SEVENTH FRAMEWORK PROGRAMME
Capacities Specific Program
Research Infrastructures

Project No.: 227887

SERIES

SEISMIC ENGINEERING RESEARCH INFRASTRUCTURES FOR EUROPEAN SYNERGIES

Work package [WP7 - TA3 Eucentre]

High-performance composite-reinforced earthquake resistant buildings with self-aligning capabilities

- Final Report -

User Group Leader: [Prof. B. Kasal

Revision: 1

March 2013

ABSTRACT

This report summarizes the key results of the international SEIES project entitled "High-performance composite-reinforced earthquake resistant buildings with self-aligning capabilities". The reports contains results of: (i) single-story, full scale mockup experiment, (ii) 2- and 3-D tests of beam-to-column connections conducted at ITAM Prague, and (iii) 1:3 scale test of frame with 3-dimensional beam-to-column connections reinforced with glass fiber (GF) rods and fabric. The results demonstrate that laminated timber frames can be designed to withstand high seismic excitations and retain their integrity under relatively large loads. One of the issues is large drift of the light frames. Joint deformations represent the main energy dissipation mechanism and a brittle failure in connections is partially mitigated by local reinforcement. 3-D connections ultimately fail in a brittle mode but under extreme excitations not realistically expected.

Keywords: laminated timber frames, local reinforcement, 3-D connections, rigid decks, seismic tests, drift

ACKNOWLEDGMENT

The research leading to these results has received funding from the European Union Seventh Framework Programme [FP7/2007-2013] under grant agreement n° 227887 [SERIES].
Additional funding was provided by Fraunhofer Wilhelm-Klauditz Institute, Brausnchweig, Germany. Support of HESS Inc., Germany is gratefully acknowledged.

REPORT CONTRIBUTORS

[**Fraunhofer WKI, TU Braunschweig, Germany**]	[Bo Kasal]
	[Norbert Rüther]
	[Tobi Polocoser]
[**Institute of theoretical and applied mechanics, Czech Academy of Sciences, Prague, Czech Republic**]	[Shotta Uruschadze]
	[Stanislav Pospisil]
[**HESS TIMBER GmbH & Co. KG Germany**]	[Andreas Heiduscke]
[**Opole University of Technology**]	[Zbigniew Zembaty]
	[Piotr Bobra]
	[Andrzej Marynowicz]

CONTENTS

List of Figures

List of Tables

1 Project description

1.1 INTRODUCTION

This document reports the analysis of results of the experiments performed at ITAM Prague (connections) Czech Republic and at the University of Bristol, UK, within the SERIES project ("Seismic Engineering Research Infrastructures for European Synergies").

The focus of this report is the analysis of experimental data generated in the above project that dealt with flexible, light, composite-reinforced laminated timber frames with self-aligning capabilities. Wood as a material is characterized with high relative strength but has low (close to zero design values) strength in tension perpendicular to fibers. Wood has relatively low values of viscous (material) damping and energy dissipation mechanism is entirely dependent on the elasto-plastic, hysteretic behavior of connections. This results in potential overstress in perpendicular-to-fibers tension and subsequent brittle failure. The brittle failure modes can be successfully mitigated via local reinforcement. This has been done in the case of plane frames but producing the 3-D (spatial) joints proves to be difficult and requires failure mode control. The frames can undergo large drift without damage and are self-aligning even at high excitation levels. Extremely high PGA and artificial spectrum containing high portion of frequencies close to the frames natural frequencies resulted in brittle failure of both tested frames (full scale mockup and 3-story scaled frame).

The performance of heavy wood frames in earthquakes has been studied both experimentally and analytically, while examples of multi-story wood frame buildings in seismically active areas are rare. This is primarily due to the difficulties in designing efficient moment-transmitting timber connections. Large inter-story drifts of wood-based moment resisting frames are caused by the low stiffness of the semi-rigid beam-to-column connections. In general, the serviceability limit state check will be the limiting criteria in the design process,

leading to over-designed cross sections of beams and columns. Apart from difficulties in balancing the moment capacities of members and connections, analyses and experiments showed that wood frames can perform well under dynamic loads due to the high strength and high energy dissipating capacity of the connections. Kikuchi [1] analysed frames up to four stories high and concluded that the frames were extremely flexible. Pinned beam-to-column connections were considered unfavourable and the analysed frames failed meeting the standard requirements of Japanese codes. Buchanan and Fairweather [2] studied various beam-to-column connections in seismic applications and concluded that moment-resisting frames can be successfully used in earthquake situations if suitable connections are available.

Strong motion earthquake tests carried out by Kasal and Heiduschke [3] revealed that the moment-resisting frames have self-aligning capabilities and showed negligible residual deformation even after large lateral displacement amplitudes. This observation is consistent with the results of shake table tests carried out by Yasumura [4]. He tested single story portal frames, shear wall systems, and a hybrid system. The moment frame used inserted steel plates to connect beams with columns. The tested MR frames as well as the hybrid system returned to the undeformed position while shear wall systems showed significant residual drifts. The self-aligning mechanism was present up to an inter-story drift of about 1/24. Palermo et al [5] investigated he performance of ductile connectors for application in multi-story laminated veneer lumber frames. The experiments showed significant hysteretic dissipation of energy, good self-aligning capacity and no damage of the moment-resisting beam-to-column connections. Glued-in mild-steel bars or external dampers designed to yield in tension and compression were responsible for the dissipation of energy. The self-aligning capabilities were achieved by a controlled rocking mechanism provided by unbonded post-tensioned tendons designed to remain elastic. The global moment-rotation response of the connection had flag-shaped hysteretic loops. These so-called post-tensioned energy dissipating (PTED) connections were previously developed for precast concrete structures [6] and later extended to steel and wood structures.

Recent earthquake scenarios caused a relatively small number of casualties but resulted in unacceptably high economic losses [7]. As a result, the demands on transient and permanent deformations became of higher importance. The absence of residual deformation allows laminated frames to be used for structures or systems that need to retain function (essential facilities) even after large magnitude events. This is a decisive advantage because such behaviour will minimize damage and the cost of reconstruction.

This report describes and summarizes the experiments conducted within the scope of the SERIES program. Significant investments of individual participants beyond the EU SERIES program has been used to finish this project. Financial support of Fraunhofer WKI is hereby acknowledged.

2 Methods and Materials

2.1 HYPOTHESES

The hypotheses of this work were as follows:

1. High drift of laminated timber frames can be controlled with relatively stiff beam-to-column connection
2. Relatively stiff beam-to-column connection s will result in brittle failures that must be mitigated
3. Composite material reinforcement will shift the failure modes from brittle to ductile
4. 3-D beam-to-column connections (BCC) are possible to design and fabricate

2.2 METHODS

The schematic in Figure 1 shows the workflow of the project. The expected response of the experimental frames was fist analytically estimated and the models will be discussed elsewhere.

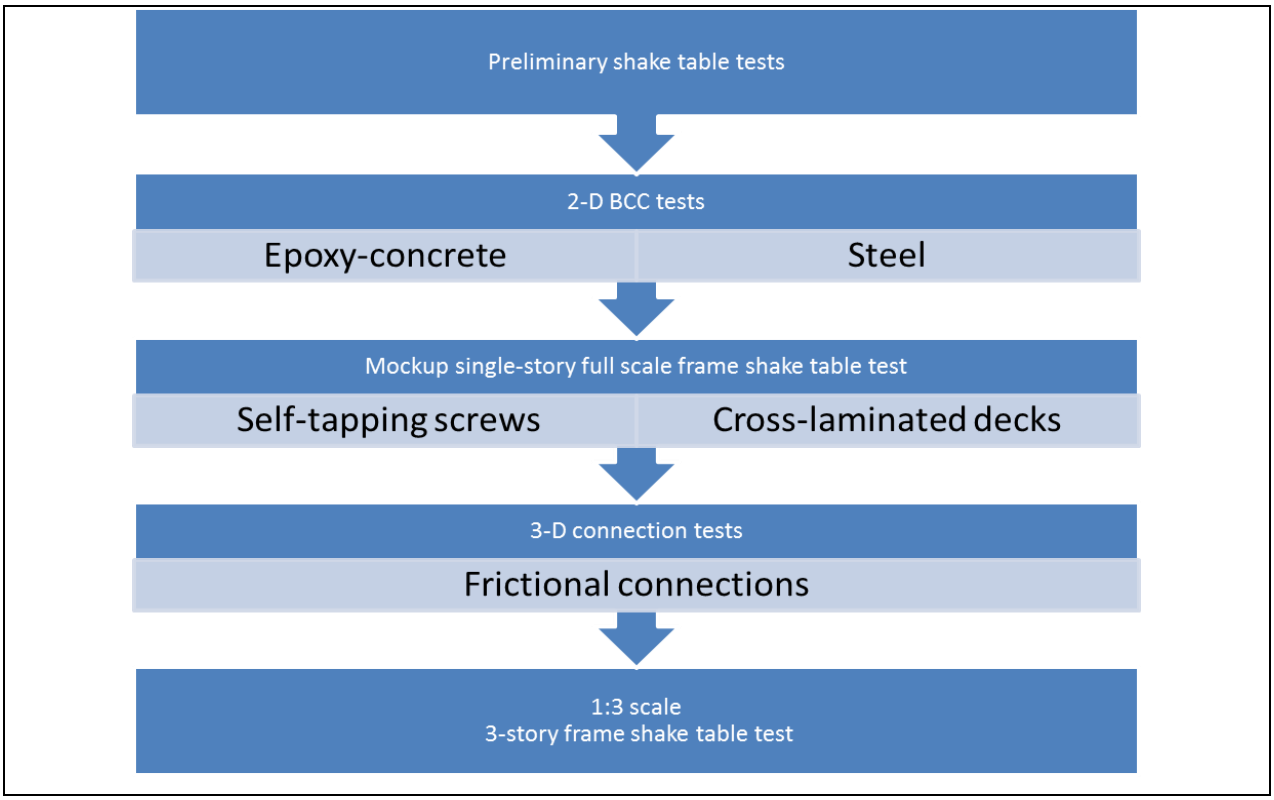

Figure 1. Schematic of the research plan and milestones.

2.3 MATERIALS

The list of materials used in the experiments is listed in

Table 1. Material parameters for 2-D BCC tests conducted at ITAM Prague

Item	Part	Average Density (kg/m^3)	E-modulus (MPa)	Yield strength (MPa)	Note
1	Laminated timber. Spruce.	400	12-14 000	80-120	Not measured
2	Steel connection plates	7850	210000	210	Not measured
3	Connection pins-steel	7850	210000	210	Not measured
4	GF reinforcement	2550	80000	2000	Not measured
5	Adhesive	--	--	--	Epoxy Resin

Table 2. Material parameters for 3-D BCC tests conducted at ITAM Prague

Item	Part	Average Density	E-modulus (MPa)	Yield strength	Note

		(kg/m^3)		(MPa)	
1	Laminated timber. Spruce.	400	12-14,000	80-120	
2	Steel connection plates	7850	210000	210	Not measured
3	Connection pins-steel	7850	210000	210	Not measured
4	GF reinforcement	2550	80000	2000	Not measured
5	Adhesive	--	--		Epoxy Resin

Table 3. Materials in mockup frame test at the University of Bristol

Item	Part	Average Density (kg/m^3)	E-modulus (MPa)	Yield strength (MPa)	Note
1	Laminated timber. Spruce.	400	12-14,000		Not measured
2	Fasteners – BCC – Decks to beams	7850	210000	210	Not measured
3	Supporting blocks of beech wood	680-830	15,000	--	Not measured
4	GF reinforcement Thickness Weight per m^2	--	--	--	Not measured
5	Adhesive	--	--	--	Epoxy Resin

3 The experiments

3.1 FULL SCALE CYCLIC STATIC TESTS OF 2-D BEAM-TO-COLUMN CONNECTIONS

The goal of these experiments was to evaluate the proposed solution for the beam-to-column, 3-D moment connections. 2-D cross-type fragments were tested using static cyclic load with increasing amplitude and relative displacements between the beams and a column were recorded.

3.1.1 Test setup and test protocol

The tests were two-dimensional and a single hydraulic cylinder was used to generate the required moment. Specimen testing was done in the ITAM laboratory in Prague. The laboratory temperature averaged 30˚C and the relative humidity was not measured. The specimens were placed horizontally on a dynamic laboratory floor with supports as shown in Figure 4. The bottom of the column was pin connected and the ends of the beams were roller connected. The top of the column was connected to the load cell.

A model 661.22C/D-01 load cell with a maximum force of 250kN, and an output of 2mV/V was used in the cyclical load tests. This load cell was driven by a Model 244.31 Hydraulic Actuator with a maximum force of 250kN. The maximum dynamic and static stroke of the actuator was 254.2mm and 264.2mm respectively. The hydraulic actuator and load cell were controlled by a MTS Model 407 Servocontroller. Each specimen was tested at a constant frequency with varied amplitudes. All amplitudes were run for three cycles with a pseudo static loading. Table 1 gives the frequency and amplitudes for each specimen tested.

Table 4. Test parameters for the 2-D beam-to-column connections

Specimen	Cycle Frequency (Hz)	Applied Amplitude Sequence (mm)
1	0.1	1-2-3-4-6-8-10-12-16-20-25-30-35…110-115
2	0.05	2-4-6-8-12-16-24-32-48-64-80-96-112-120
3	0.05	2-4-6-8-12-16-24-32-48-64-80-96-112-120
4	0.05	2-4-6-8-12-16-24-32-48-64-80-96-112-120

In each test potentiometers were used to measure displacements of the frame at defined spots on the specimen, see Figure 4 and 5. Potentiometers 10 thru 13, 20, and 21 had a maximum recordable displacement of ±25mm. The potentiometers labeled 14 and 22 had a max displacement of ±250mm and ±50mm respectively. V0 was the force output of the load cell in kilonewtons. The data was acquired with AUTOSOFT "C", a data acquisition program. The data acquired from potentiometers 10 thru 13, 20, and 21 showed positive when the angle between the beam and column was decreasing and negative when the angle was increasing. For V0, 14, and 21 the data was positive for motion away from the load cell and negative for motion toward the load cell. After completion of the tests the data was analyzed to determine if results were reasonable and followed test protocol.

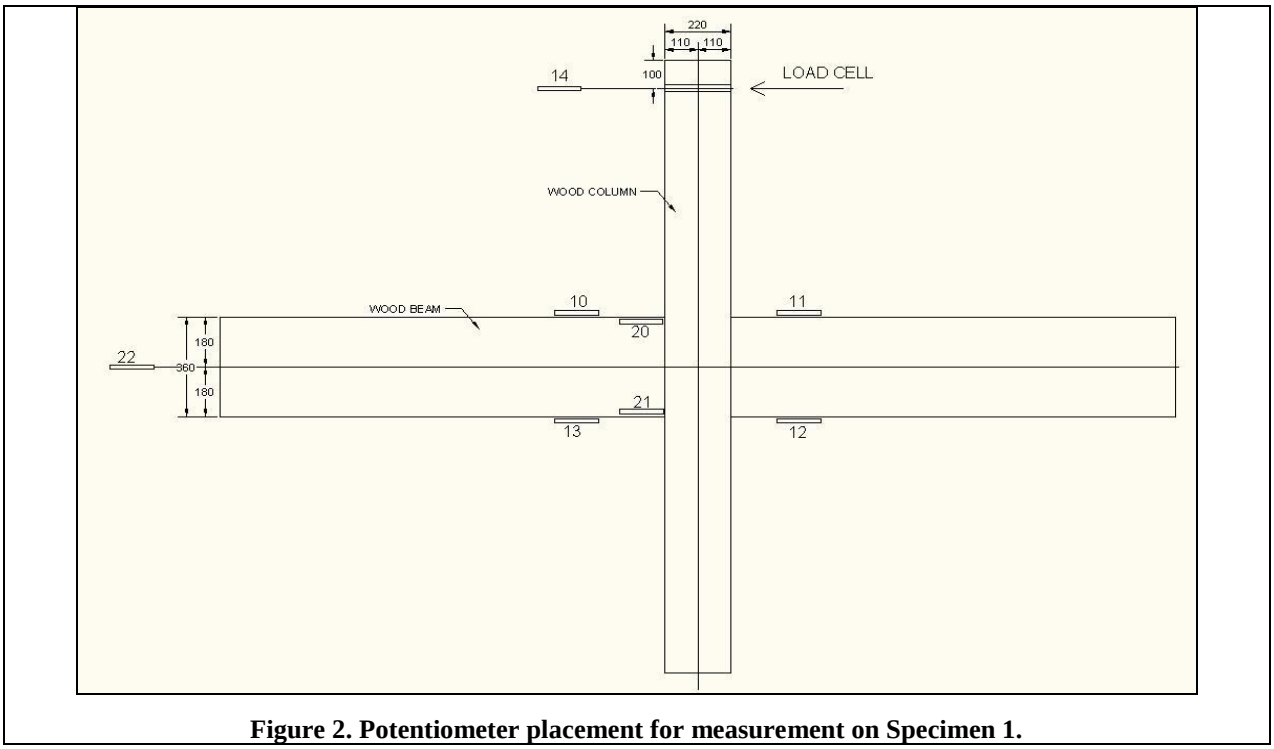

Figure 2. Potentiometer placement for measurement on Specimen 1.

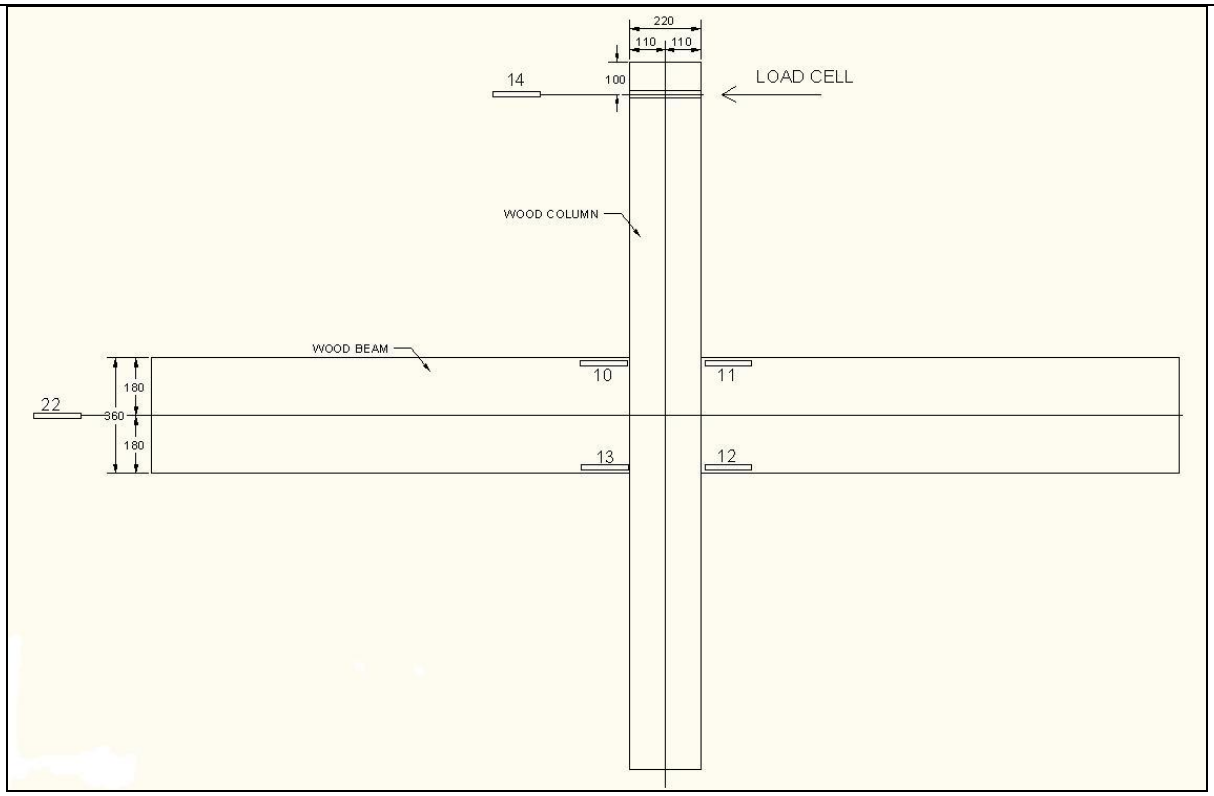

Figure 3. Potentiometer placement for measurement on Specimen 2-4.

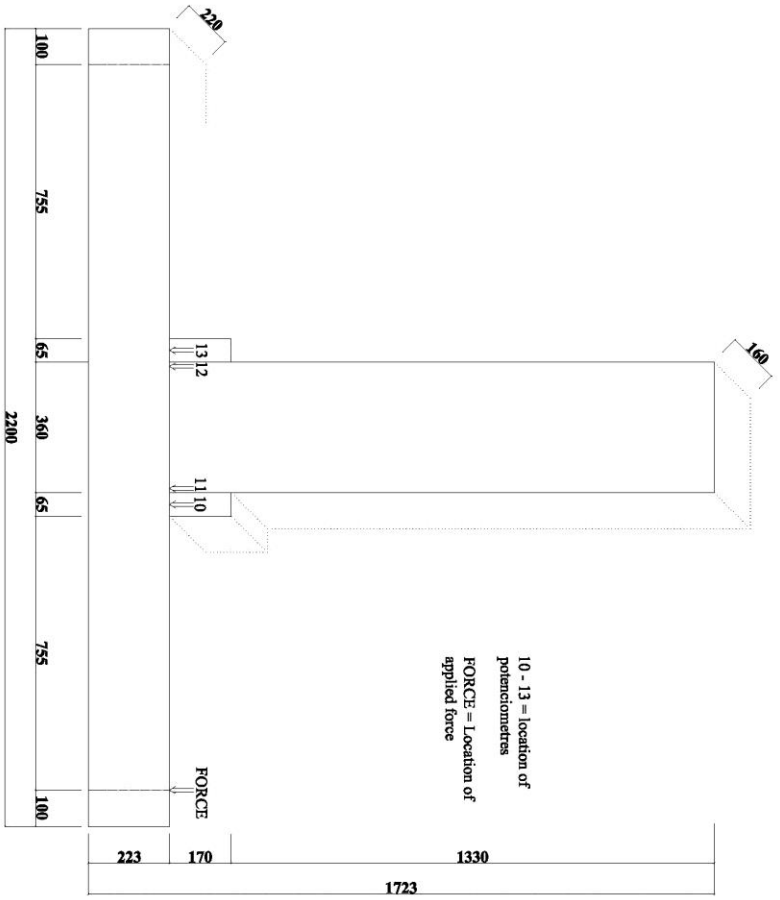
220
160
100
755
65
360
65
755
100
2200
13
12
11
10
FORCE
10 - 13 = location of potenciometres
FORCE = Location of applied force
223
170
1330
1723

(a)

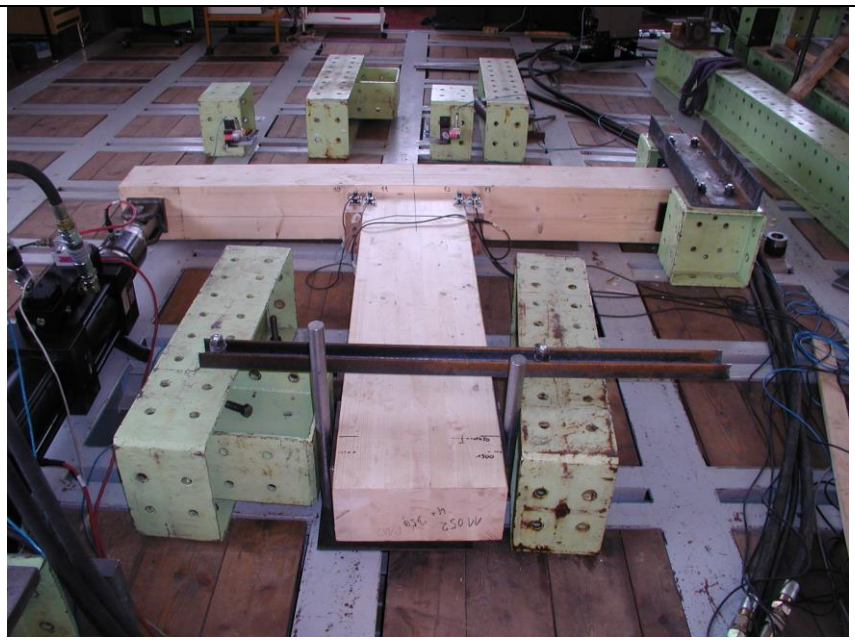

(b)

Figure 4. Test setup for 2-D beam-to-column connections (ITAM Prague) (mockup connection). (a) schematic of the test with dimensions, and (b) test setup.

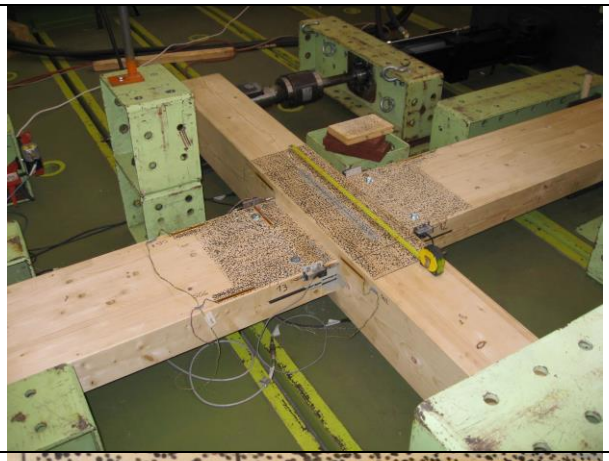

Figure 5. Details of the 2-D moment connection tests.

3.1.2 Materials

All specimens were manufactured using spruce. The specimens were GL24h laminated wood columns and beams produced by Hess Laminator. The moisture content and density of each specimen was 10 to 12% and about 400 kg/m^3 respectively. Each specimen consisted of one 220mm x 220mm x 2200mm laminated wood column and two 120mm x 360mm x 1490mm laminated wood beams that were later assembled in a cross frame using 3 different types of beam-to-column (BC) moment connections.

Four laminated wood frames were assembled for testing under cyclic loading. All frames consisted of moment resisting BC connections. Specimen 1 and 2 were assembled using connection Type 1 shown in Figure 1. Hess Laminator made all cuts and glued the M 16 threaded rods into the beams. The frames were assembled on site at the Institute of Theoretical and Applied Mechanics in Prague, Czech Republic. Two 8mm diameter screws were drilled into the shear key area on each beam for additional shear reinforcement. Polymer concrete filled in the assembly openings in the frame and provided extra compression strength in the connection zone of the column.

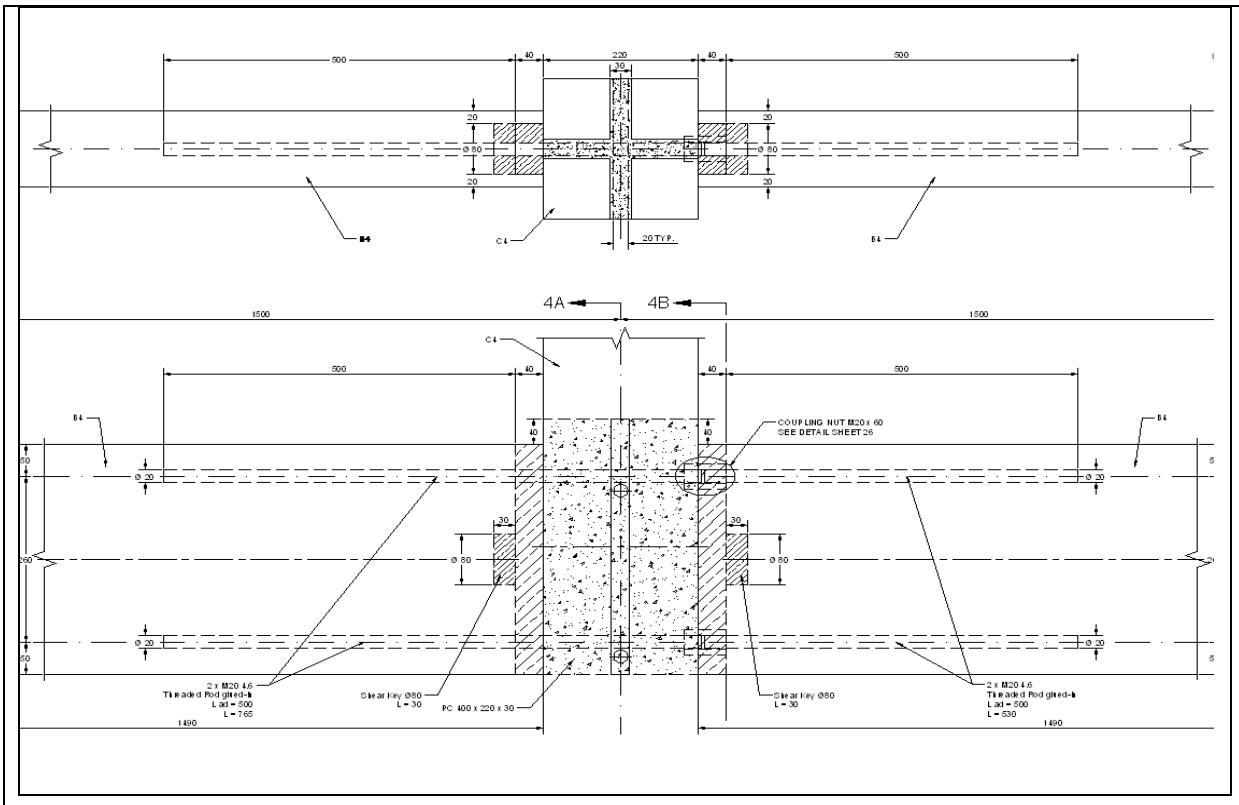

Figure 6. Specimen 1 and 2 Connection Details

Specimen 3 was assembled using connection Type 2 shown in Figure 2. Hess Laminator made all the cuts and holes in the specimen needed for assembly. The moment connection frame was assembled at ITAM in Prague. The pre-manufactured steel plates were connected using 12mm diameter bolts, and the beams were connected to the steel plates using 10mm diameter steel dowel connectors. Polymer concrete was used to fill openings in the connection and hold the steel plates in place within the column.

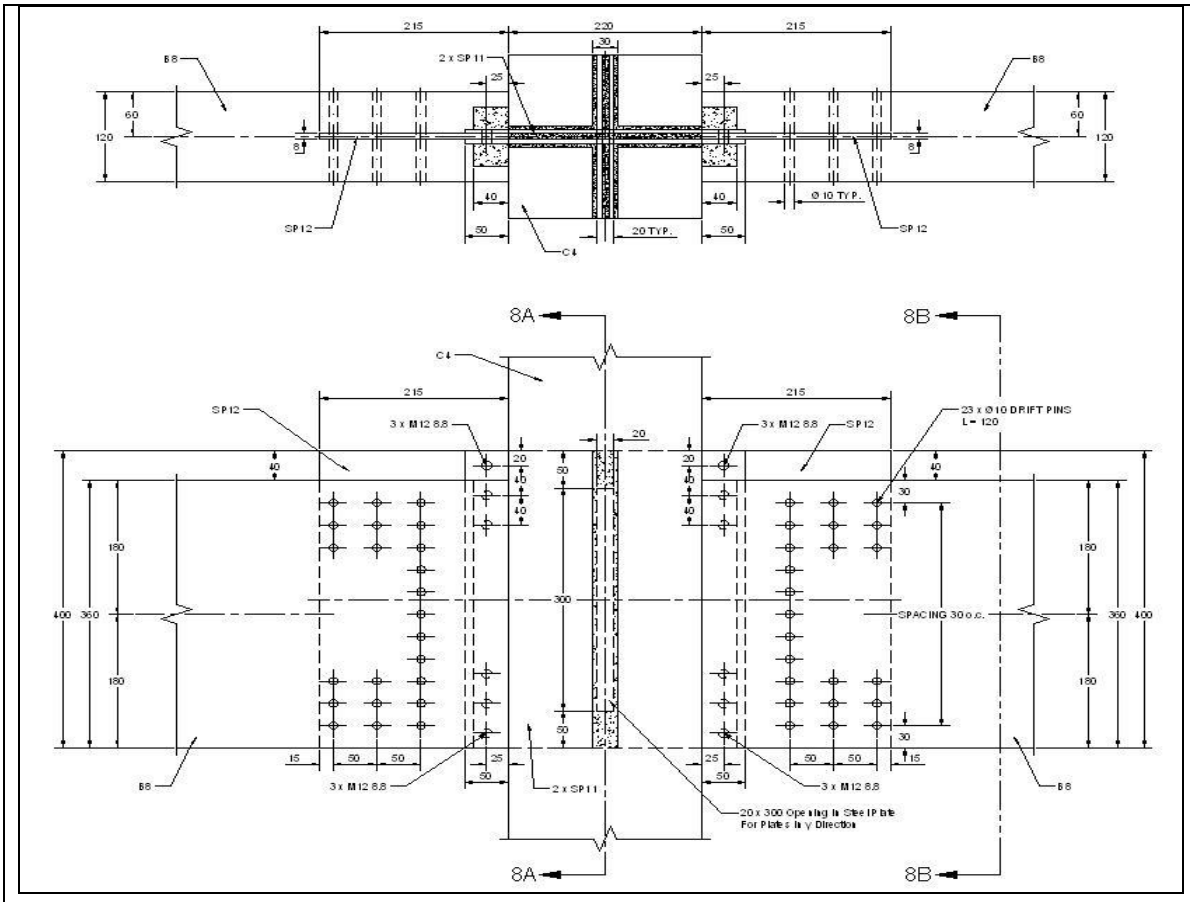

Figure 7. Specimen 3 Connection Details

Specimen 4 was assembled using connection Type 3 shown in Figure 4. The laminated wood pieces were produced by Hess Laminator. All cuts, holes, and assembly were done on site at ITAM. The moment connection was created using prefabricated steel plates, and dowel type fasteners. Steel plates were connected to the column using M 16 steel bolts, and 10mm diameter steel dowels were used to connect the beams to the steel plates.

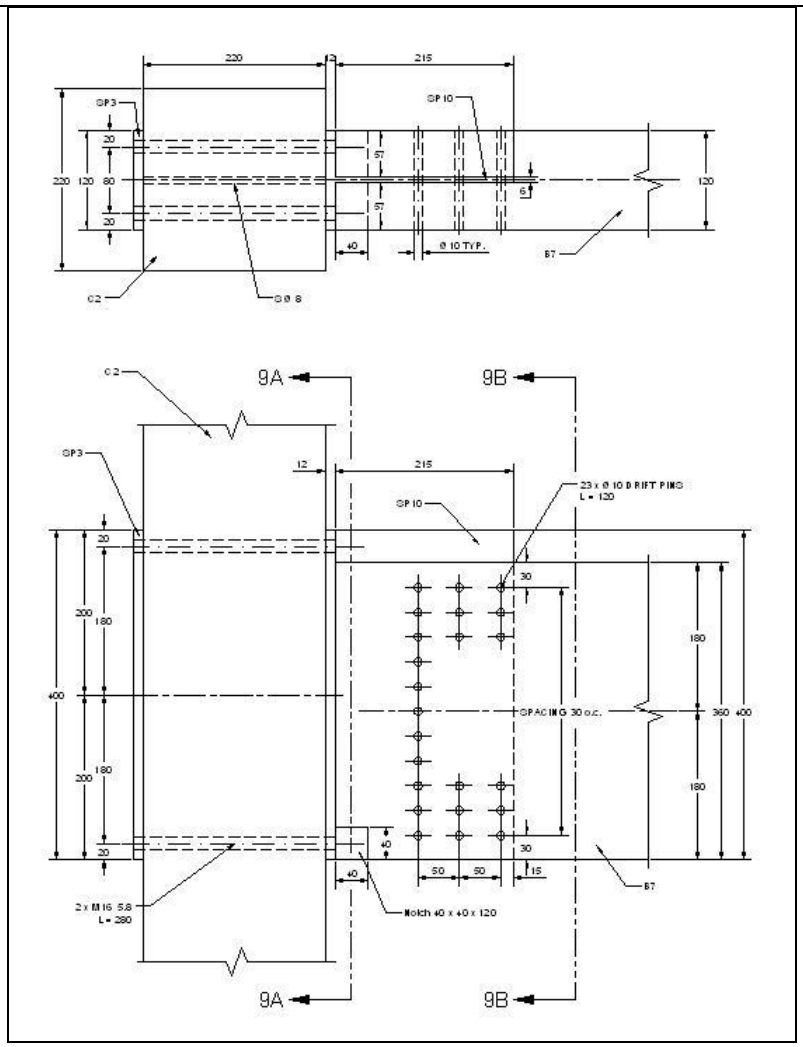

Figure 8. Specimen 4 Connection Details

Each assembled moment connection frame was a cross shape with an end to end column distance of 2200mm and an end to end beam distance of 3200mm. The restraints were placed 100mm in from each end of the column making the applied moment arm 1m (1000mm). The beams each had a moment arm of 1340mm.

3.1.3 Results

Upon completion of the tests the data was analyzed and evaluated to determine the performance of the beam-to-column connections of two dimensional laminated wood frames under cyclic loads. Figure 6 shows the plotted results of piston displacement vs. time for the tests performed on Specimen 1. One problem with these plots and results is the displacement is not symmetric

about the x-axis. This means problems occurred with controlling the load cell to meet test protocol and the problems would need to be fixed before the test of Specimen 2.

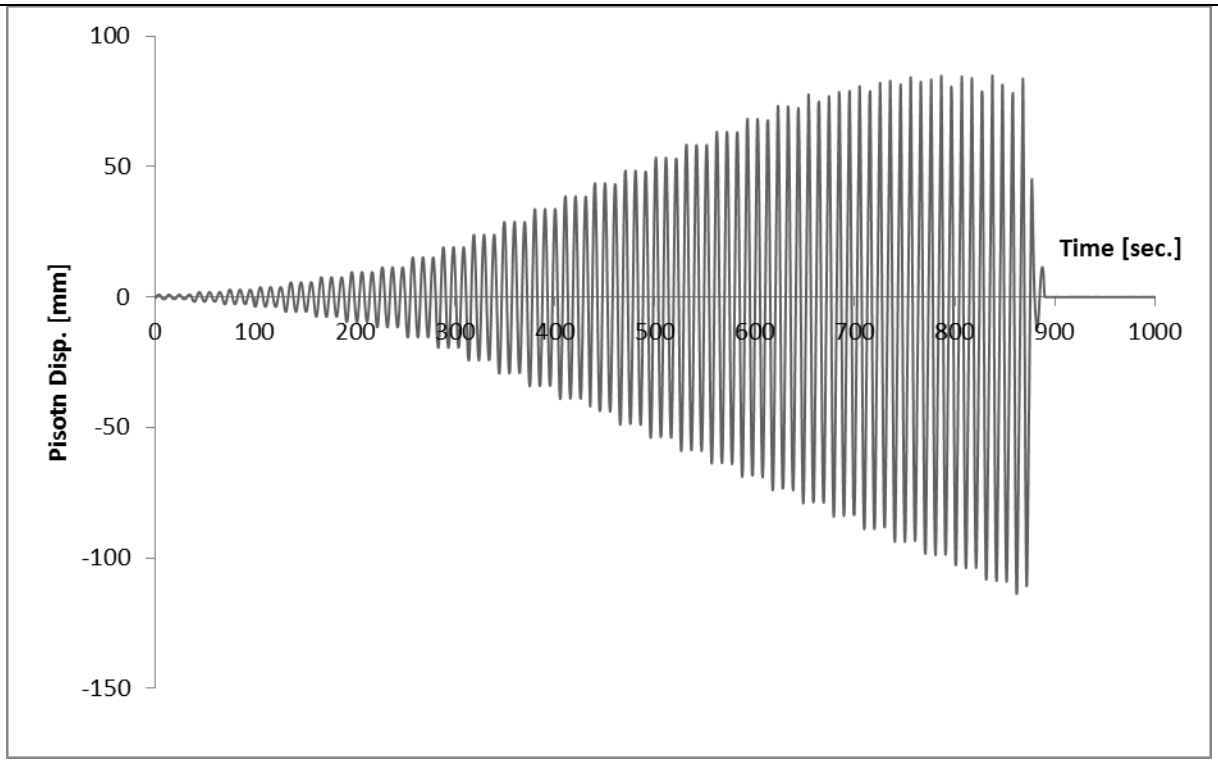

Figure 9. Piston displacement vs. time for Specimen 1.

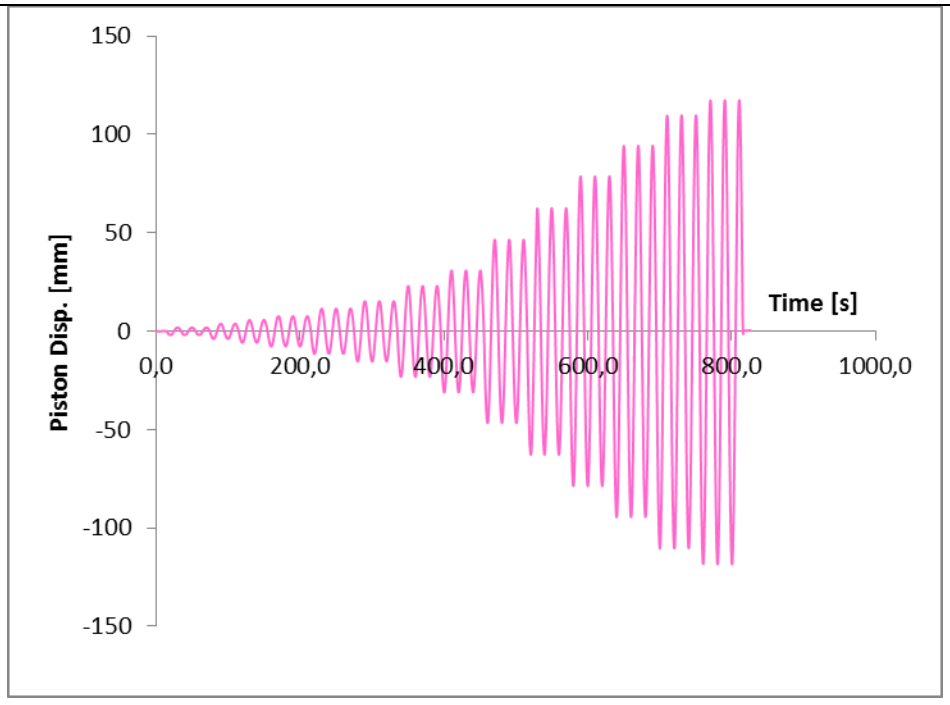

Figure 10. Piston displacement vs. time for Specimen 2

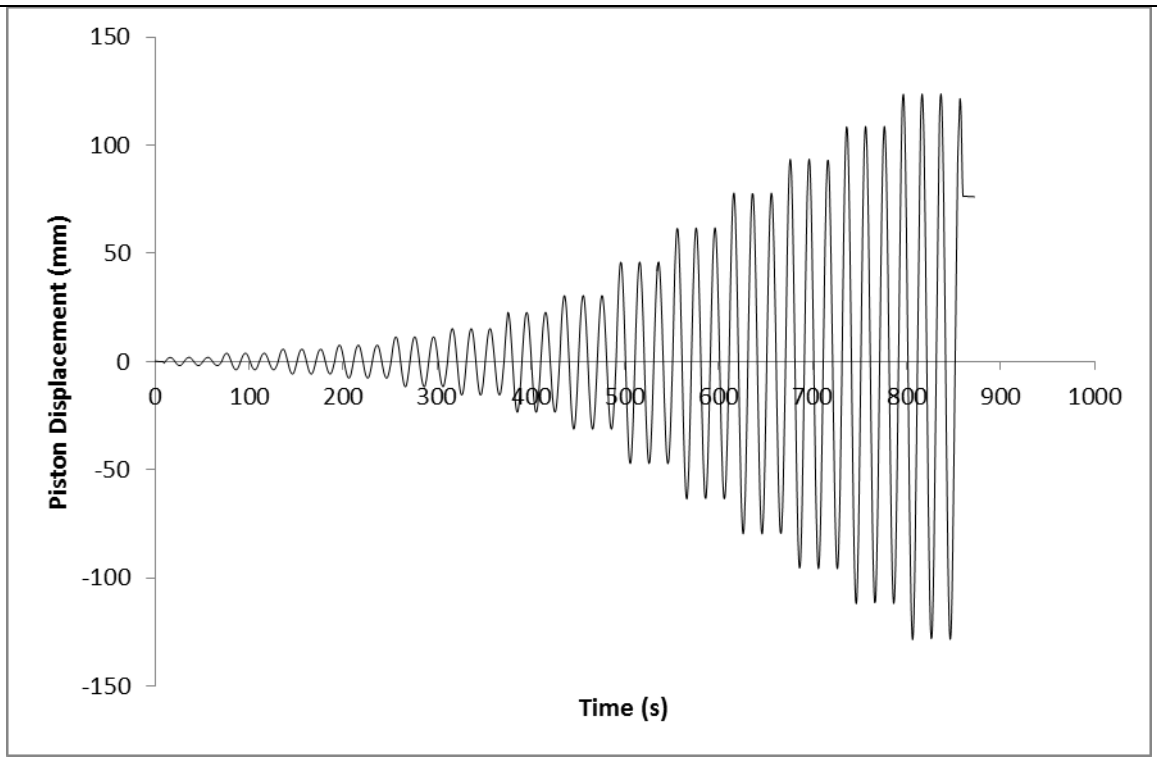

Figure 11. Piston displacement vs. time for Specimen 3

Figure 16 shows the cumulative energy dissipation in moment connection in Specimen 2. At low amplitudes of cyclic loading the energy dissipated in the joint is very small and increases as the applied amplitude increases.

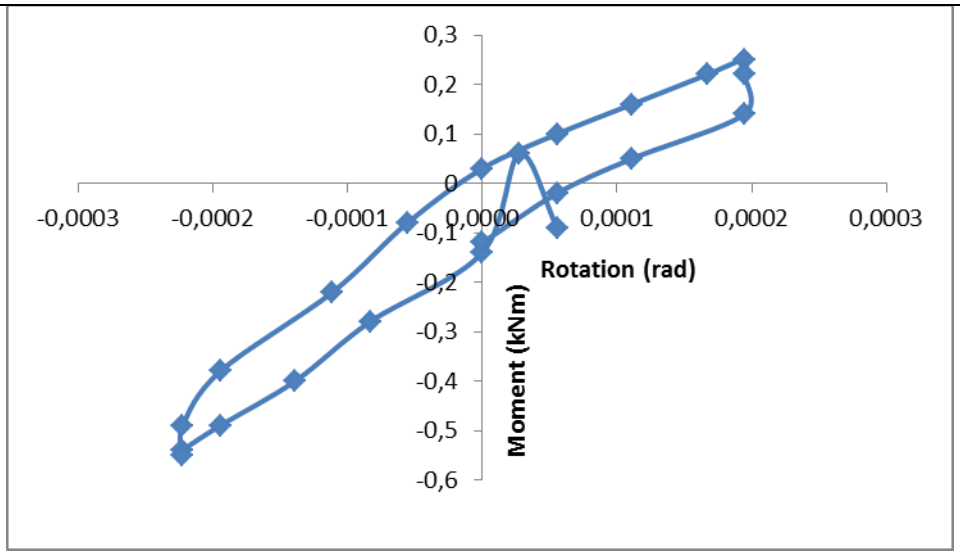

Figure 12. Specimen 1. Moment-rotation at small amplitudes (cycle 1).

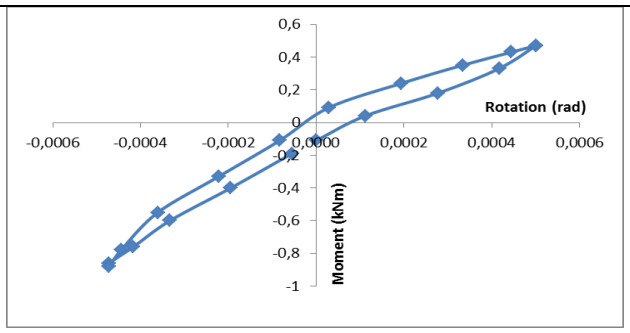

Figure 13. Specimen 1. Moment-rotation at small amplitudes (cycle 6).

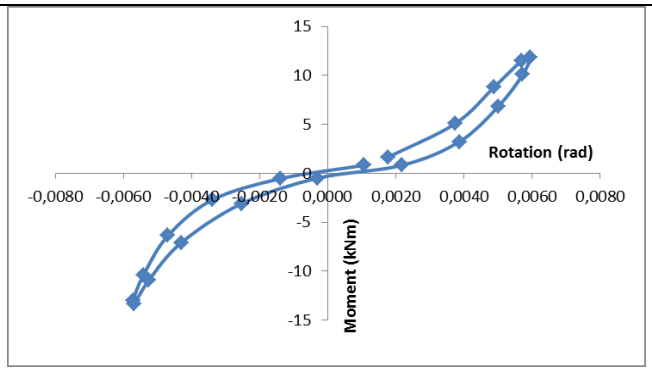

Figure 14. Specimen 1. Moment-rotation at large amplitudes (cycle 32). Note the pinching of the curve but relatively tight loop indicating limited energy dissipation capacity.

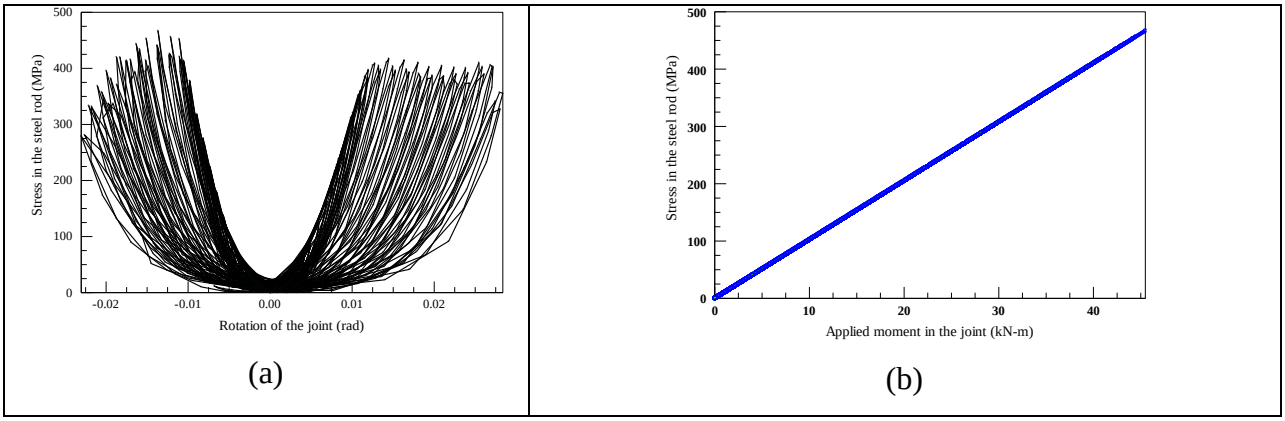

Figure 15. Rotation of the joint versus tensile stress in the steel rods (a) and applied moment versus stress in the rods (b) for the connection 1.

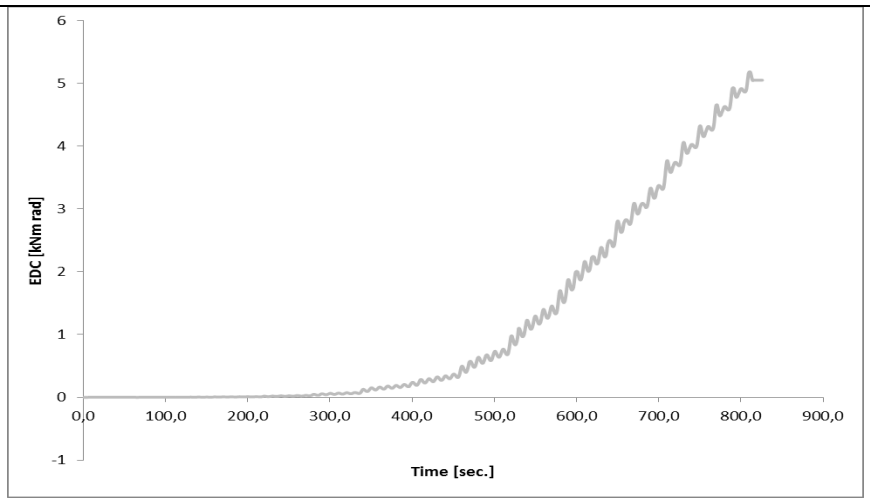

Figure 16. Cumulative energy dissipation vs. time for specimen 2.

Moment-rotation curves for the specimens 1-3 are shown in Figure 18.

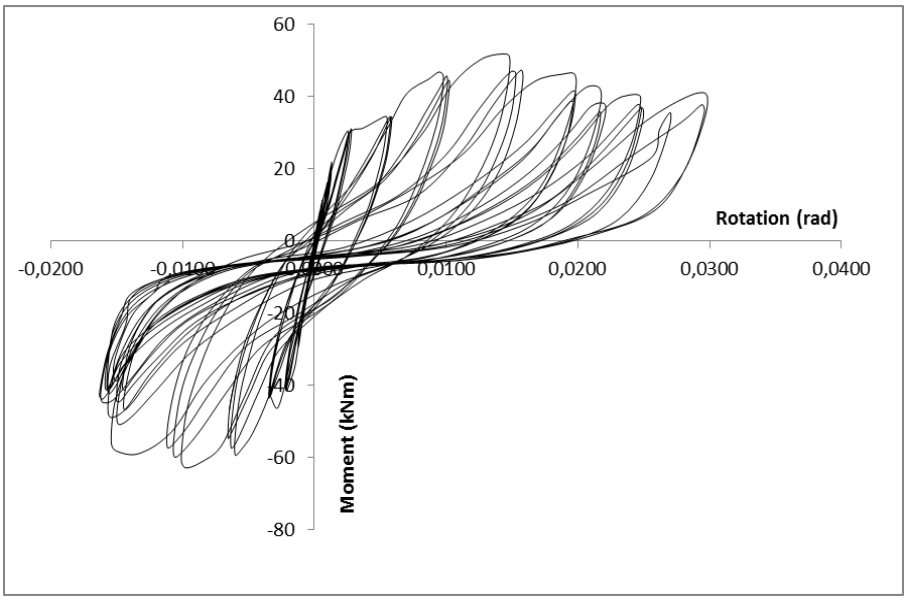

Figure 17. Moment-rotation curves (hysteretic curves) for the specimens 3.

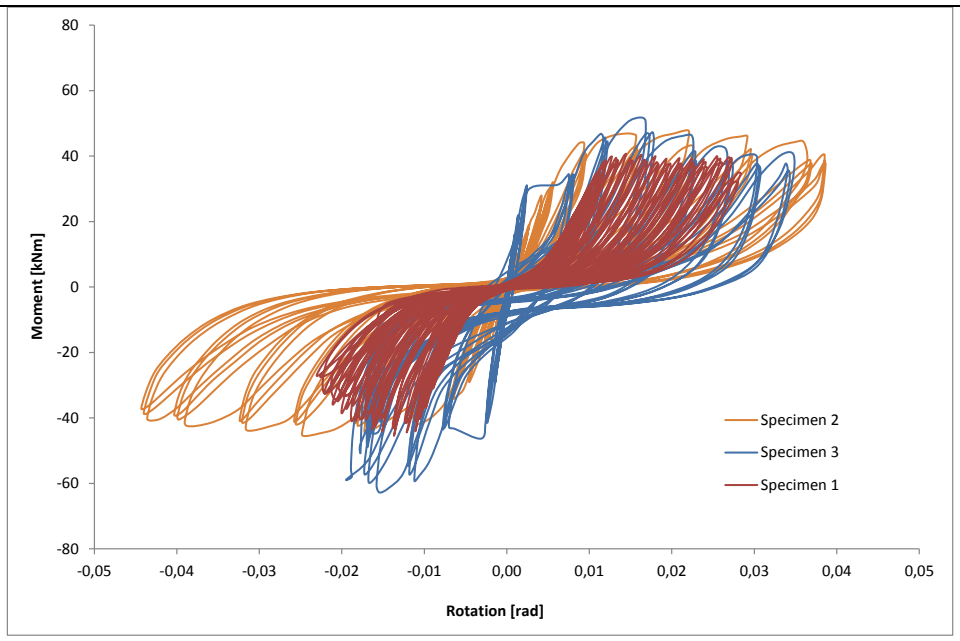

Figure 18. Moment-rotation curves (hysteretic curves) for the specimens 1, 2, and 3.

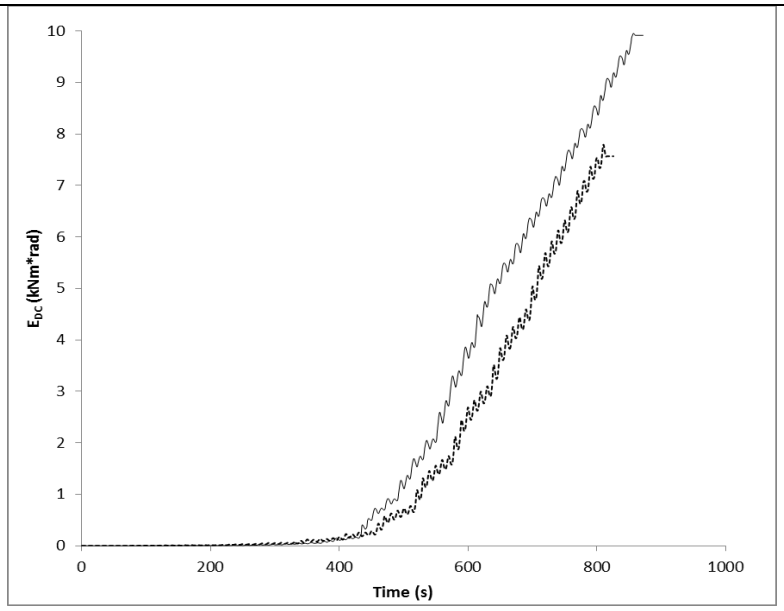

Figure 19. Cumulative dissipated energy. Specimens 2 and 3.

Based on the experiments above, it was decided that the beam-to-column connections will be designed as close-to-rigid to minimize the drift.

3.2 SHAKE TABLE MOCKUP TESTS OF FULL-SCALE SINGLE-STORY MOMENT FRAME

The mockup frame was a single-story, full-size frame with relatively rigid beam-to-column connections – see Figure 24.

3.2.1 Test setup and test protocol

The instrumentation of the mockup test frame is shown in Table 5, **Figure 20** and Figure 21.

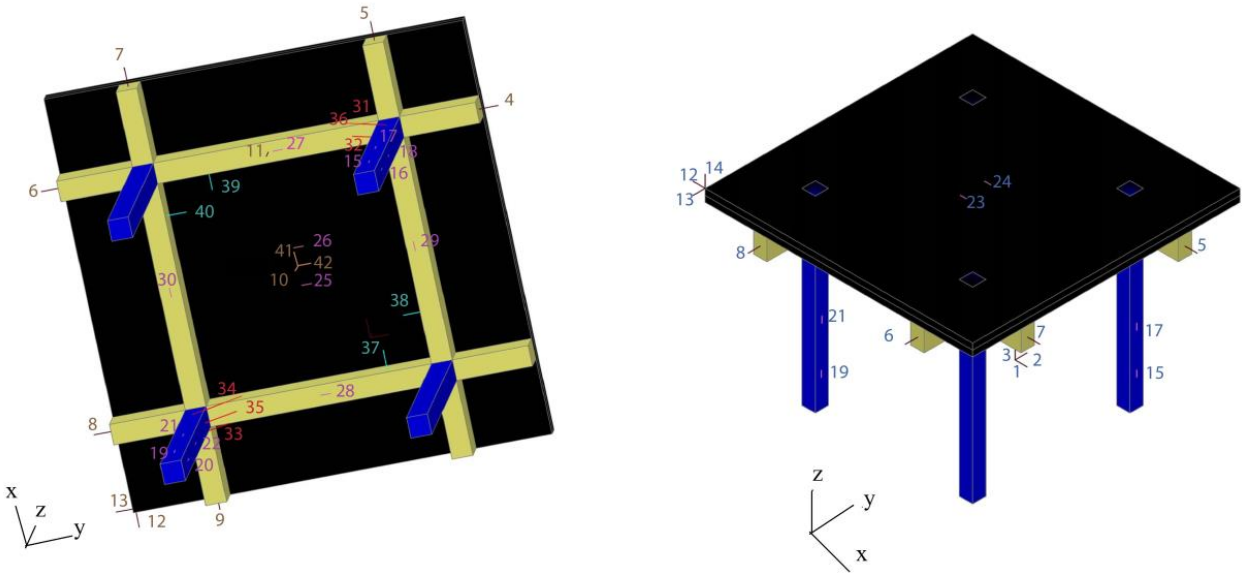

(a)

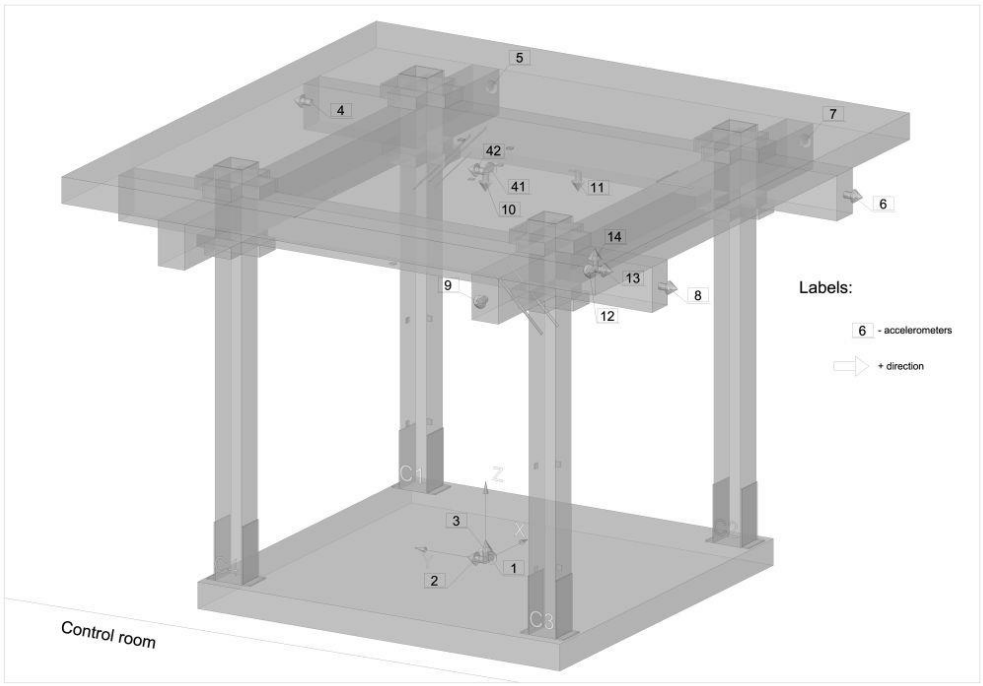

(b)

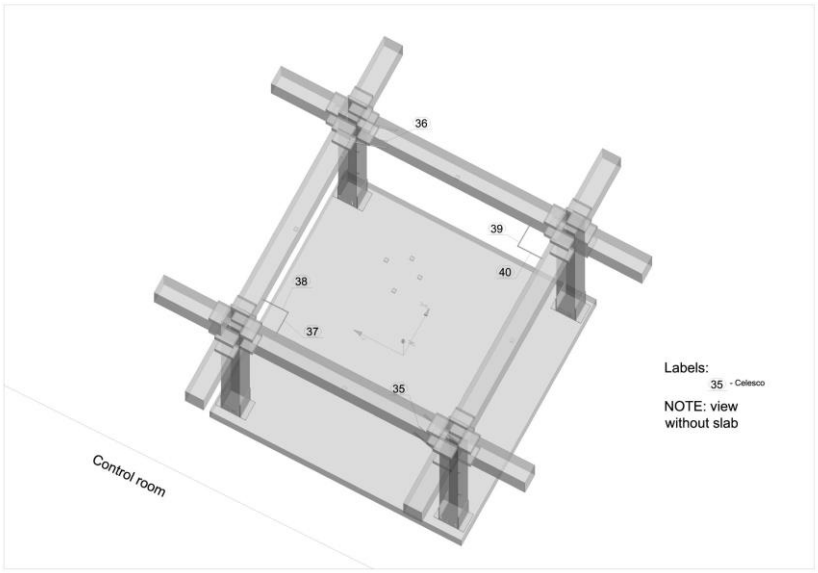

(c)

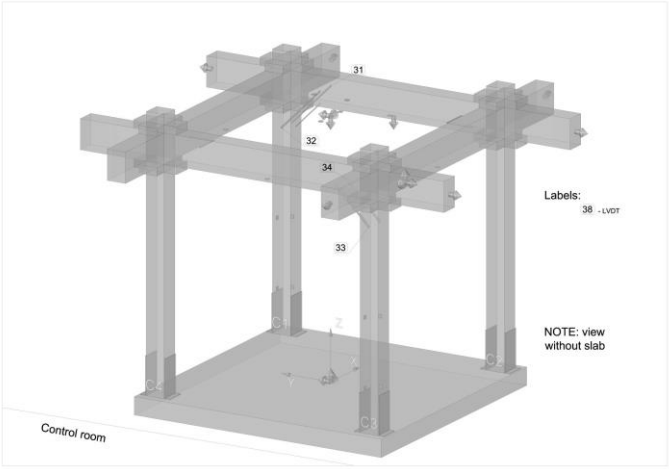

(d)

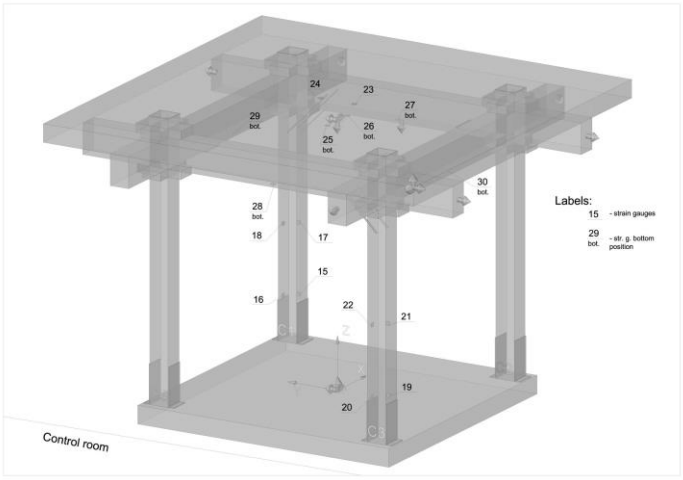

(e)

Figure 20. Instrumentation of the mockup frame. Instrument type and location – see Table 5. (a) overall view, (b) accelerometers, (c) string potentiometers, (d) LVDT´s, and (d) strain gauges.

Table 5. Location and type of the sensors for the mockup frame – see Figure 20

Channel	*Type*	*Location*	*Calibration constant*
1	Acc SETRA	Shaking table (-300,1000,0) Direction +X	0.9745V/g
2	Acc SETRA	Shaking table (-300,1000,0) Direction +Y	0.9787V/g
3	Acc SETRA	Shaking table (-300,1000,0) Direction +Z	0.9721V/g
4	Acc SETRA	Connection 1 (1300,2210,2730) Direction Y	0.9808V/g
5	Acc SETRA	Connection 1 (2210,1300,2730) Direction x	0.9746V/g
6	Acc SETRA	Connection 2 (1300,-2210,2730) Direction Y	0.9822V/g
7	Acc SETRA	Connection 2 (2210,-1300,2730) Direction x	0.9725V/g
8	Acc SETRA	Connection 3 (-1300,-2210,2730) Direction Y	0.9792V/g
9	Acc SETRA	Connection 3 (-2210,-1300,2730) Direction x	0.9489V/g
10	Acc SETRA	Deck 1 under side (0, 0, 2900) Direction z	0.9818V/g
11	Acc SETRA	Beam C1C2 under side (middle) 1300,0,2560 Direction z	0.9801V/g
12	Acc SETRA	Deck, top (-2210,-2210,3100) Direction X	0.9673V/g
13	Acc SETRA	Deck, top (-2210,-2210,3100) Direction Y	0.9778V/g
14	Acc SETRA	Deck, top (-2210,-2210,3100) Direction Z	0.9762V/g
15	Strain gauge	Column 1 SP1B, bottom (1410,1300,460) +X face Z direction	100 με/ V
16	Strain gauge	Column 1 SP1B, bottom (1310,1410,460 +Y face Z direction	100 με/ V
17	Strain gauge	Column 1 SP1M, middle (1410, 1300,1230)	100 με/ V

		+X face Z direction	
18	Strain gauge	Column 1 SP1M, middle (1300,1410,1230) +Y face Z direction	100 με/ V
19	Strain gauge	Column 3 SP3B, bottom (-1190,-1310,460) +X face Z direction	100 με/ V
20	Strain gauge	Column 3 SP3B, bottom (-1300,-1190,460) +Y face Z direction	100 με/ V
21	Strain gauge	Column 3 SP3M, middle (-1190,-1300,1230) +X face Z direction	100 με/ V
22	Strain gauge	Column 3 middle (-1300,-1190,1230) +Y face Z direction	100 με/ V
23	Strain gauge	Deck top +Z face (0,-200,3100) For Direction x	100 με/ V
24	Strain gauge	Deck top +Z face (0,200,3100) For Direction x	100 με/ V
25	Strain gauge	Deck bottom -Z face (-200,0,2900) For Direction y	100 με/ V
26	Strain gauge	Deck bottom -Z face (200,0,2900) For Direction y	100 με/ V
27	Strain gauge	Beam C1-C2 Middle underside (1300,50,2560) -Z face Y direction	100 με/ V
28	Strain gauge	Beam C3-C4 Middle underside (-1300,0,2560) -Z face Y direction	100 με/ V
29	Strain gauge	Beam C1-C4 Middle underside (0,1275,2560) -Z face X direction	100 με/ V
30	Strain gauge	Beam C2-C3 Middle underside (0,-1300,2550) -Z face X direction	100 με/ V
31	LVDT	Connection 1 B1P1 (1410,830,2730) To col 1 (1410,1300,2260) Direction 45° outside face	1.958mm/V

32	LVDT	Connection 1 B1P1 (1190,830 ,2730) To col 1 (1190,1300,2260) Direction 45° inside face	4.062mm/V
33	LVDT	Connection 3 B3P3 (1410,-850 ,2730) To col 3 (-1910,-1300,2260) Direction 45° outside face	3.972mm/V
34	LVDT	Connection 3 B3P3 (-1190,-830 ,2730) To col 3 (-1190,-1300,2260) Direction 45° inside face	3.936mm/V
35	celesco	Connection 3 B3P3 (-1300,-890,2560) To col 3 (-1300,-1190,2260) Direction 45° Mid. Fibre	3.86mm/V
36	celesco	Connection 1 B1P1 (1300,890,2560) To col 1 (1300,1190,2260) Direction 45° Mid. fibre	3.84mm/V
37	celesco	Sway Near Col. 4 (-1190,705,2730) X	47.49mm/V
38	celesco	Sway Near Col. 4 (-670,1190,2730) y	25.63mm/V
39	celesco	Sway Near Col. 2 (1190,-675,2730) X	41.89mm/V41.79
40	celesco	Sway Near Col. 2 (810,-1190,2730) y	41.79mm/V
41	setra	Deck 1 under side (0, 0, 2900) X direction	.9767V/g

42	setra	Deck 1 under side (0, 0, 2900) Y direction	.9832V/g
43	Shaking Table Roll angle		0.25 deg/V
44	Shaking Table Pitch angle		0.25 deg/V
45	Shaking Table Roll accel		1 rad/s2/V
46	Shaking Table Pitch accel		1 rad/s2/V
47	Load cell		0.981V/kN

(a)

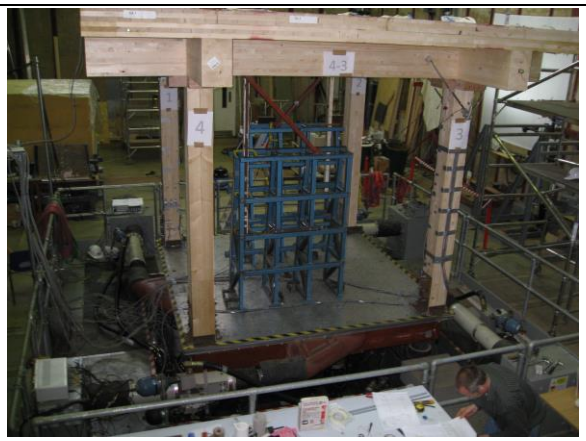

(b)

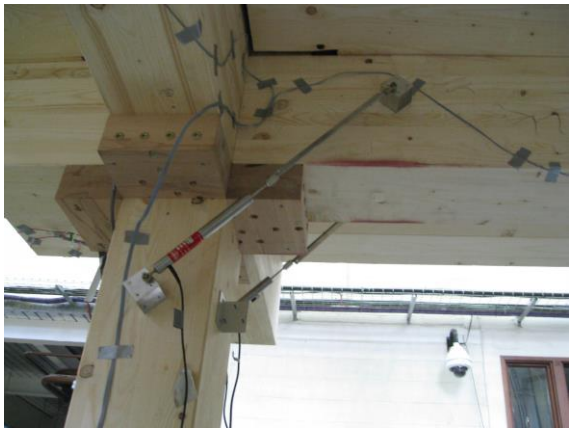

(c)

(d)

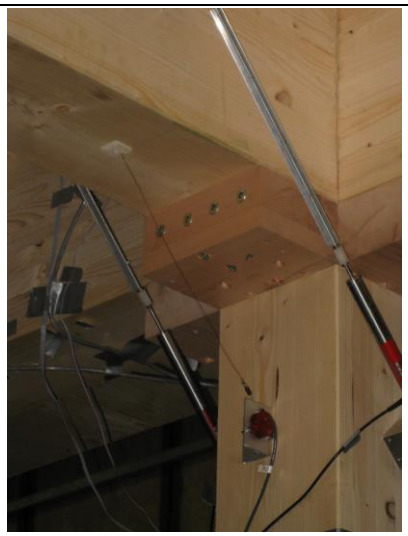

(e)

(f)

Figure 21. Instrumentation of the mockup frame. (a) bare frame prior to the installation, (b) designation of columns and beams, (c) LVDT´s measuring the relative displacement between beams and columns, (d) string potentiometer measuring the horizontal displacement of the beam relative to the shaking table, (e) additional string potentiometer, and (f) column support instrumentation.

The test protocol and schedule is in the Table 6.

Table 6. Test protocol for the mockup frame.

EARTHQUAKE ENGINEERING RESEARCH CENTRE

Queen's Building
University Walk
Bristol BS8 1TR

Tel: 0117-9287708
Fax: 0117-9287783

UNIVERSITY OF BRISTOL
Department of Civil Engineering

EARTHQUAKE SIMULATOR TEST LOG

Date	Time	Test No.	Run No.	Title	TIR Ref.	Computer files ACQ	Computer files DRIVER	Gain %	Notes
23/05/11	**12.30**	**1**	**1**	**TA3_1105_N1R1 noise, y axis**	**TA3_11006_R1(TIR1)**		**ADVANTEST**	**0.5 mm/V**	**0-100Hz, Acq rate = 256Hz, Py = 6dB, AuxIn filt = 1000Hz Sensors setra 6409 & setra 6978 added after test.**
23/05/11									
23/05/11	12.30	2	1	TA3_1105_N2R1 noise, y axis	TA3_11006_R1(TIR1)		ADVANTEST	0.5 mm/V	0-100Hz, Acq rate = 256Hz, Py = 6dB, AuxIn filt = 1000Hz
23/05/11	13.40	3	1	TA3_1105_N3R1 noise, y axis	TA3_11006_R1(TIR1)		ADVANTEST	1 mm/V	0-100Hz, Acq rate = 256Hz, Py = 6dB, AuxIn filt = 1000Hz

23/05/11	14.20	4	1	TA3_1105_N4R1 noise, X axis	TA3_11006_R1(TIR1)	ADVANTEST	0.5 mm/V	0-100Hz, Acq rate = 256Hz, Py = 6dB, AuxIn filt = 1000Hz
23/05/11	14.20	5	1	TA3_1105_N5R1 noise, X axis	TA3_11006_R1(TIR1)	ADVANTEST	1 mm/V	0-100Hz, Acq rate = 256Hz, Py = 6dB, AuxIn filt = 1000Hz
23/05/11	14.50	6	1	TA3_1105_N6R1 noise, X axis	TA3_11006_R1(TIR1)	ADVANTEST	2.5 mm/V	0-100Hz, Acq rate = 256Hz, Py = 6dB, AuxIn filt = 1000Hz
23/05/11	15.00	7	1	TA3_1105_N7R1 noise, Y axis	TA3_11006_R1(TIR1)	ADVANTEST	2.5 mm/V	0-100Hz, Acq rate = 256Hz, Py = 6dB, AuxIn filt = 1000Hz
23/05/11	15.35	8	1	TA3_1105_S1R1 sweep, Y axis	TA3_11006_R1(TIR1)	Frqswp32	2-16 Hz 2 oct/min 0.1g	0-100Hz, Acq rate = 256Hz, Py = 6dB, AuxIn filt = 1000Hz 16Hz resonance associated with oscillation of the instrumentation support frame
23/05/11	15.35	9	1	TA3_1105_S2R1 sweep, Y axis	TA3_11006_R1(TIR1)	Frqswp32	1-12 Hz 2 oct/min 0.05 g	Acq rate = 256Hz, Py = 6dB, AuxIn filt = 1000Hz
23/05/11	15.55	10	1	TA3_1105_S3R1 sweep, Y axis	TA3_11006_R1(TIR1)	Frqswp32	1-12 Hz 2 oct/min 0.05 g	Acq rate = 256Hz, Py = 6dB, AuxIn filt = 1000Hz
24/05/11								
24/05/11	11.30	11	1	TA3_1105_P1R1 Snapback test, Y axis	TA3_11006_R1(TIR1)			Acq rate = 256Hz Snap shackle failed to release.

24/05/11								
24/05/11	16.00	12	1	TA3_1105_N8R1 Noise, y axis	TA3_11006_R1(TIR1)	ADVANTEST	2.5 mm/V	0-100Hz, Acq rate = 256Hz, Py = 6dB, AuxIn filt = 1000Hz
24/05/11	16.30	13	1	TA3_1105_N9R1 Noise, y axis	TA3_11006_R1(TIR1)	ADVANTEST	1 mm/V	0-100Hz, Acq rate = 256Hz, Py = 6dB, AuxIn filt = 1000Hz
24/05/11	16.42	14	1	TA3_1105_N10R1 Noise, x axis	TA3_11006_R1(TIR1)	ADVANTEST	1 mm/V	0-100Hz, Acq rate = 256Hz, Py = 6dB, AuxIn filt = 1000Hz
24/05/11	16.55	15	1	TA3_1105_N11R1 Noise, x axis	TA3_11006_R1(TIR1)	ADVANTEST	2.5 mm/V	0-100Hz, Acq rate = 256Hz, Py = 6dB, AuxIn filt = 1000Hz
25/05/11	09.10	16	1	TA3_1105_P2R1 Snapback test, Y axis	TA3_11006_R1(TIR1)			Acq rate = 256Hz
25/05/11	09.29	17	1	TA3_1105_P3R1 Snapback test, Y axis	TA3_11006_R1(TIR1)			Acq rate = 256Hz
25/05/11	9.49	9	1	TA3_1105_S4R1 sweep, X axis	TA3_11006_R1(TIR1)	Frqswp32	1-12 Hz 2 oct/min 0.01 g	Acq rate = 256Hz, Px= 10dB, AuxIn filt = 1000Hz
25/05/11	9.49	9	1	TA3_1105_S5R1 sweep, X axis	TA3_11006_R1(TIR1)	Frqswp32	1-12 Hz 2 oct/min 0.01 g	Acq rate = 256Hz, Px= 10dB, AuxIn filt = 1000Hz
25/05/11	10.01	9	1	TA3_1105_S6R1 sweep, Y axis	TA3_11006_R1(TIR1)	Frqswp32	1-12 Hz 2 oct/min 0.01 g	Acq rate = 256Hz, Px= 10dB, AuxIn filt = 1000Hz

25/05/11	10.01	9	1	TA3_1105_S7R1 sweep, Y axis	TA3_11006_R1(TIR1)	Frqswp32	1-12 Hz 2 oct/min 0.01 g	Acq rate = 256Hz, Px= 10dB, AuxIn filt = 1000Hz
25/05/11	11.56	9	1	TA3_1105_T1R1 sweep, Y axis	TA3_11006_R1(TIR1)		5%	Acq rate = 256Hz, Px= 10dB, AuxIn filt = 1000Hz

For illustration, the accelerogram for the test No TA3_1105_T1R1 is shown in Figure 22. Graphical description of individual tests (accelerograms) has little value and digital records are available from the investigators.

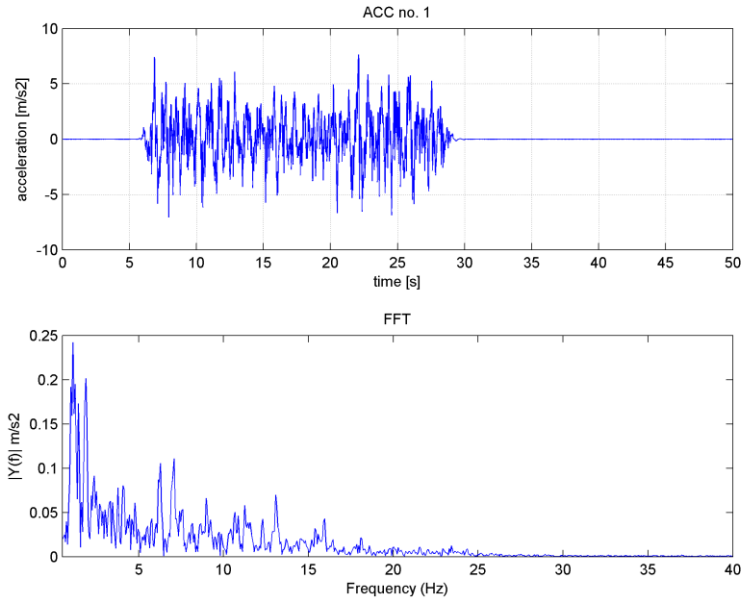

Figure 22. Accelerogram (shaking table y motion) and FFT for the test TA3_1105_T1R1.

3.2.2 Materials

The design drawings of the mockup frame are located in the Figure 23.

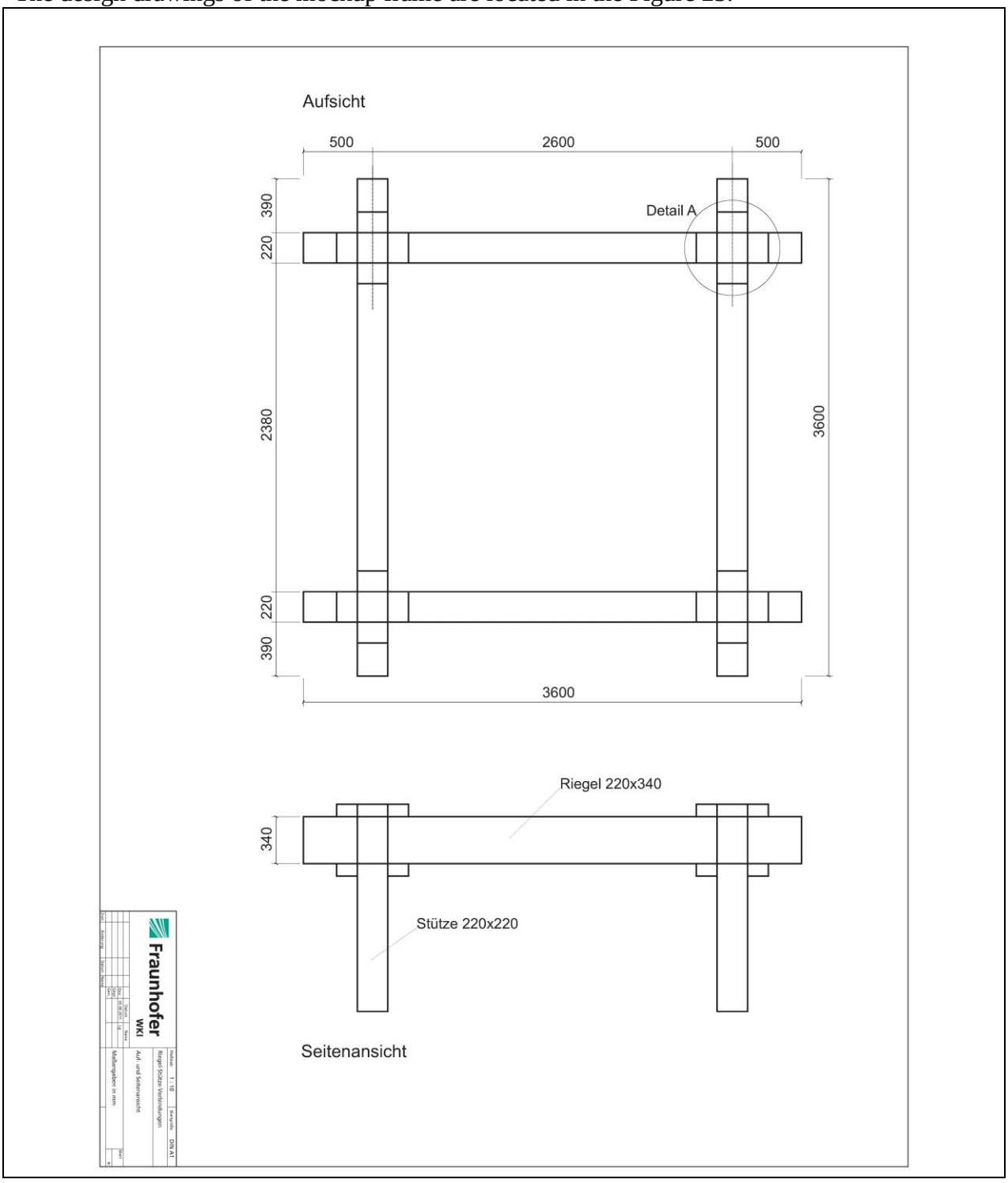

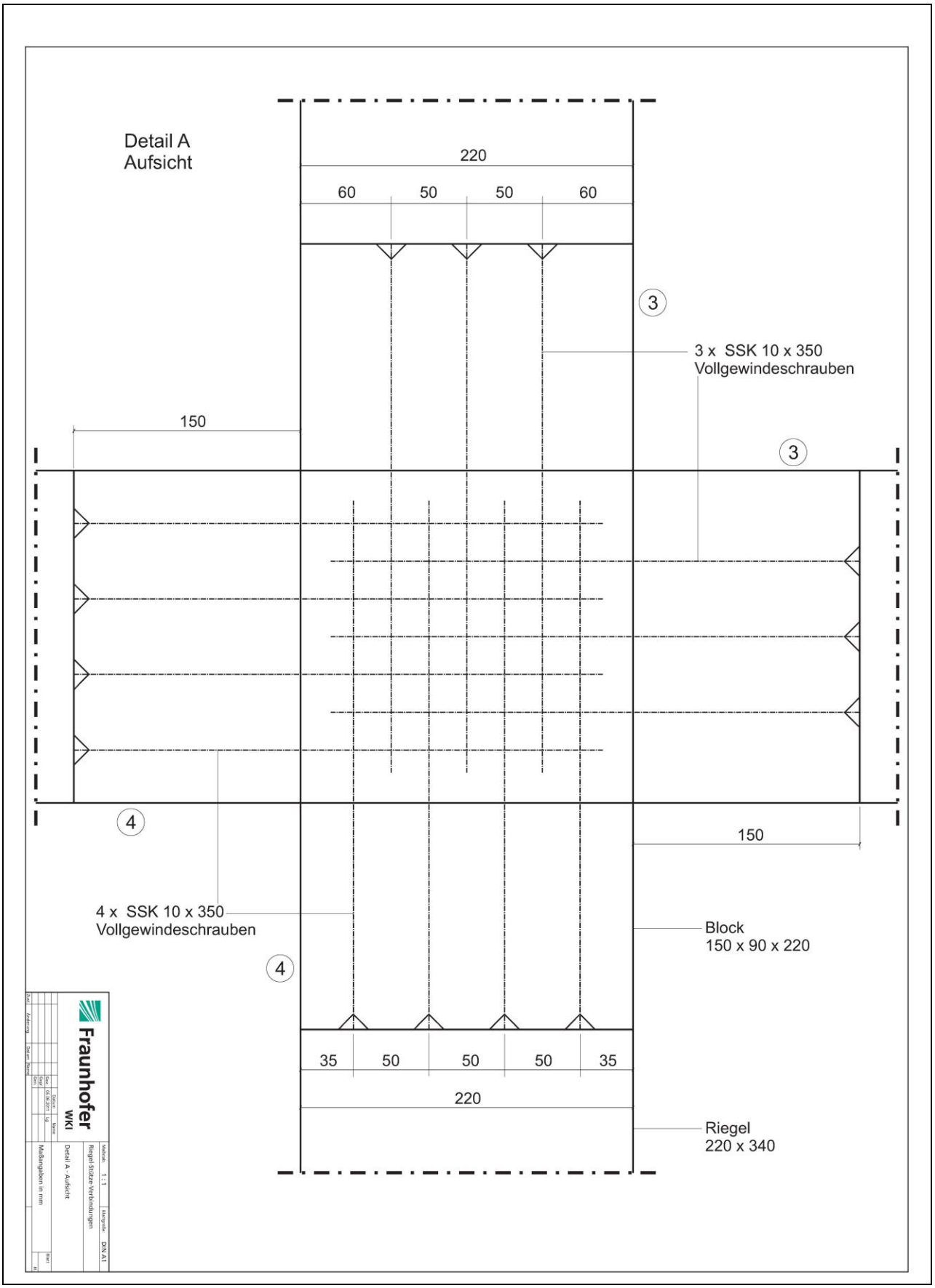
Detail A
Aufsicht
220
60
50
50
60
3
3 x SSK 10 x 350
Vollgewindeschrauben
150
3
4
150
4 x SSK 10 x 350
Vollgewindeschrauben
Block
150 x 90 x 220
4
35
50
50
50
35
220
Riegel
220 x 340
Fraunhofer
WKI
Detail A - Aufsicht
Riegel-Stütze-Verbindungen
Maßangaben in mm
1 : 1
DIN A1

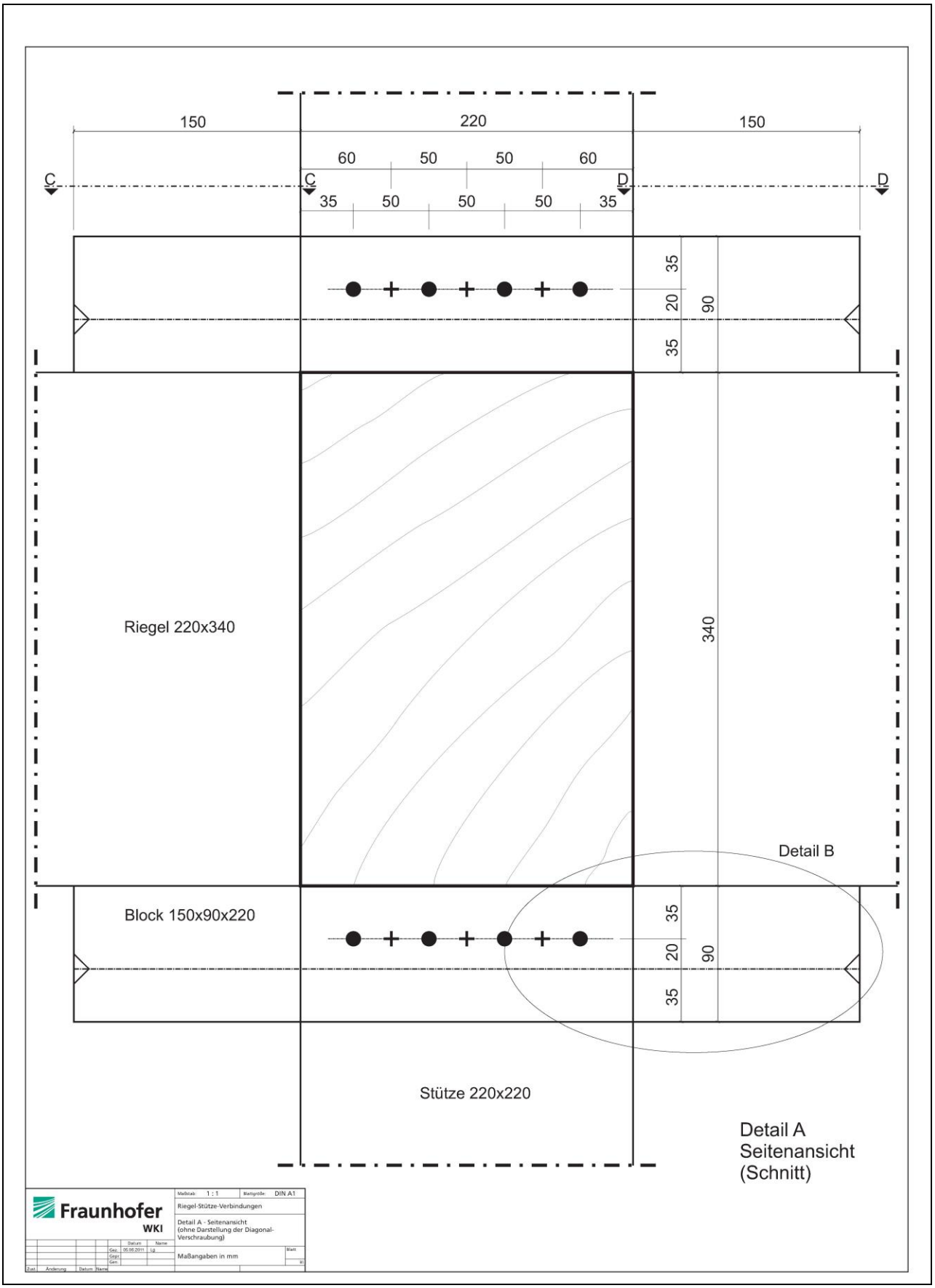
150
220
150
60
50
50
60
C
C
D
D
35
50
50
50
35
35
20
35
90
340
Riegel 220x340
Detail B
Block 150x90x220
35
20
35
90
Stütze 220x220
Detail A
Seitenansicht
(Schnitt)
Fraunhofer
WKI
Maßstab: 1 : 1
Blattgröße: DIN A1
Riegel-Stütze-Verbindungen
Detail A - Seitenansicht
(ohne Darstellung der Diagonal-
Verschraubung)
Maßangaben in mm
Blatt

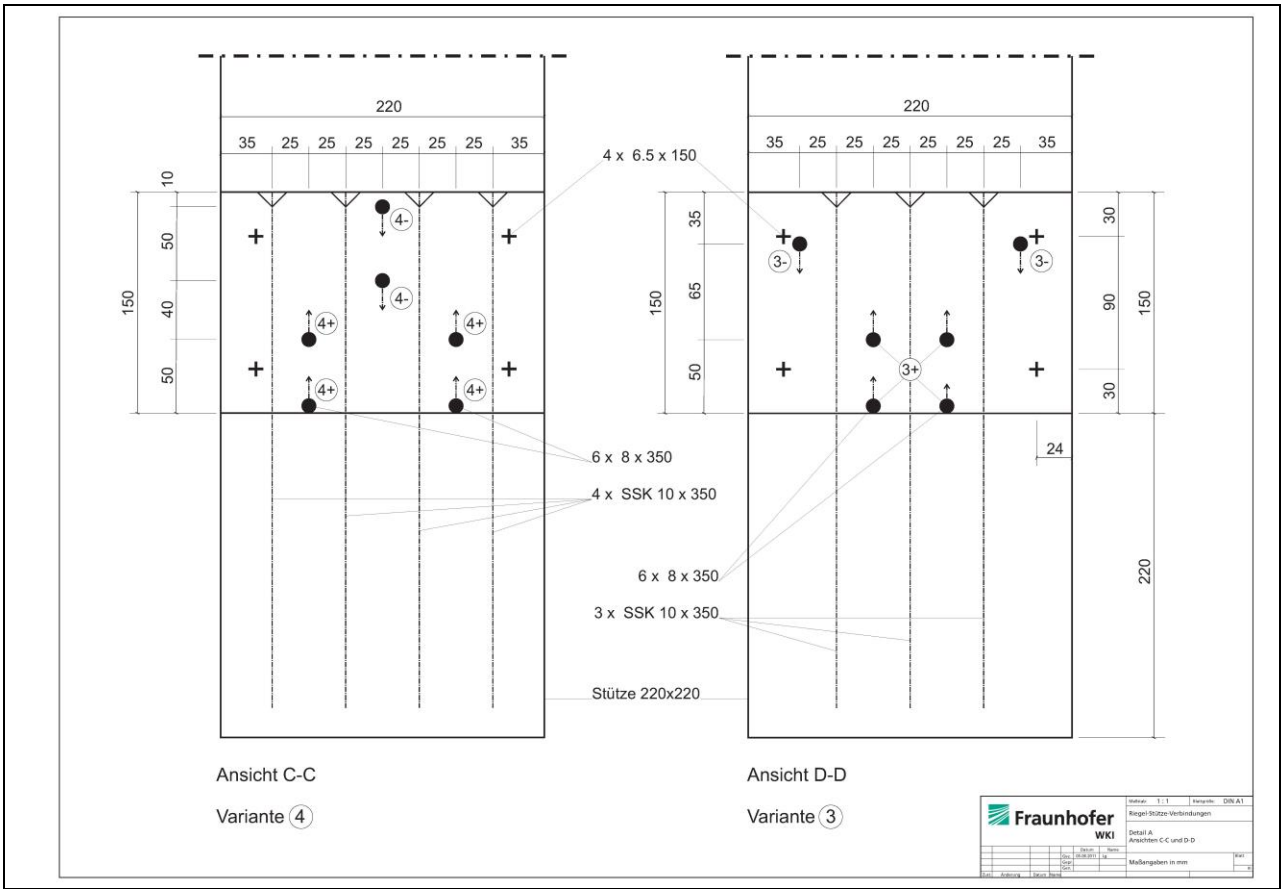
220
35 25 25 25 25 25 25 35
10
50
40
50
150
4-
4+
4 x 6.5 x 150
6 x 8 x 350
4 x SSK 10 x 350
6 x 8 x 350
3 x SSK 10 x 350
Stütze 220x220
3-
3+
35
65
50
30
90
30
24
220
Ansicht C-C
Variante 4
Ansicht D-D
Variante 3
Fraunhofer WKI
Riegel-Stütze-Verbindungen
Detail A
Ansichten C-C und D-D
Maßangaben in mm

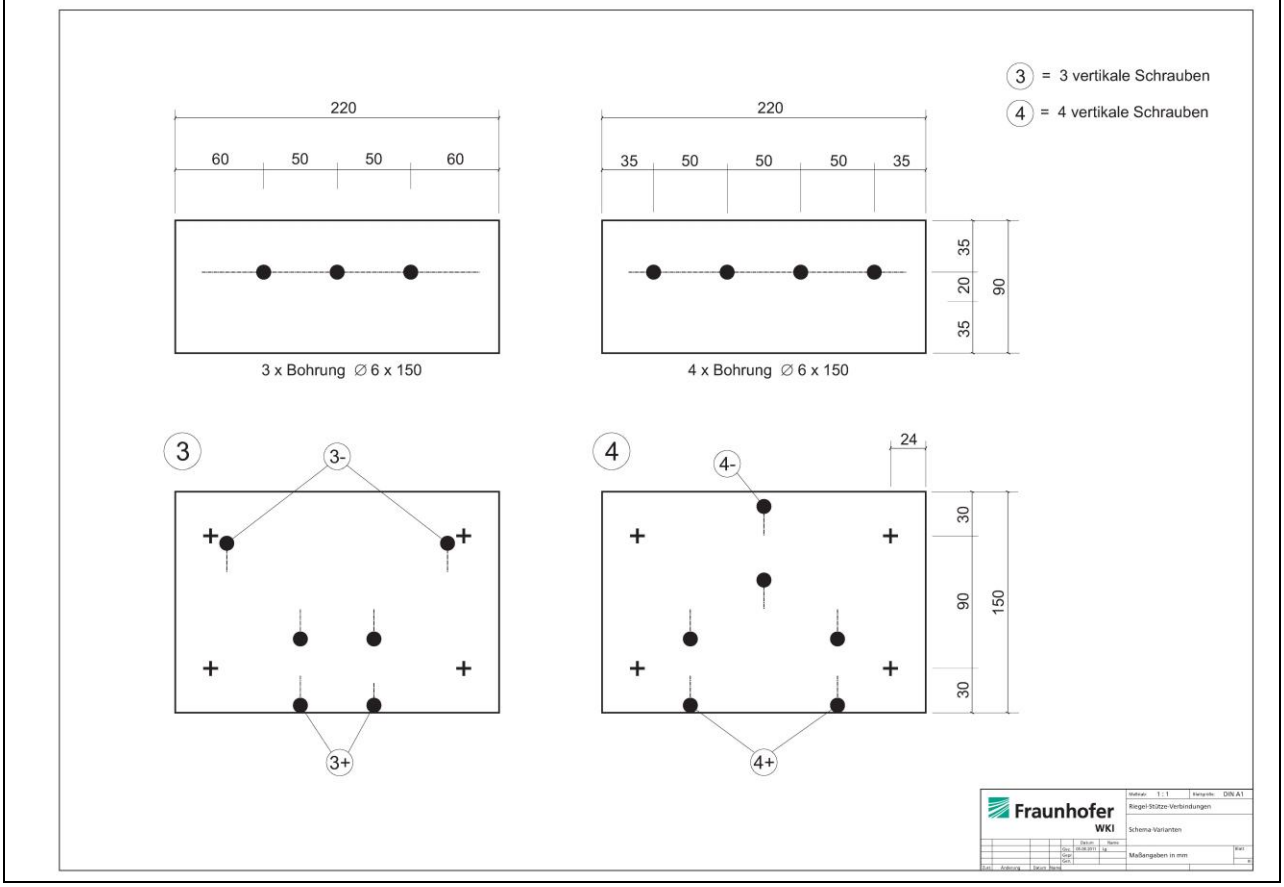
3 = 3 vertikale Schrauben
4 = 4 vertikale Schrauben
220
60 50 50 60
3 x Bohrung ∅ 6 x 150
35 50 50 50 35
4 x Bohrung ∅ 6 x 150
35
20
35
90
3
3-
3+
4
4-
4+
24
30
90
30
150
Fraunhofer WKI
Riegel-Stütze-Verbindungen
Schema-Varianten
Maßangaben in mm

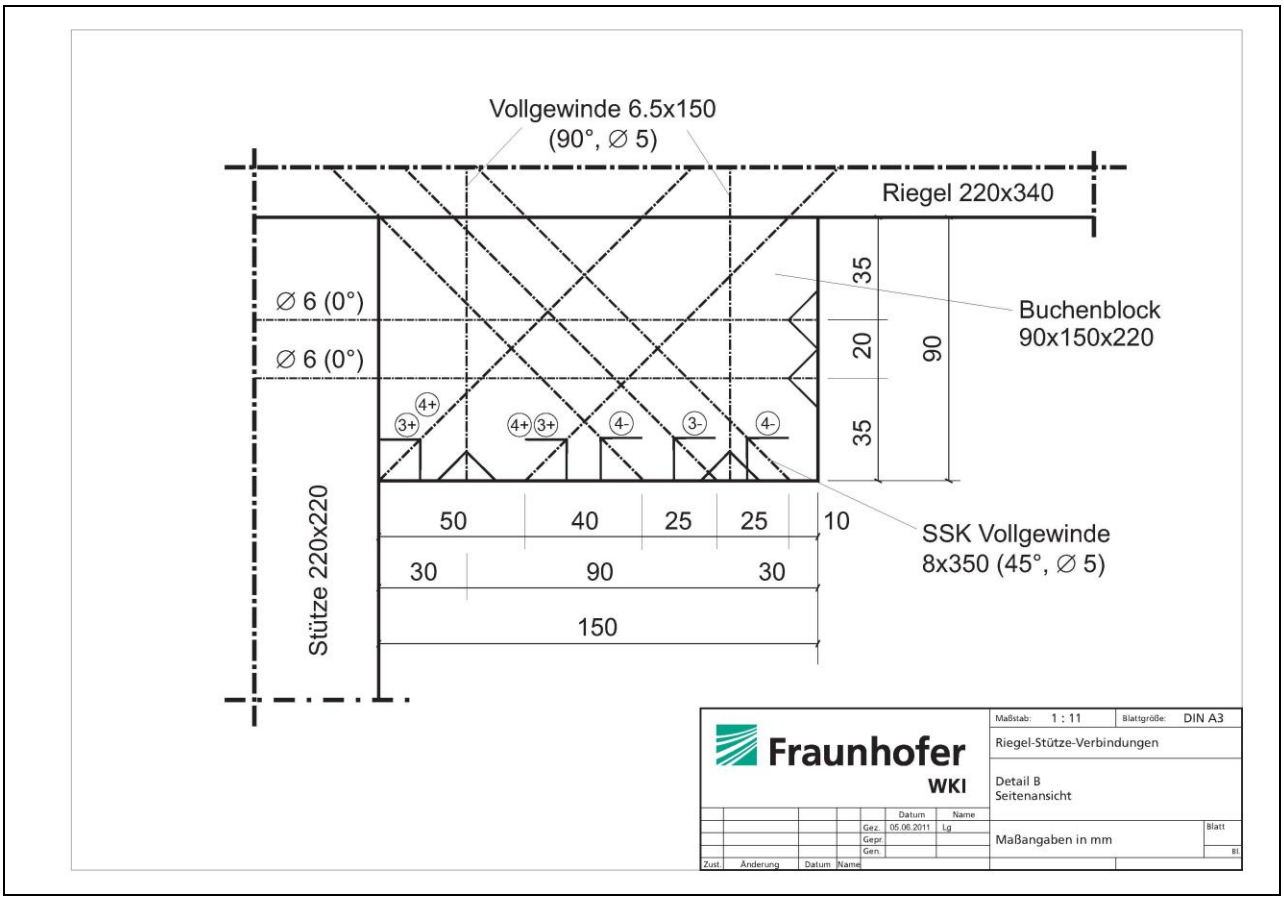

Figure 23. Design drawings of the mockup frame.

Figure 24. Details of the BTC for the single-story mockup frame

3.2.3 Results

During the experiment, accelerations of columns and beams, rotation between connections displacement of the beams and tension in the columns were measured. We are able to extract from the measured data information about the changes in the natural frequencies. This helped us to describe the degradation of the structure -weakening of the joints. Shift in the natural frequencies can be shown in first natural frequency measured by accelerometer in Y-direction located in the middle of the upper slab. After 1st seismic test frequency was 2.57 Hz, after 2nd test frequency was 2.01 Hz and after 3rd test it was 1.56 Hz.

The rotation in the connection between column and beam was measured.After 1st seismic test the rotation was almost negligible, it reaches value 0.015 degrees. In 2nd test rotation was 0.3 degrees, after the 3rd test it was 1 degree and after the signifcant cracks appeared, rotation was 4 degrees.

Also the strain on the column was important .For the strain gauge, glued in the middle of the column strain increases from 0.01 mm after the 1st test to 0.58 mm after the 2nd test and reached fnally to 0.9 mm after the 3rd test.

3.3 TEST OF THE BEAM-TO-COLUMN CONNECTION FOR THE MOCKUP FRAME

3.3.1 Test setup and test protocol

The test setup is in the Figure 25 and the test protocol is in the **Figure 26**.

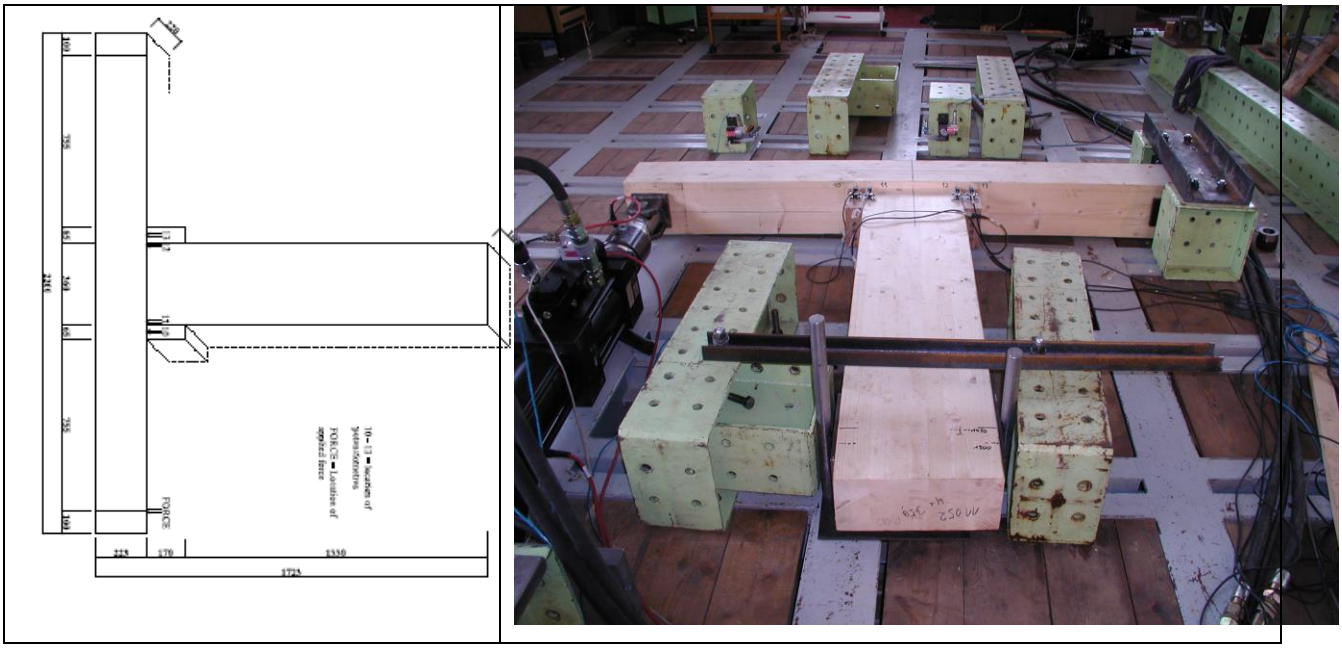

Figure 25. Schematic of the beam-to-column connection test setup. Mockup frame connection test.

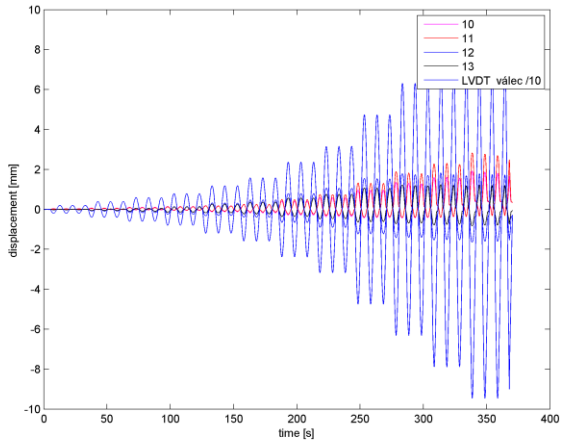

Figure 26. Test protocol for the BTC test of the mockup frame (LVDT valec=LVDT hydraulic actuator).

3.3.2 Materials

The material for the beam-to-column connection was identical to the one of the mockup frame (manufacturer HESS TIMBER GmbH & Co. KG, Germany, http://www.hess-timber.com/). The spruce (Picea) wood was used for the BTC and the joint shown in Figure 23 and Figure 24 was tested. The moisture contents of the material was not recorded. The room temperature in the laboratory during the test was about 20° C and the relative humidity of the air about 50% (none of these parameters were recorded).

Table 7. Material characteristics and test parameters for the 2-D BTC of the mockup frame.

Material property		Note
Specie/type	Spruce/glue laminated wood.	
Density	400 kg/m^3	From tables, not measured
Moisture contents	10 %	estimated
Air temperature during the test	Not recorded	
Air relative humidity during the test	Not recorded	

3.3.3 Results

The results are presented in the following charts

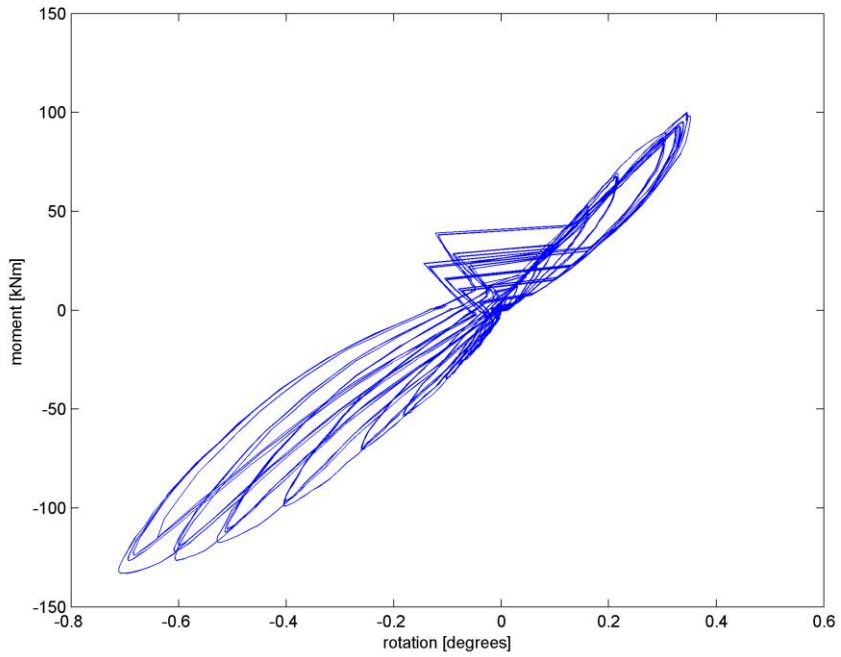

Figure 27. Moment-rotation curve for the BCF of the mockup frame.

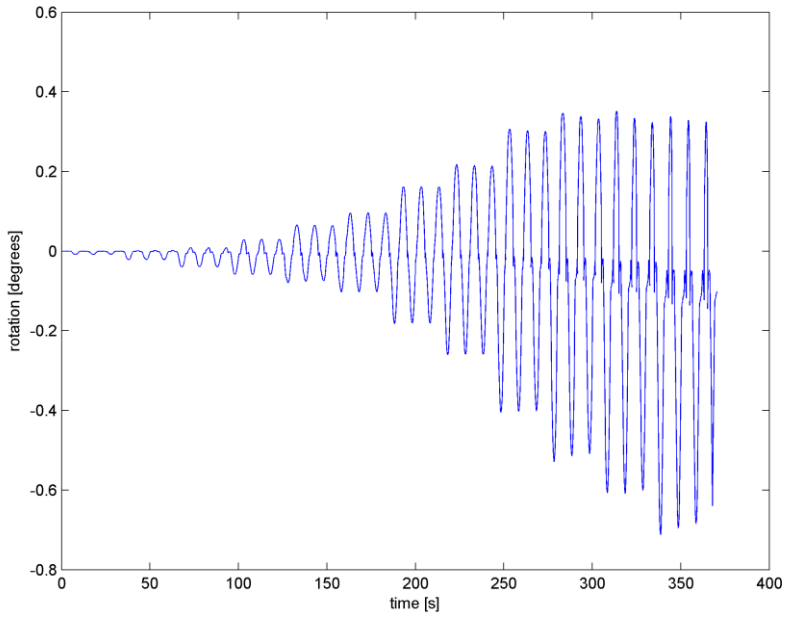

Figure 28. Time versus rotation of the BTC of the mockup frame.

3.4 FULL SCALE CYCLIC STATIC TESTS OF 3-D BEAM-TO-COLUMN CONNECTIONS

3.4.1 Test setup and test protocol

The test setup and the results of the cyclic tests are shown in **Figure 29**.

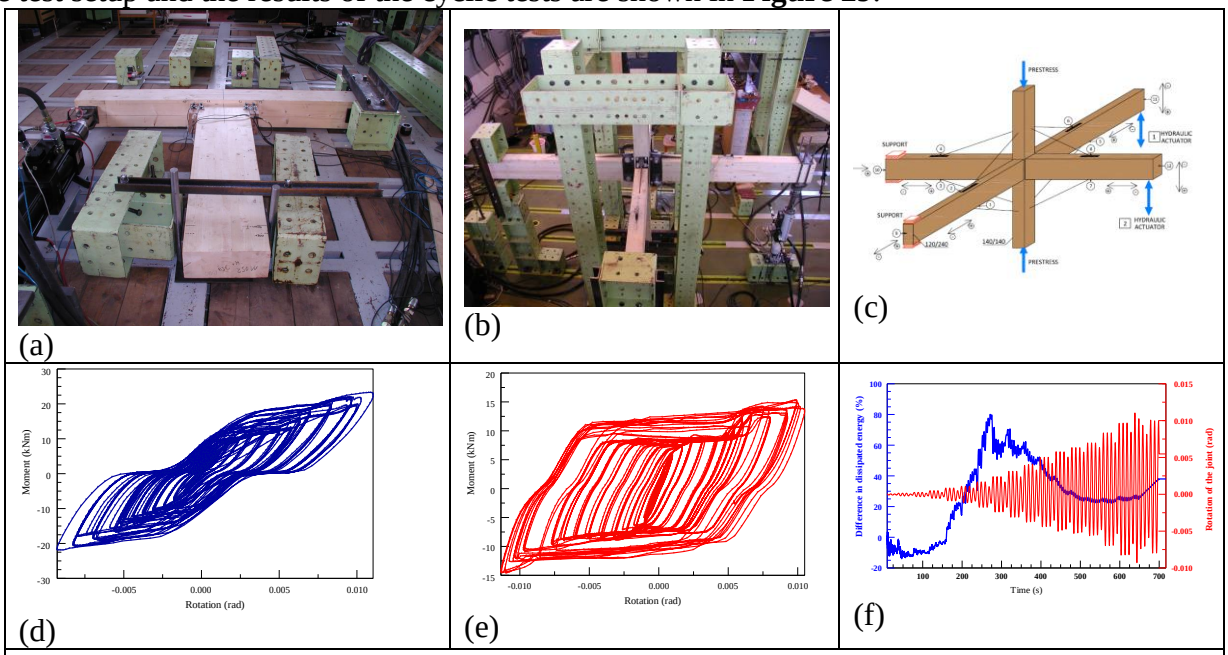

Figure 29. Beam to column connection tests. (a) 2-D (plane frame) joint using self-tapping screws, (b) 3-D spatial frame frictional joint, (c) test schematic and instrumentation, (d) moment-rotation curve for joint with no friction , (e) moment-rotation curve for frictional joint, and (f) difference in dissipated energy for joints in (d) and (e) – see Figure 30 for connection details.

3.4.2 Materials

The materials tested was again laminated spruce with approximate properties listed in the Table 7

3.4.3 Results

The results of the cyclic test are shown in **Figure 29**. **Figure 29** (d) shows the moment-rotation curve for connection with high friction and the **Figure 29** (e) shows the behavior of the frictional joint. **Figure 29** (f) shows the difference in the energy dissipation in both joints.

3.5 SHAKE TABLE TESTS OF THE SCALED THREE-STORY MOMENT FRAME

3.5.1 Test setup and test protocol

The test setup is in **Figure 30**.

(a)

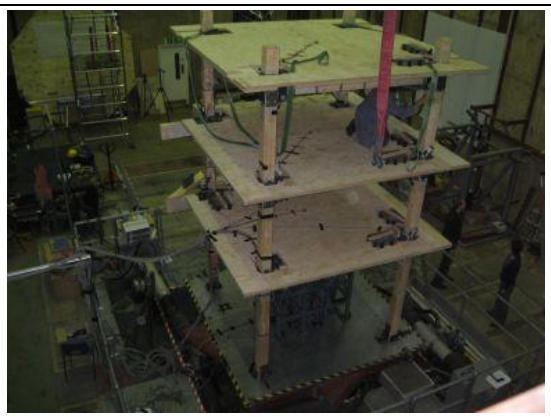

(b)

Figure 30. 3-story laminated frame with frictional connections tested under seismic loads. (a) 3-D connection with pre-stressed bolts, (b) frame on a shaking table.

3.5.2 Materials

The material of the beam-to-column connection test was identical to the material used in the mockup frame tested in Bristol.

3.5.3 Results

The results are discussed in the Appendix A

3.6 DISCUSSION OF THE RESULTS

The results showed that the initial hypothesis was not disapproved and that the frames exhibited self-correcting property. The failure of the frames occurred at relatively large excitations (the signal was artificially generated and significant energy content entailed excitation frequencies close to the natural frequencies of the frame).

4 Conclusions

From the experiments it follows that:

- Relatively rigid moment connections are possible but cannot sufficiently control the drift
- The self-correcting property of the wood-laminated frames can be achieved by balancing the stiffness and degradation parameters of the BTC and connections between the frame and the ground
- The stiffness degradation at large amplitudes prevents the frame to vibrate at resonant frequencies
- The relatively large drifts result in relatively small rotation in BTC
- The strains in the wood members did not exceed theoretical ultimate strains and the beams and columns remained in the elastic range

References

[1]Kikuchi, S. Earthquake resistance of multi-storey timber frame structures. Proceedings from Pacific Timber Engineering Conference, Gold Coast, Australia, Vol. 1, 205-214, 1994.
[2]Buchanan, A.H. & Fairweather R.H. 1993. Seismic design of glulam structures, Bulletin of the New Zealand National Society for Earthquake Engineering, Vol 26(4), pp. 415-436.
[3]Kasal, B., Pospíšil, S., Jirovsky, I., Drdacky, M., Heiduschke, A., and Haller, P. Seismic performance of laminated timber frames with fiber reinforced connections. Earthquake Engineering and Structural Dynamics. John Wiley & Sons Ltd. London, K, Vol. 33. (5): 633-646, 2004.
[4]Yasumura, M. Structural behavior of timber joints under earthquake loading. COST C1. Control of the semi-rigid behaviour of civil engineering structural connections. Proceedings of the International Conference, Liege, Belgium, Ed. Maquoi R., pp. 337-346, 1998.
[5]Palermo, A.; Pampanin, S.; Buchanan, A.; Fraggiacomo, M.; Deam, M, B. Code provisions for seismic design of multi-storey post-tensioned timber buildings. Proc. of CIB, Florence, Italy, CIB-W18/39-15-6, 2006.
[6]Priestley MJN. Seismic design philosophy for precast concrete frames. SEI 1996 6(1):25-31
[7]Pinto, A. Achievements of the COST C1 seismic group. COST C1. Control of the semi-rigid behaviour of civil engineering structural connections. Proceedings of the International Conference, Liege, Belgium, Ed. Maquoi R., pp. 349-358, 1998.

APPENDIX A

Report on the evolution of natural frequencies of the three story frame during the "SERIES" shaking table tests

Piotr Bobra, Andrzej Marynowicz, Zbigniew Zembaty

In table 1 the sequence of tests of wooden frame is presented. The aim of this report is to analyze changes in natural frequencies between intact model and various damage levels. For this purpose white noise low level excitations carried out before the first and after each damaging seismic tests were used. These tests are highlighted in respective rows of table 1.

To calculate transfer function the following equation was applied:

$$|H_{uv}(f)| = \left|\frac{G_{uv}(f)}{G_{uu}(f)}\right|,$$

where:

$H_{uv}(f)$ – transfer function estimate between input signal *u* and output *v*,
$G_{uu}(f)$ – power spectral density (PSD),
$G_{uv}(f)$ – cross power spectral density (CPSD).

To compute the respective transfer function estimate MATLAB procedure "*tfestimate(u,v,…)*" was used, where windowing parameter (number of sample used – section - for *u* and *v*) set as 2048, which covers time window of about 8 sec.

To analyze changes in natural frequencies, every accelerometer connected to the beams was chosen for output readouts (ch31-ch42). As the input channels ch19 (on X direction) and ch20 (on Y direction) were selected. Sensors applied in the middle of each deck were ignored, because they wouldn't show the torsional mode of vibrations on the graphs. Figure 1 presents the model of frame with accelerometers used in our calculations. In the figures 2-7 transfer function estimates for channel 40 (set on X direction) are plotted, which is also collected in table 2. Additionally the readout from Y direction (ch41) is presented to show differences in the third NF for the intact model.
The calculated transfer function estimates, for all analyzed channels (see fig. 1) are summarized in Appendix (table A1.) together with corresponding plots.

Table 1. Sequence of the shaking table experiments.

No.	Excitation type	TIR file Ref. (TA3_1110_)	Excitation level PGA/RMS/amplitude	Direction of excitation
1	Impact test	-	-	X
2		-	-	Y
3	Static load test	L1R1	No dead load	-
4		L2R1	150 kg on 1st floor (column 1)	-
5	Snapback-pullover test	P1R1	2300 N	Y
6	White noise	N1R1	~0.1g (RMS)	X
7		N2R1	~0.1g (RMS)	Y
8	White noise	**N3R1**	~0.1g (RMS)	X+Y

9	Sweep sine	S1R1	~0.1g (amplitude)	X
10		S2R1	~0.03g (amplitude)	X
11		S3R1	~0.03g (amplitude)	Y
12	First seismic test	T1R1	~0.1g / 0.02g* (PGA)	X+Y+Z
13	White noise	**N4R1**	~0.1g (RMS)	X+Y
14	Second seismic test	T2R1	~0.3g / 0.06g* (PGA)	X+Y+Z
15	White noise	**N5R1**	~0.1g (RMS)	X+Y
16	Third seismic test	T3R1	~0.5g / 0.1g* (PGA)	X+Y+Z
17	White noise	**N6R1**	~0.1g (RMS)	X+Y
18	Fourth seismic test	T4R1	~1.0g / 0.2g* (PGA)	X+Y+Z
19	White noise	**N7R1**	~0.1g (RMS)	X+Y
20	Fifth seismic test	T5R1	~2.0g (PGA)	X+Y
* vertical excitation (Z)				

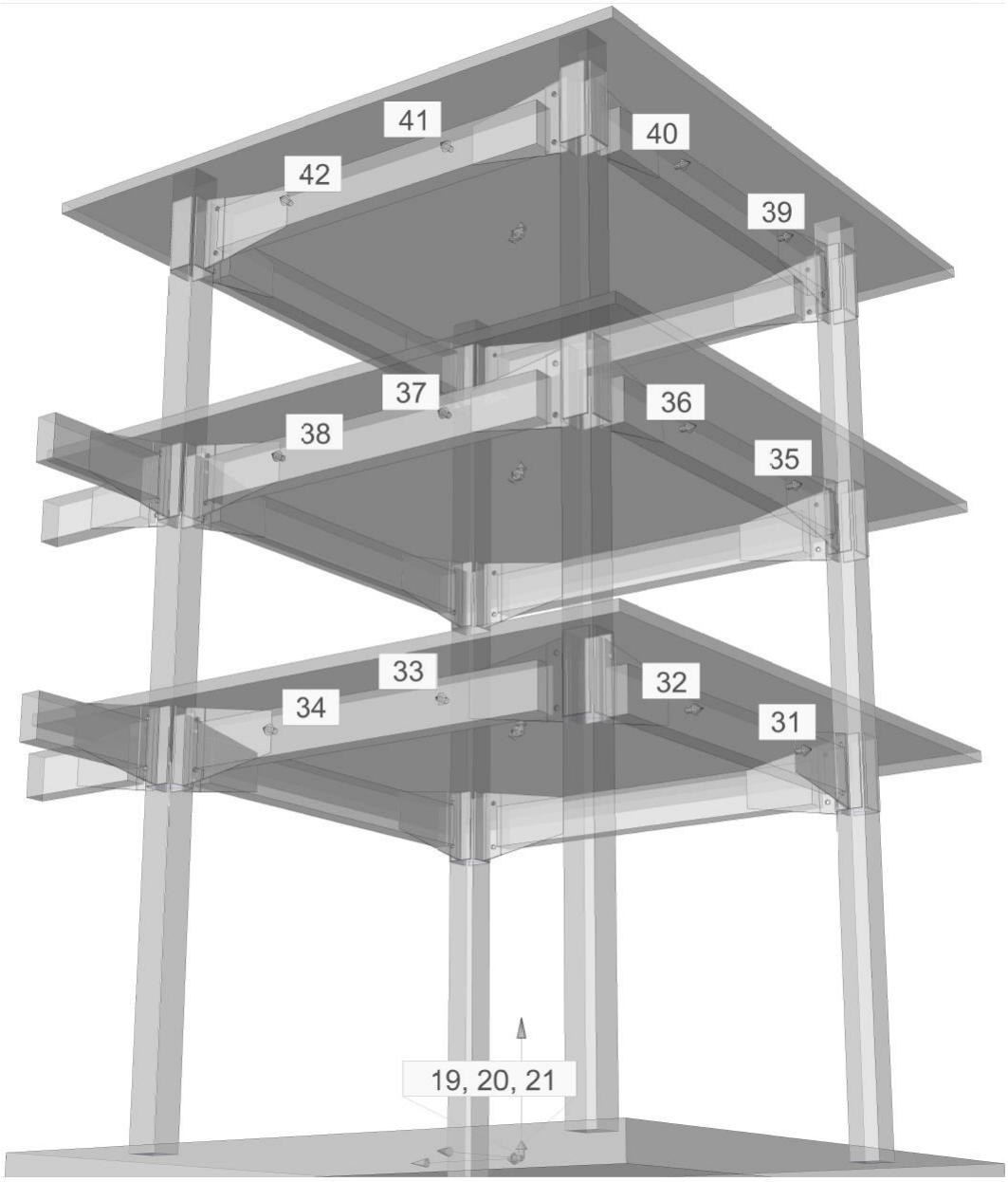

Fig. 1 Model of three story frame with selected accelerometers (ch*xx*) position marked.

Table 2. Evaluation of natural frequencies for input sensor ch19 and output ch40 located on 3rd floor.

Channel no.	TIR file Ref. (TA3_1110_)	1st natural frequency [Hz]	2nd natural frequency [Hz]	3rd natural frequency [Hz]
ch40X-ch19X	N3R1	4.25	5.63	16.38
	N4R1	2.00	2.75	8.13
	N5R1	2.00	2.75	8.00
	N6R1	2.00	2.75	8.00
	N7R1	1.63	2.50	7.38

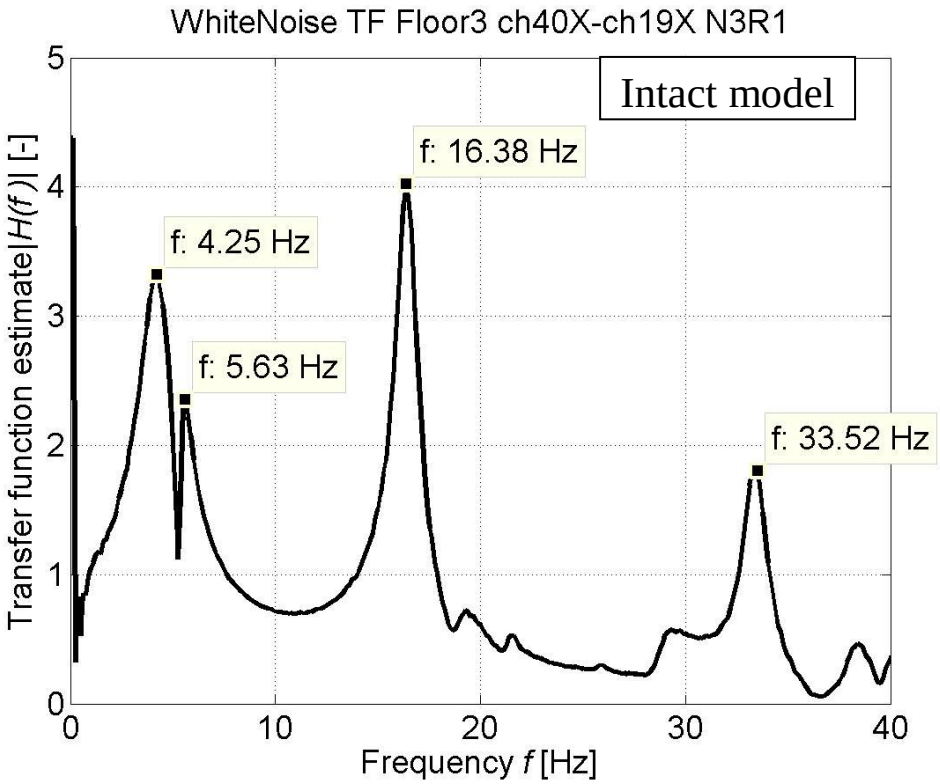

Fig. 2 Transfer function estimate given by input sensor ch19 and output ch40 located on 3rd floor for INTACT model.

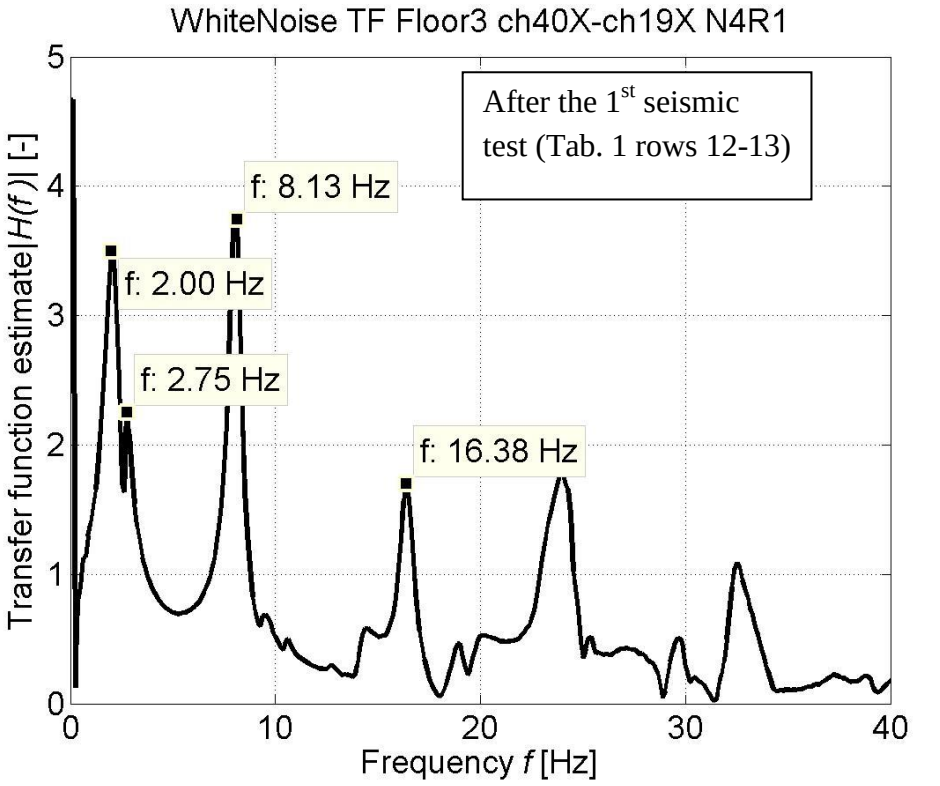

Fig. 3 Transfer function estimate given by input sensor ch19 and output ch40 located on 3rd floor after first seismic test.

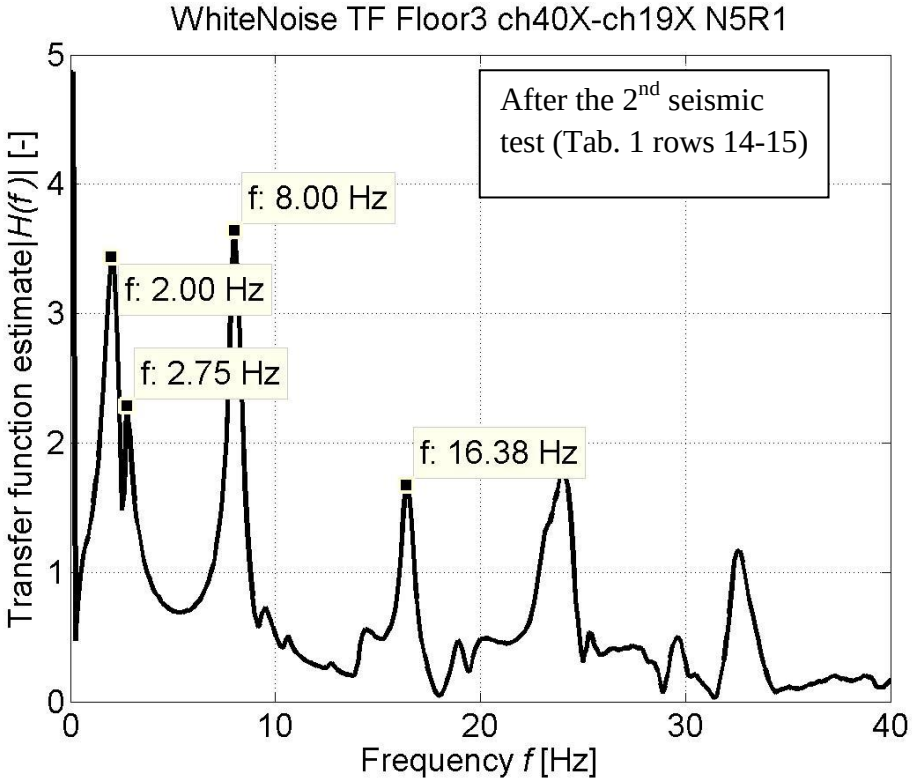

Fig. 4 Transfer function estimate given by input sensor ch19 and output ch40 located on 3rd floor after second seismic test.

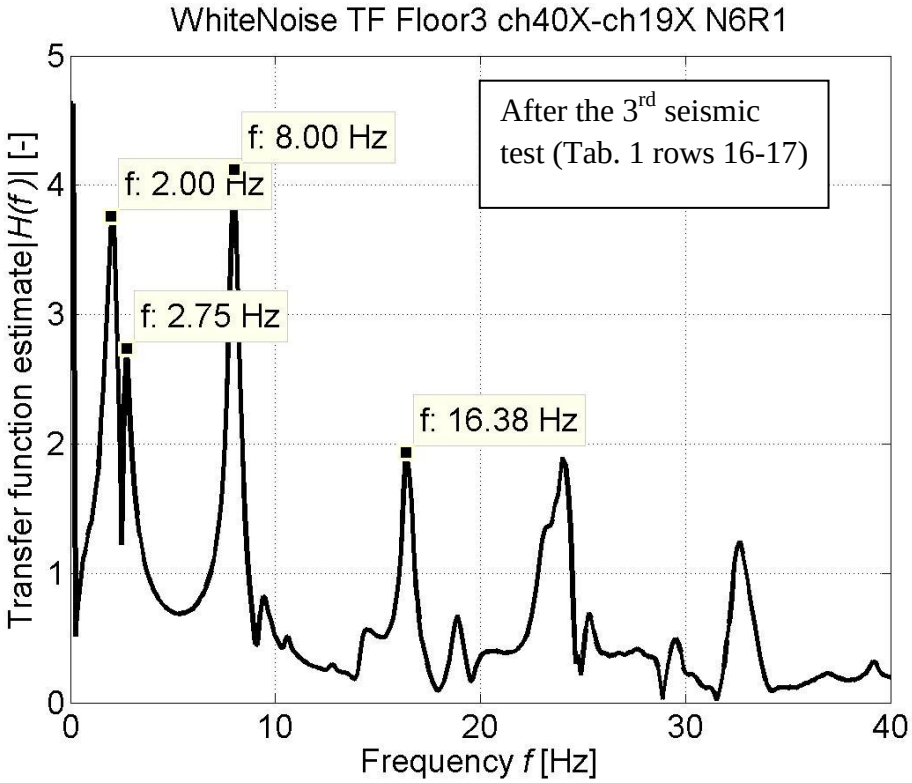

Fig. 5 Transfer function estimate given by input sensor ch19 and output ch40 located on 3rd floor after third seismic test.

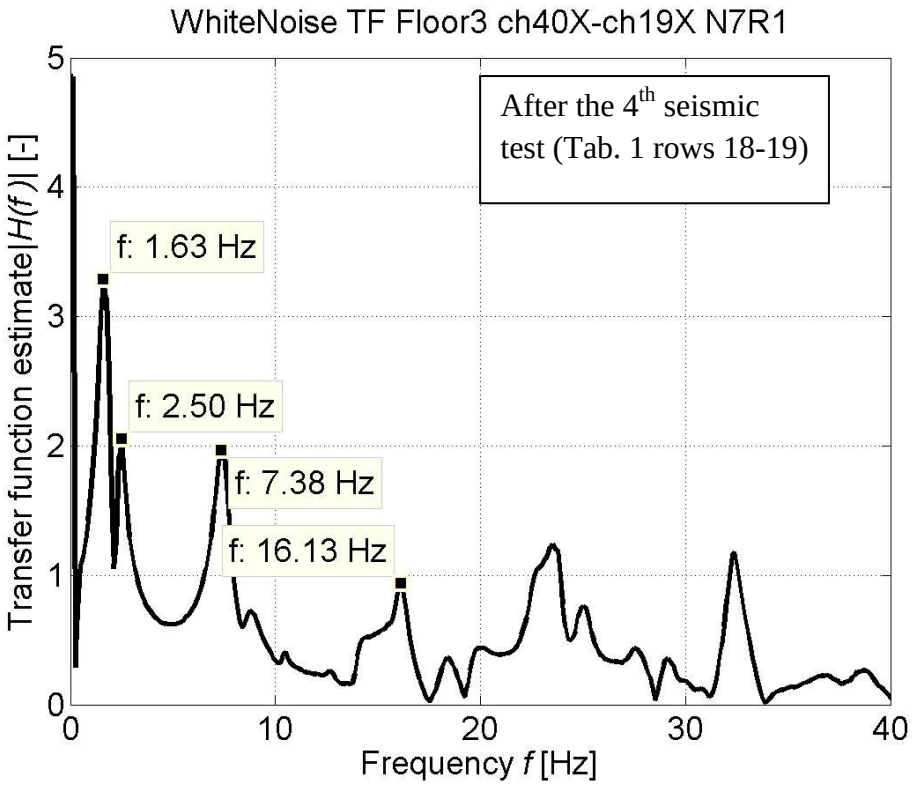

Fig. 6 Transfer function estimate given by input sensor ch19 and output ch40 located on 3rd floor after fourth seismic test.

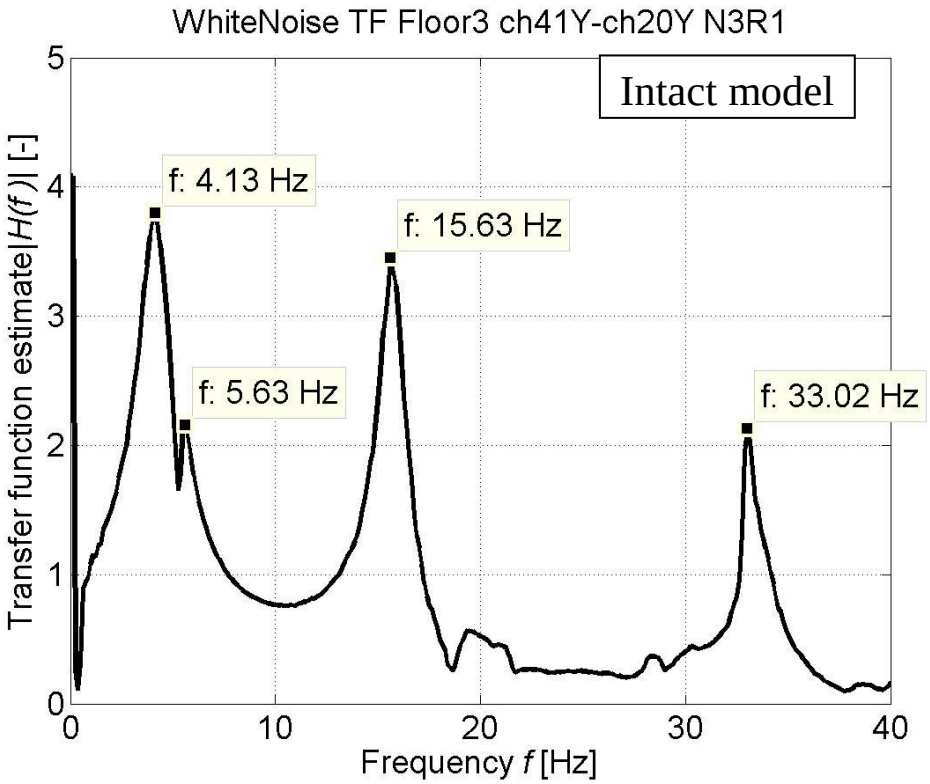

Fig. 7 Transfer function estimate given by input sensor ch20 and output ch41 located on 3rd floor for INTACT model.

APPENDIX B

Comment about the plots of transfer function estimates.

The title of each plot clearly describes from which accelerometer the signals were taken. Also the excitation types are described.

For example: "*White Noise TF Floor1 ch31X-ch19X N3R1*"

ch19X – input, channel 19 located on the shacking table (X direction)

Floor1 ch31X – output, channel 31 located on 1st floor (X direction)

N3R1 – the last four symbols of the test title (see LOG file "*TA3_1110_R2(LOG).doc*" from "*SERIES_TA3_1110*" folder)

Table B1. Display of the first, second & the third natural frequencies.

Channel no.	TIR file Ref. (TA3_1110_)	1st natural frequency [Hz]	2nd natural frequency [Hz]	3rd natural frequency [Hz]
FLOOR 1				
ch31X-ch19X	N3R1	4.13	-	16.38
	N4R1	2.00	-	8.13
	N5R1	2.00	-	8.00
	N6R1	2.00	-	8.00
	N7R1	1.63	-	7.50
ch32X-ch19X	N3R1	4.13	5.50	16.38
	N4R1	2.00	2.75	8.13
	N5R1	2.00	2.75	8.00
	N6R1	2.00	2.63	8.00
	N7R1	1.63	2.38	7.38
ch33Y-ch20Y	N3R1	4.00	5.50	15.63
	N4R1	2.00	-	7.63
	N5R1	2.00	-	7.75
	N6R1	2.00	2.63	7.75
	N7R1	1.75	-	7.13
ch34Y-ch20Y	N3R1	4.13	5.25	15.63
	N4R1	2.00	-	7.63
	N5R1	2.00	-	7.75
	N6R1	2.00	-	7.75
	N7R1	1.75	-	7.25
FLOOR 2				
ch35X-ch19X	N3R1	4.25	-	16.63
	N4R1	2.13	-	8.13
	N5R1	2.13	-	8.13
	N6R1	2.13	-	8.00
	N7R1	1.63	-	7.63
ch36X-ch19X	N3R1	4.13	5.50	16.63
	N4R1	2.00	2.75	8.13
	N5R1	2.00	2.75	8.13
	N6R1	2.00	2.75	8.00
	N7R1	1.63	2.50	7.50
ch37Y-ch20Y	N3R1	4.13	5.50	15.88
	N4R1	2.00	2.75	7.75
	N5R1	2.00	2.75	7.75

	N6R1	2.00	-	7.75
	N7R1	1.75	-	7.25
ch38Y-ch20Y	N3R1	4.13	5.25	15.88
	N4R1	2.00	-	7.75
	N5R1	2.00	-	7.75
	N6R1	2.13	-	7.75
	N7R1	1.88	-	7.25
FLOOR 3				
ch39X-ch19X	N3R1	4.25	-	16.38
	N4R1	2.13	-	8.13
	N5R1	2.13	-	8.00
	N6R1	2.13	-	8.00
	N7R1	1.75	-	7.38
ch40X-ch19X	N3R1	4.25	5.63	16.38
	N4R1	2.00	2.75	8.00
	N5R1	2.00	2.75	8.00
	N6R1	2.00	2.75	8.00
	N7R1	1.63	2.50	7.38
ch41Y-ch20Y	N3R1	4.13	5.63	15.63
	N4R1	2.00	2.75	7.63
	N5R1	2.00	2.75	7.75
	N6R1	2.00	2.75	7.75
	N7R1	1.75	-	7.13
ch42Y-ch20Y	N3R1	4.25	5.25	15.63
	N4R1	2.00	-	7.63
	N5R1	2.13	-	7.75
	N6R1	2.13	-	7.75
	N7R1	1.88	-	7.25

F L O O R 1
Channels 31-34

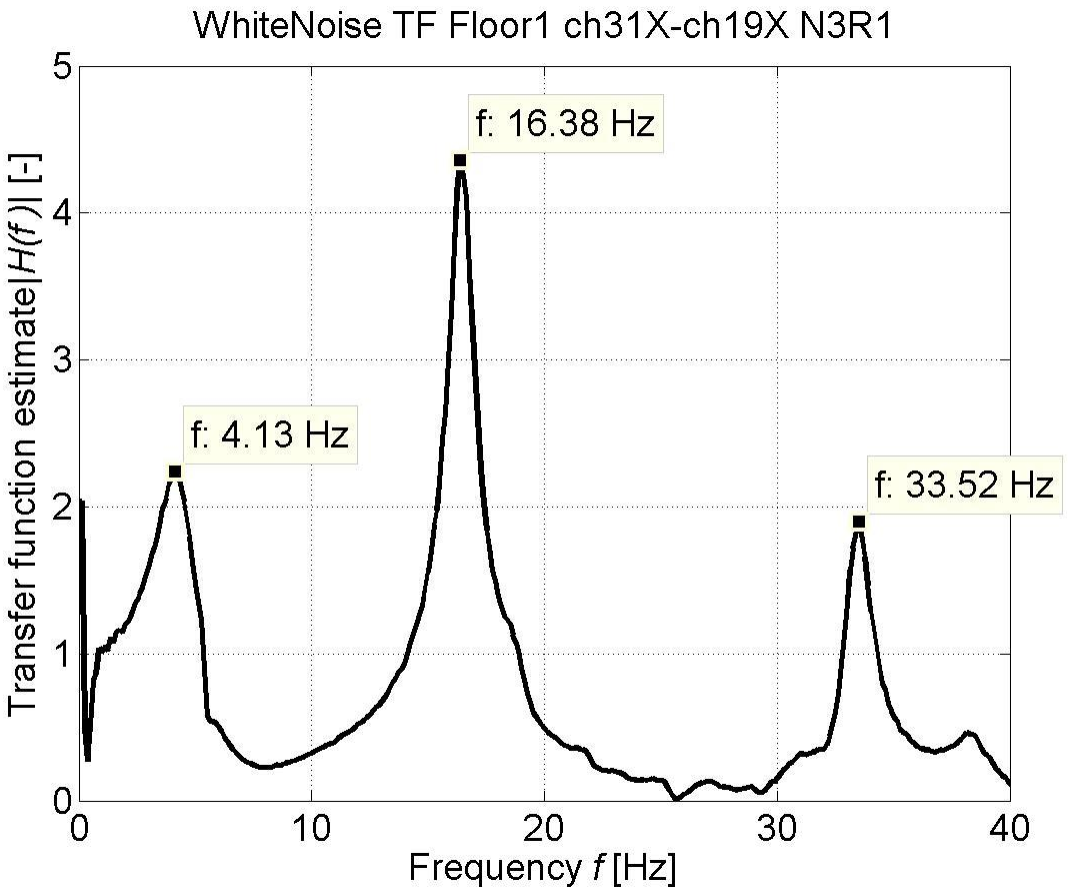
WhiteNoise TF Floor1 ch31X-ch19X N3R1
f: 16.38 Hz
f: 4.13 Hz
f: 33.52 Hz
Transfer function estimate|H(f)| [-]
Frequency f [Hz]
0
1
2
3
4
5
0
10
20
30
40

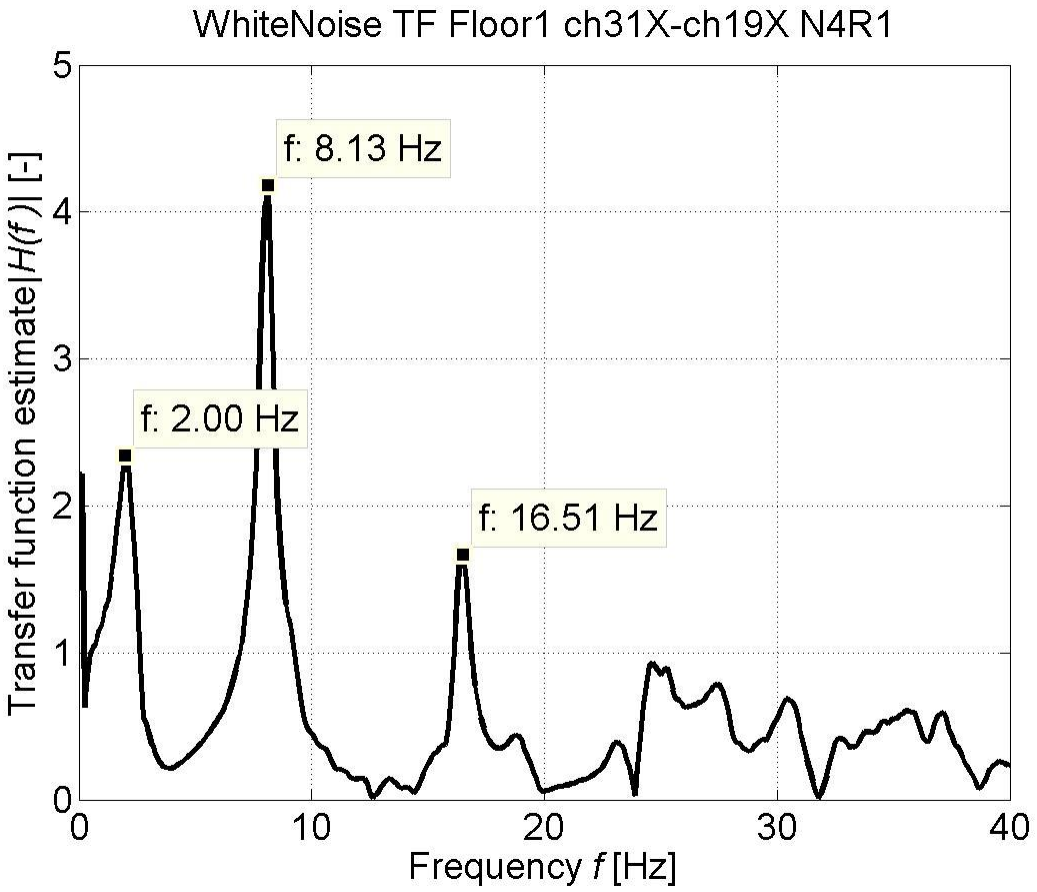
WhiteNoise TF Floor1 ch31X-ch19X N4R1
f: 8.13 Hz
f: 2.00 Hz
f: 16.51 Hz
Transfer function estimate|H(f)| [-]
Frequency f [Hz]
0
1
2
3
4
5
0
10
20
30
40

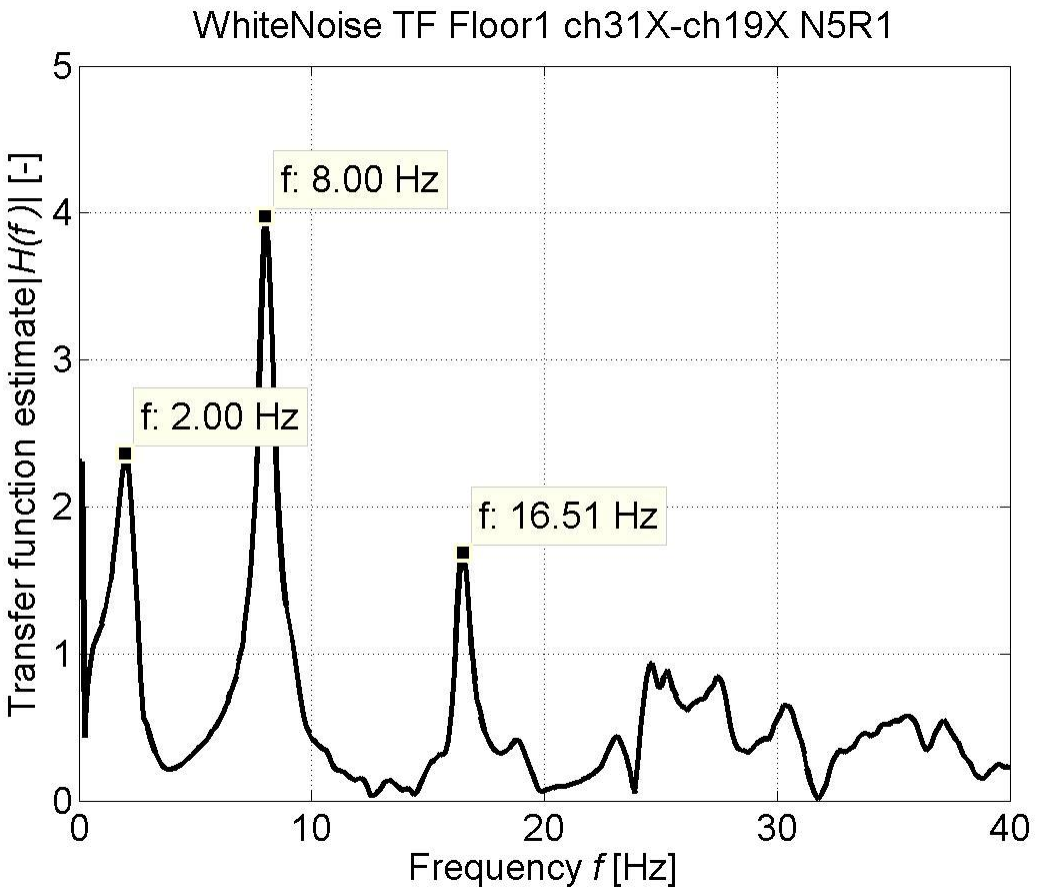
WhiteNoise TF Floor1 ch31X-ch19X N5R1
f: 8.00 Hz
f: 2.00 Hz
f: 16.51 Hz
Transfer function estimate|H(f)| [-]
Frequency f [Hz]
0
1
2
3
4
5
0
10
20
30
40

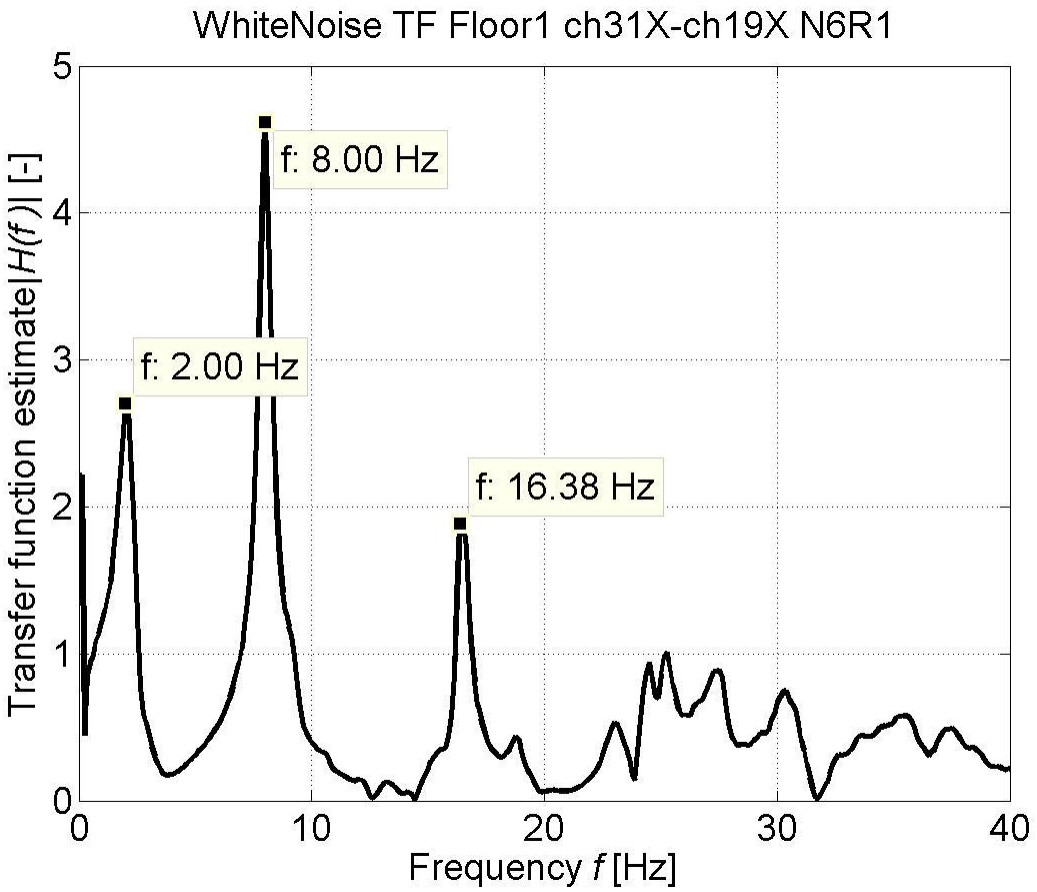
WhiteNoise TF Floor1 ch31X-ch19X N6R1
f: 8.00 Hz
f: 2.00 Hz
f: 16.38 Hz
Transfer function estimate|H(f)| [-]
Frequency f [Hz]
0
1
2
3
4
5
0
10
20
30
40

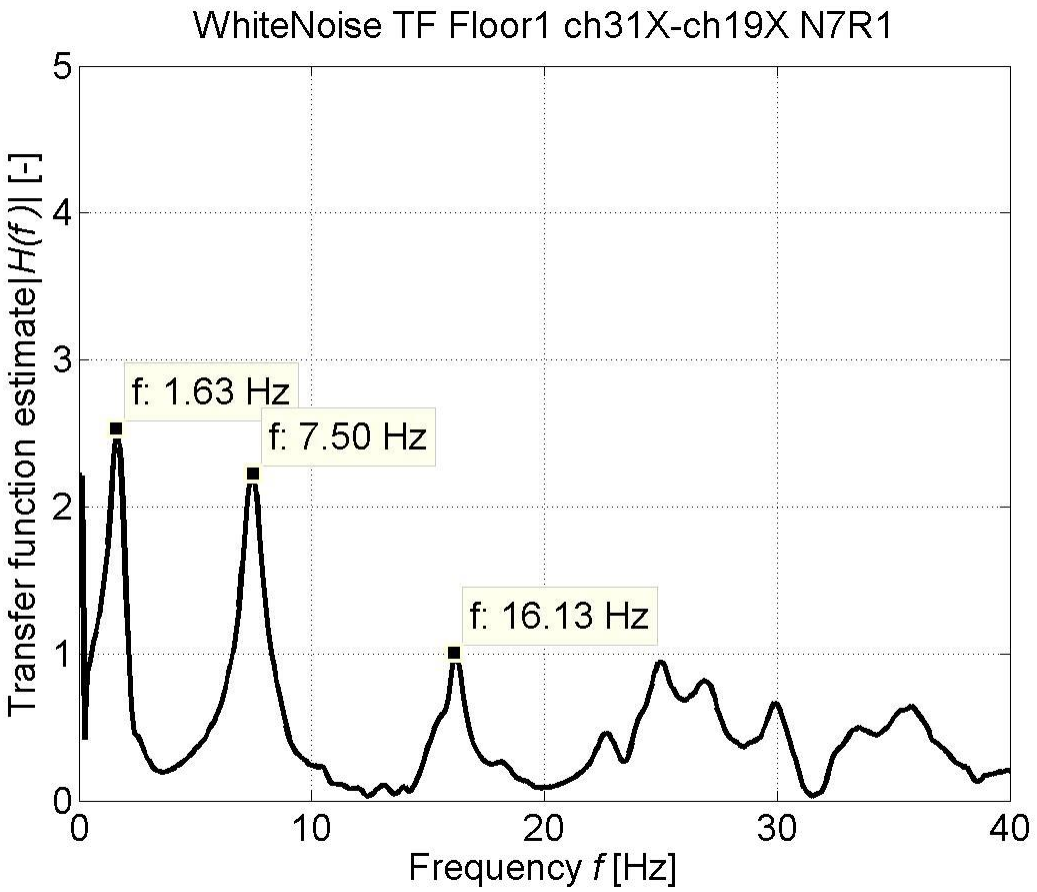
WhiteNoise TF Floor1 ch31X-ch19X N7R1
Transfer function estimate|H(f)| [-]
Frequency f [Hz]
f: 1.63 Hz
f: 7.50 Hz
f: 16.13 Hz
0
1
2
3
4
5
0
10
20
30
40

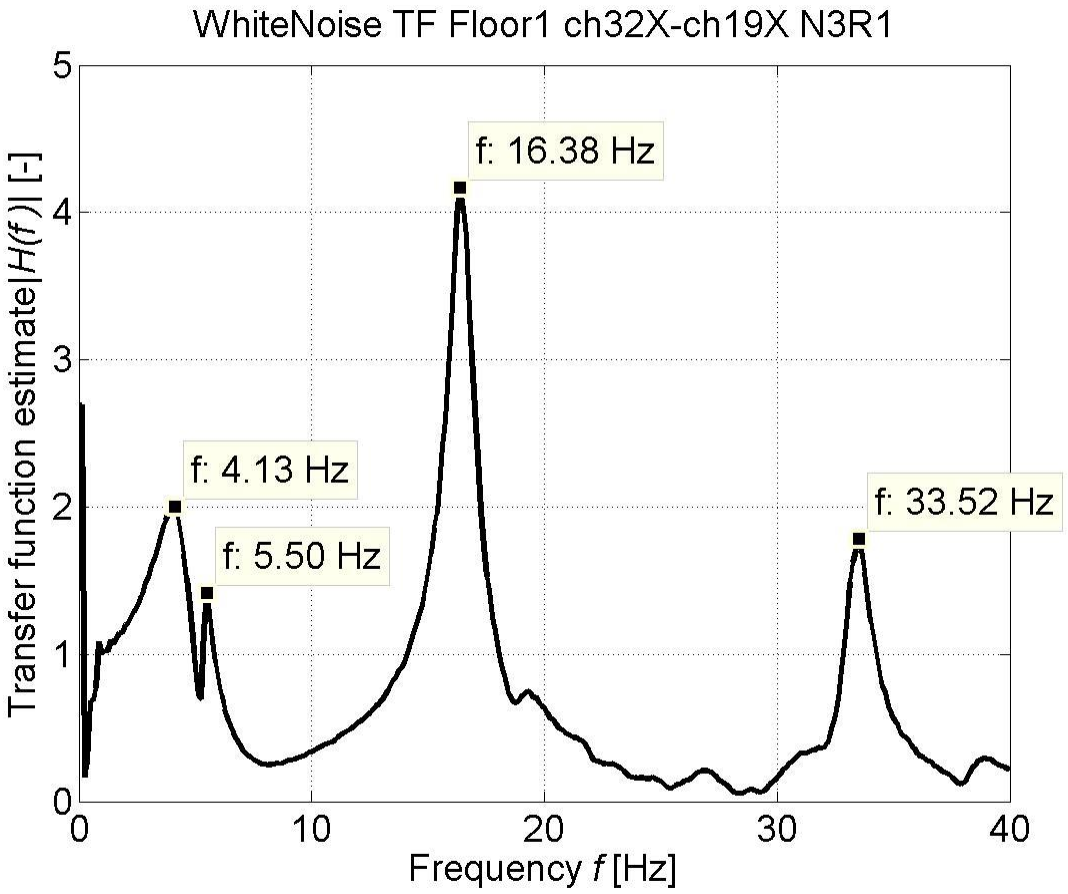
WhiteNoise TF Floor1 ch32X-ch19X N3R1
f: 16.38 Hz
f: 4.13 Hz
f: 5.50 Hz
f: 33.52 Hz
Transfer function estimate |H(f)| [-]
Frequency f [Hz]
0
1
2
3
4
5
0
10
20
30
40

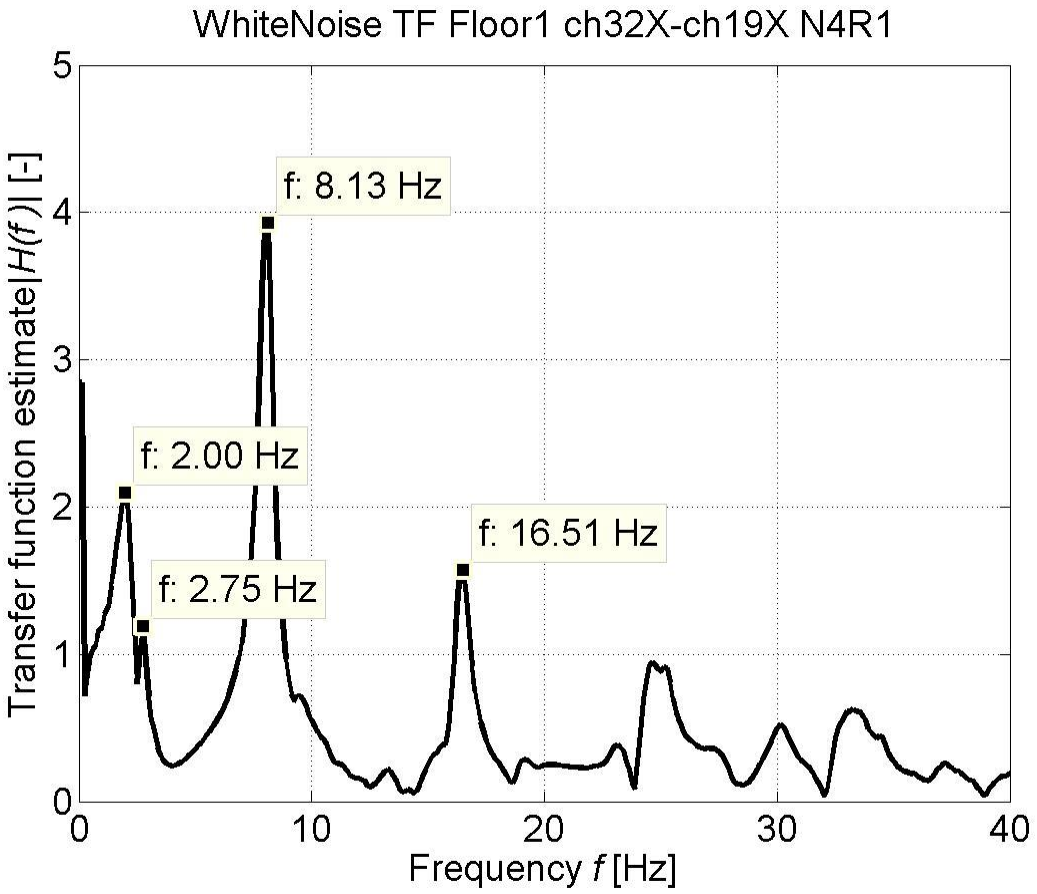
WhiteNoise TF Floor1 ch32X-ch19X N4R1
f: 8.13 Hz
f: 2.00 Hz
f: 2.75 Hz
f: 16.51 Hz
Transfer function estimate |H(f)| [-]
Frequency f [Hz]
0
1
2
3
4
5
0
10
20
30
40

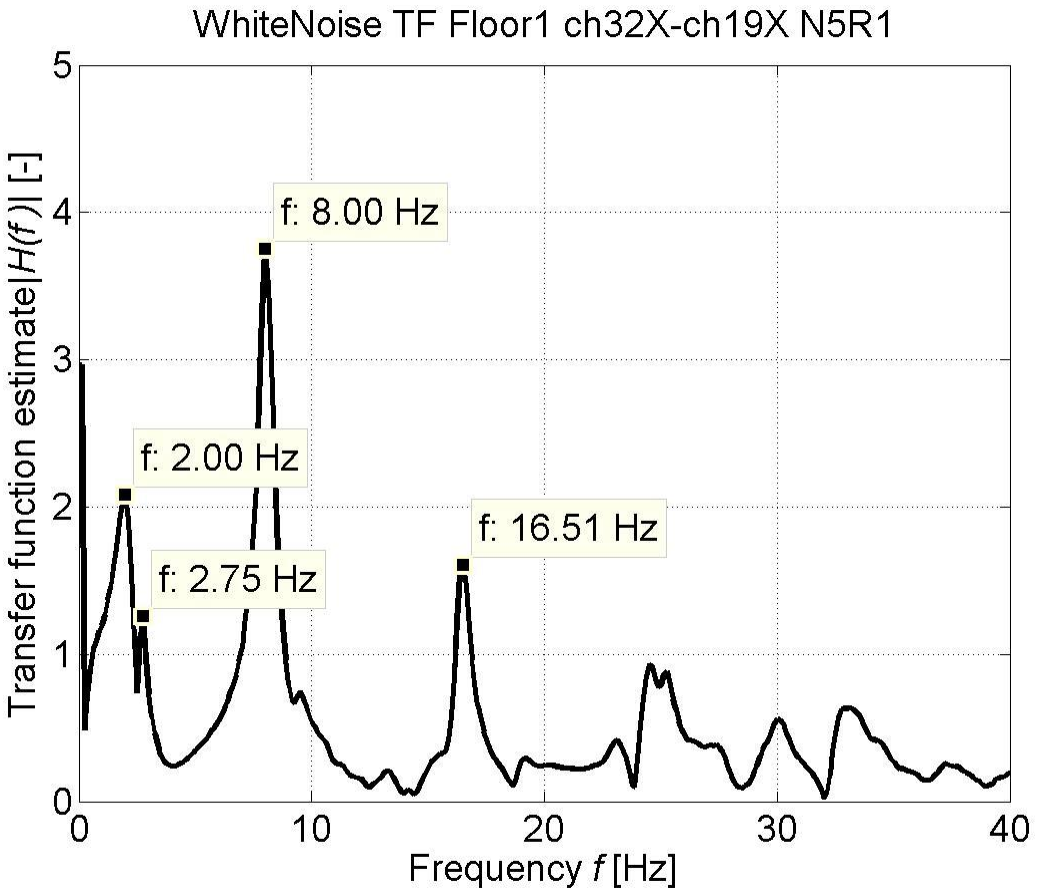
WhiteNoise TF Floor1 ch32X-ch19X N5R1
Transfer function estimate |H(f)| [-]
Frequency f [Hz]
f: 8.00 Hz
f: 2.00 Hz
f: 2.75 Hz
f: 16.51 Hz
0
1
2
3
4
5
0
10
20
30
40

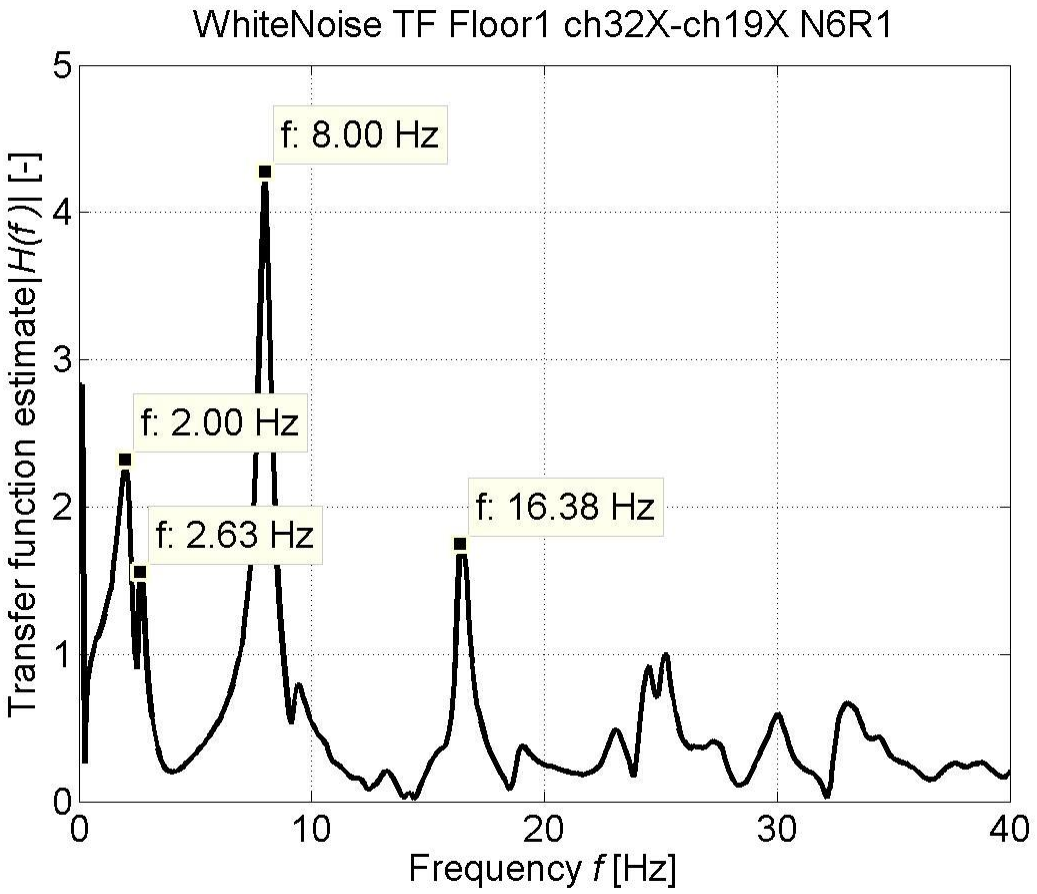
WhiteNoise TF Floor1 ch32X-ch19X N6R1
f: 8.00 Hz
f: 2.00 Hz
f: 2.63 Hz
f: 16.38 Hz
Transfer function estimate |H(f)| [-]
Frequency f [Hz]
0
1
2
3
4
5
0
10
20
30
40

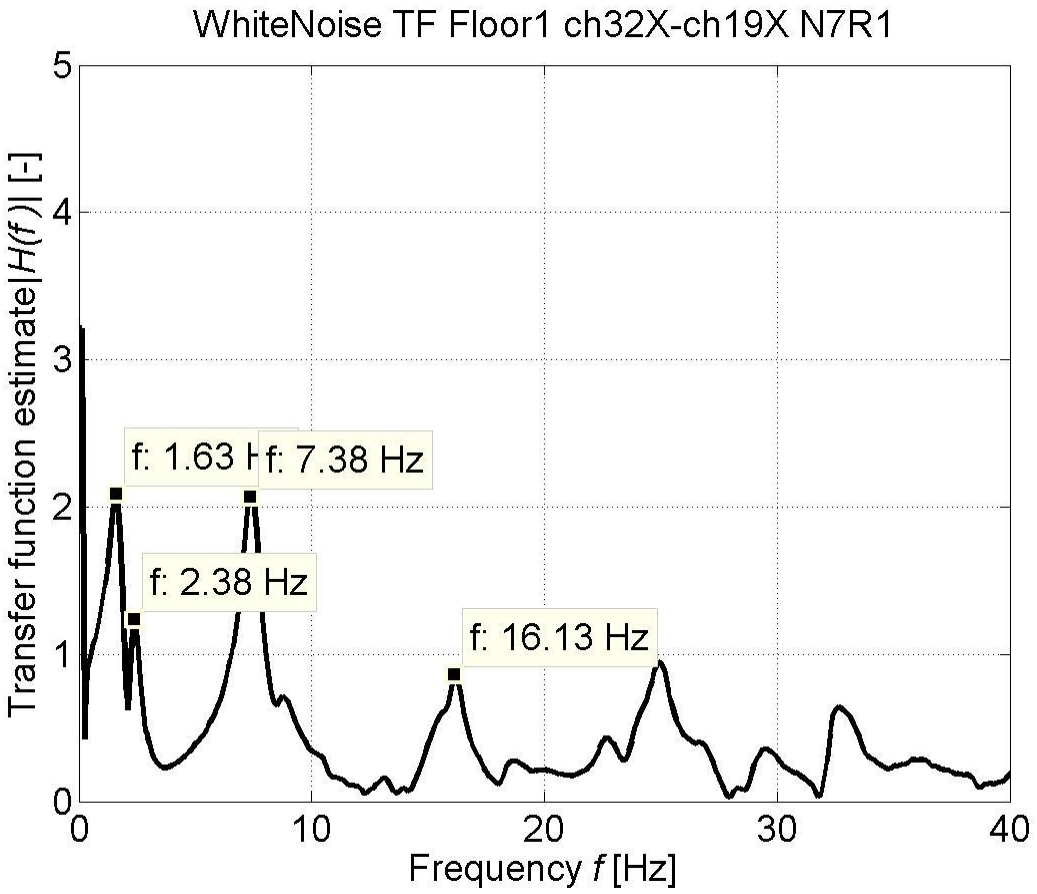
WhiteNoise TF Floor1 ch32X-ch19X N7R1
Transfer function estimate |H(f)| [-]
Frequency f [Hz]
f: 1.63 H
f: 7.38 Hz
f: 2.38 Hz
f: 16.13 Hz
0
1
2
3
4
5
0
10
20
30
40

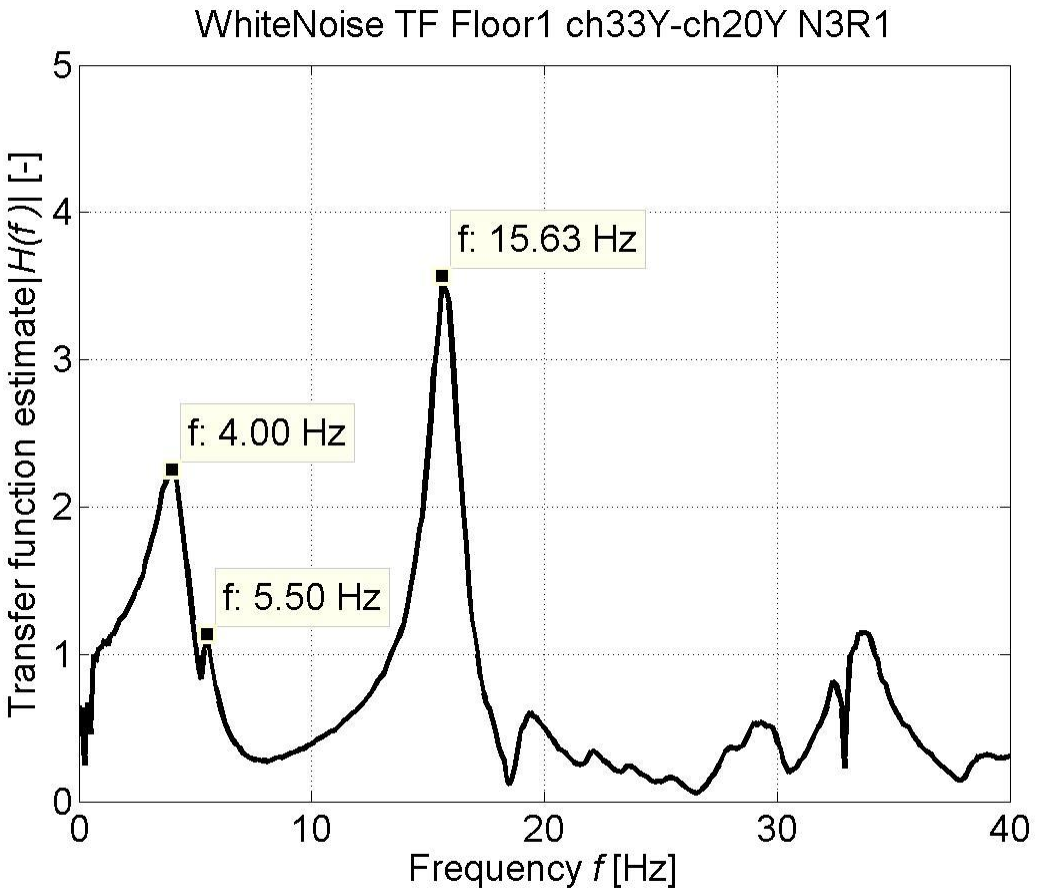
WhiteNoise TF Floor1 ch33Y-ch20Y N3R1
Transfer function estimate |H(f)| [-]
Frequency f [Hz]
f: 15.63 Hz
f: 4.00 Hz
f: 5.50 Hz
0
1
2
3
4
5
0
10
20
30
40

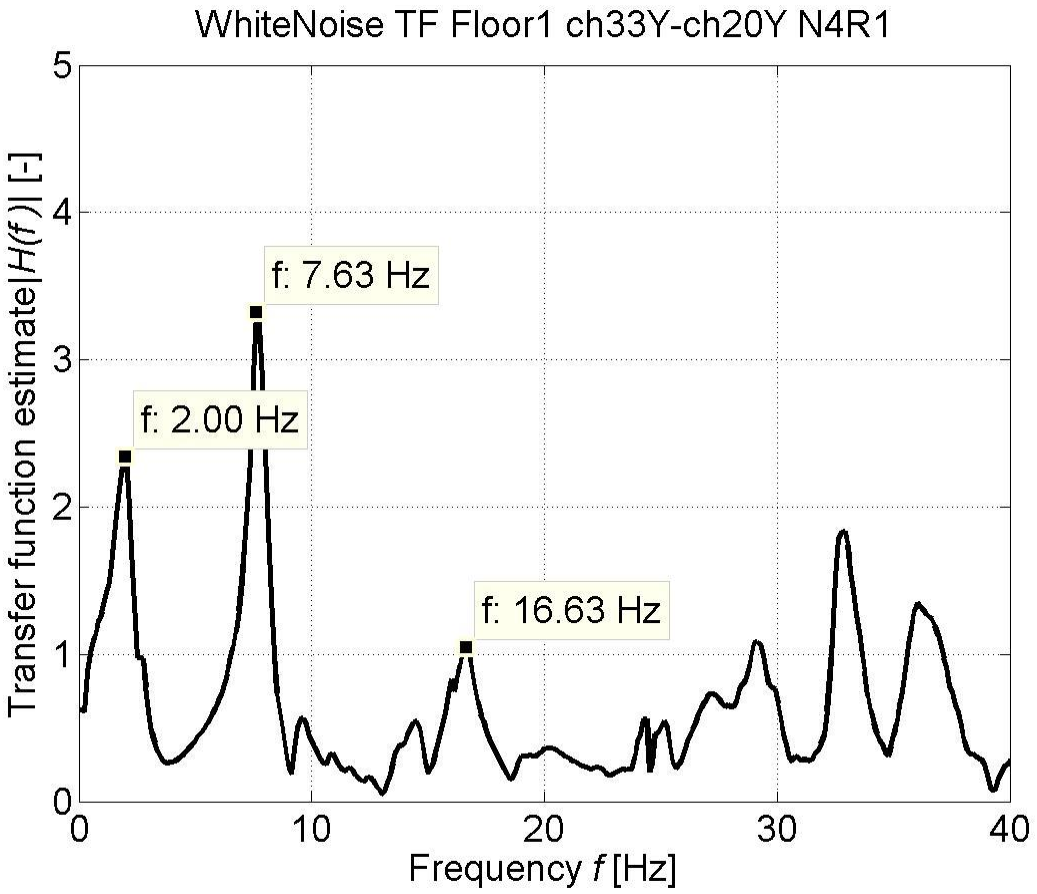
WhiteNoise TF Floor1 ch33Y-ch20Y N4R1
Transfer function estimate |H(f)| [-]
Frequency f [Hz]
f: 2.00 Hz
f: 7.63 Hz
f: 16.63 Hz
0
1
2
3
4
5
0
10
20
30
40

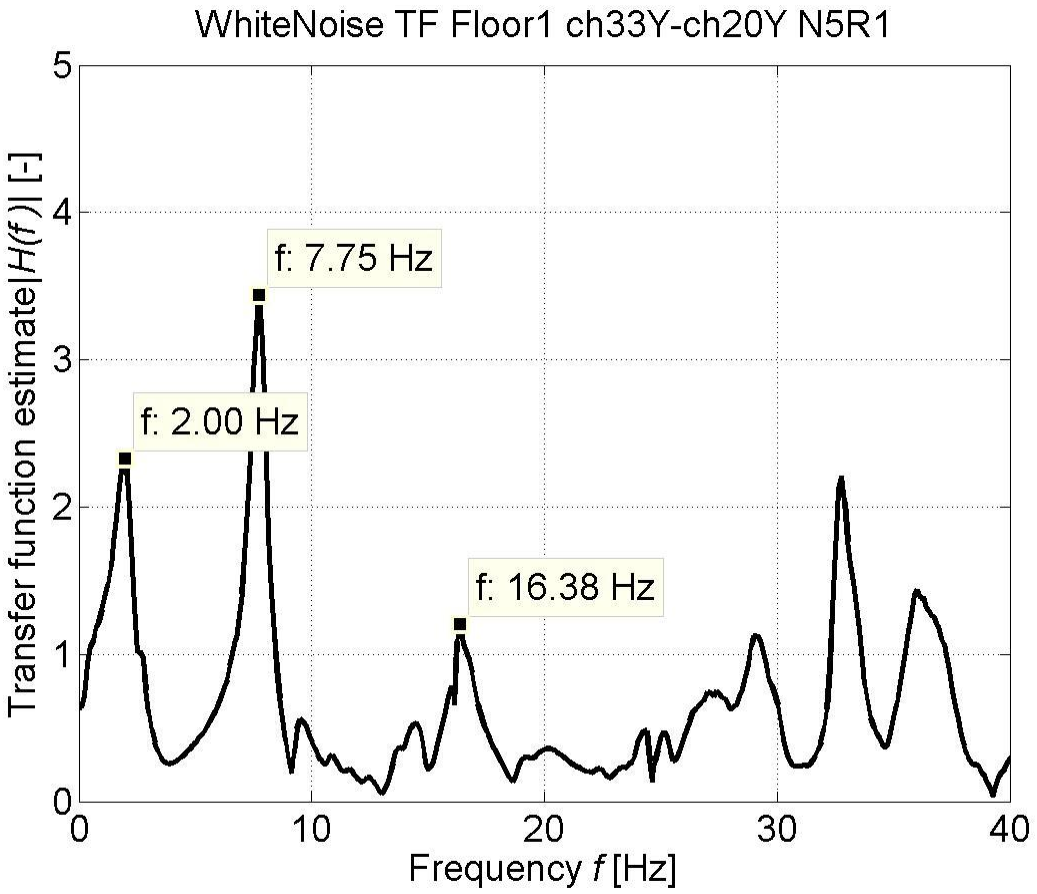
WhiteNoise TF Floor1 ch33Y-ch20Y N5R1
Transfer function estimate |H(f)| [-]
Frequency f [Hz]
f: 7.75 Hz
f: 2.00 Hz
f: 16.38 Hz
0
1
2
3
4
5
0
10
20
30
40

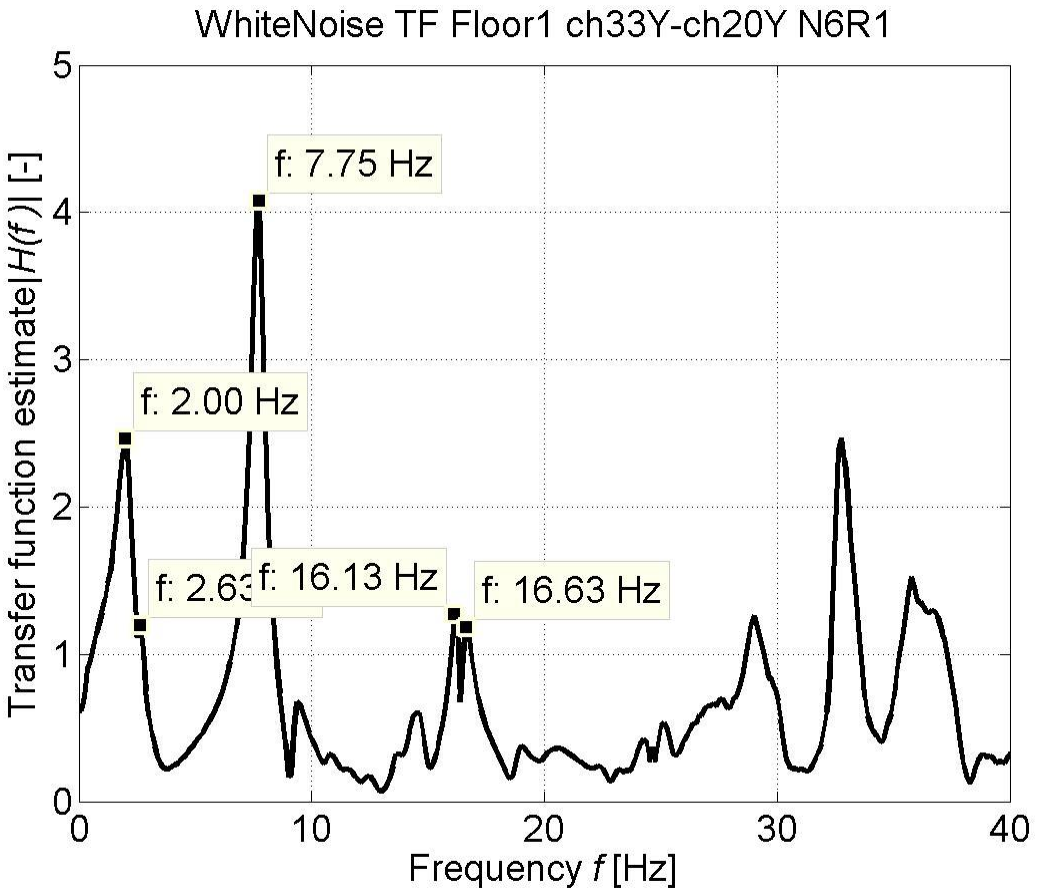
WhiteNoise TF Floor1 ch33Y-ch20Y N6R1
f: 7.75 Hz
f: 2.00 Hz
f: 2.63
f: 16.13 Hz
f: 16.63 Hz
Transfer function estimate |H(f)| [-]
Frequency f [Hz]
0
1
2
3
4
5
0
10
20
30
40

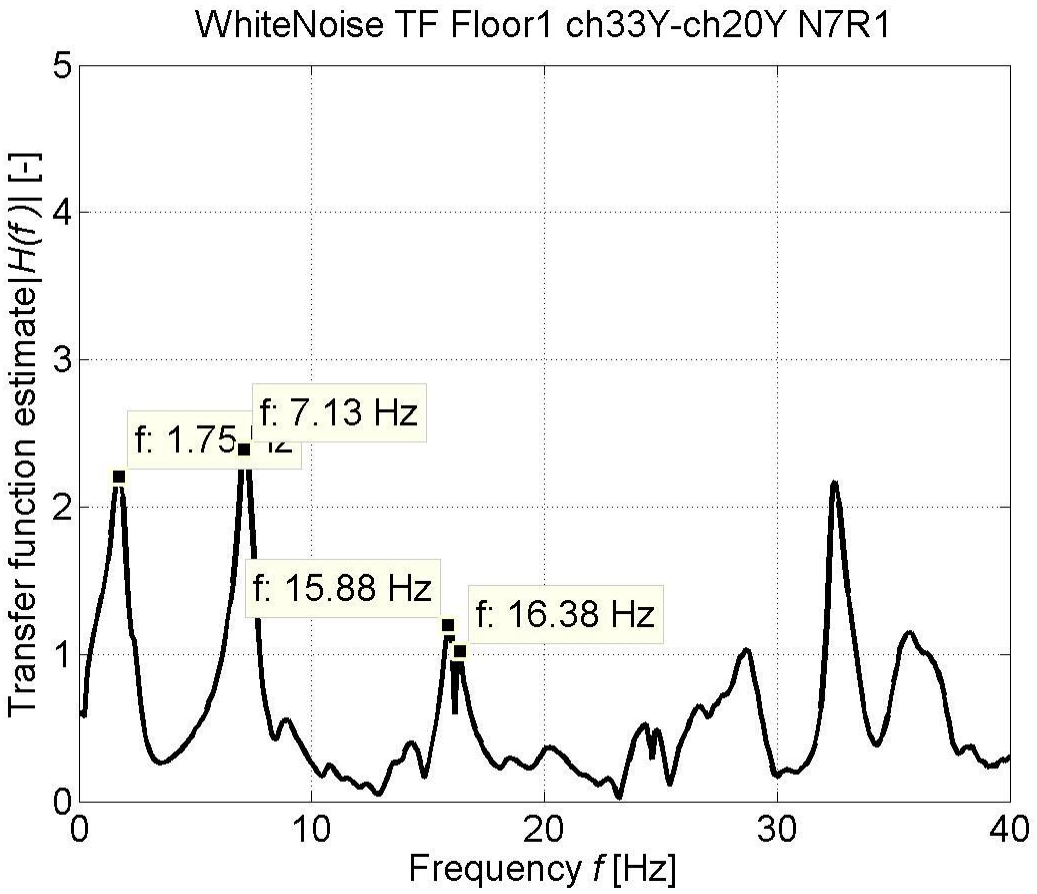
WhiteNoise TF Floor1 ch33Y-ch20Y N7R1
Transfer function estimate|H(f)| [-]
Frequency f [Hz]
f: 1.75
f: 7.13 Hz
f: 15.88 Hz
f: 16.38 Hz
0
1
2
3
4
5
0
10
20
30
40

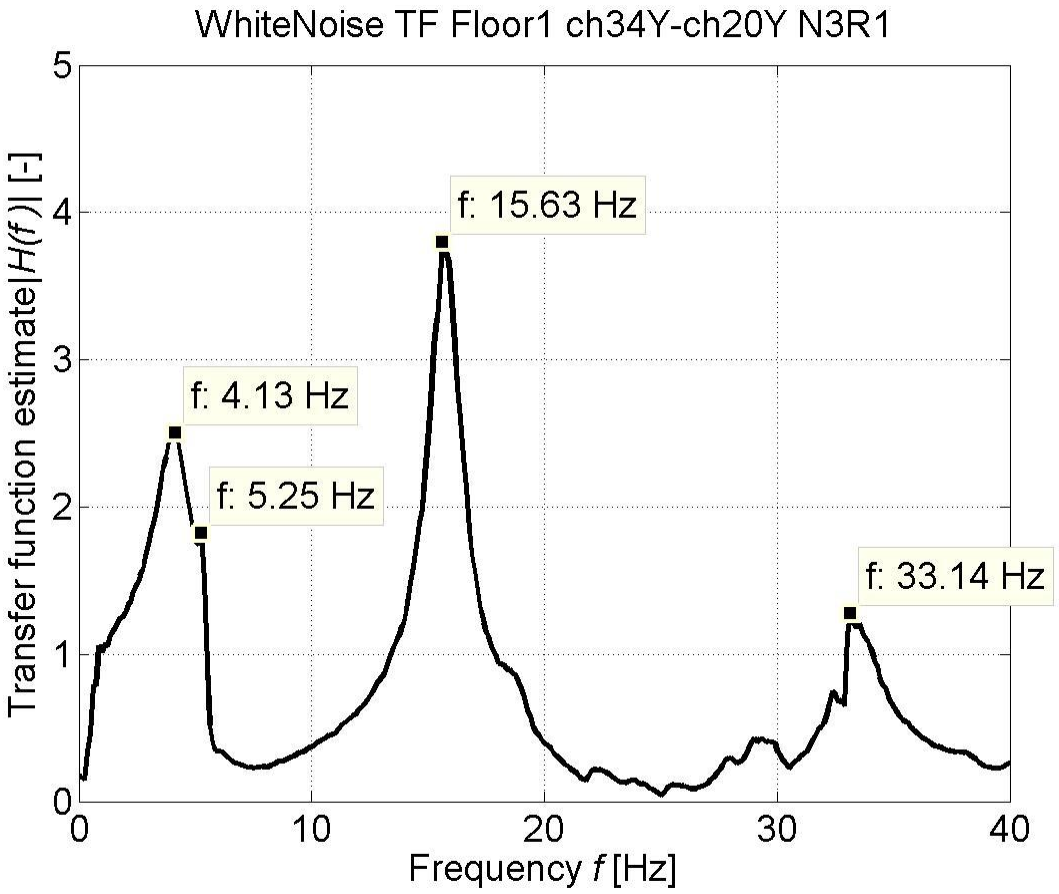
WhiteNoise TF Floor1 ch34Y-ch20Y N3R1
Transfer function estimate |H(f)| [-]
Frequency f [Hz]
f: 4.13 Hz
f: 5.25 Hz
f: 15.63 Hz
f: 33.14 Hz
0
1
2
3
4
5
0
10
20
30
40

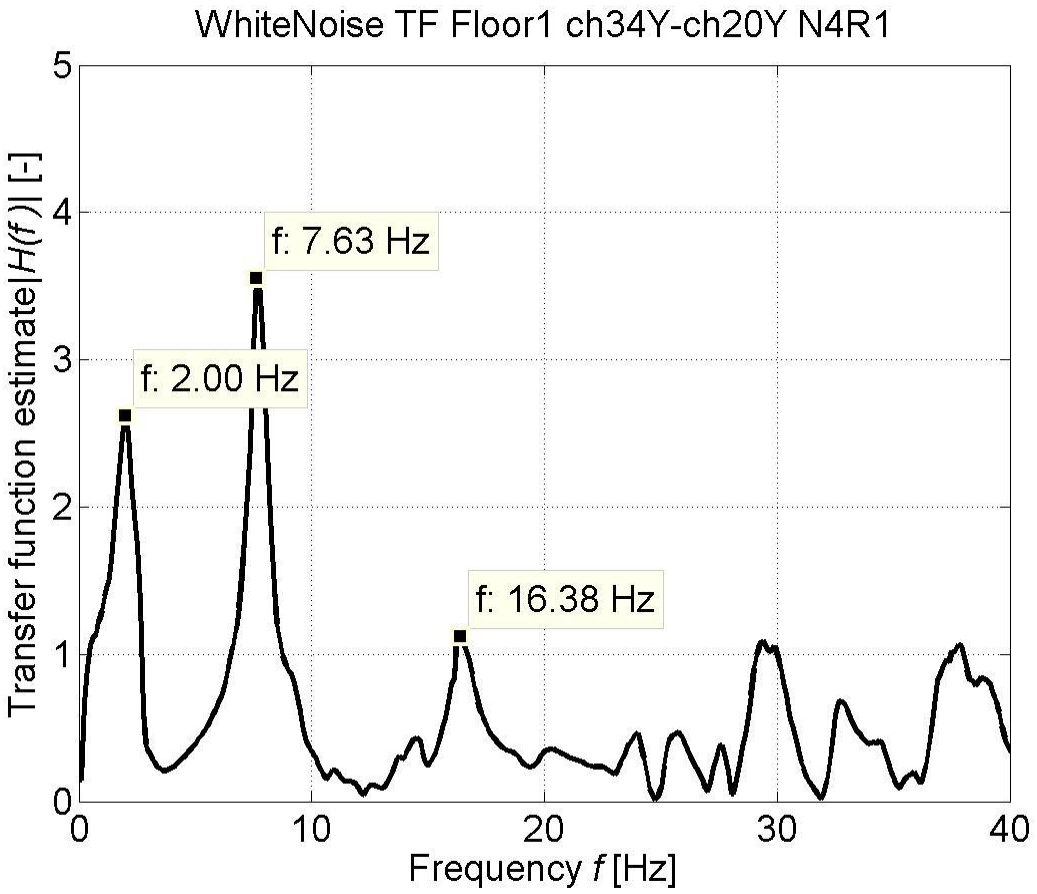
WhiteNoise TF Floor1 ch34Y-ch20Y N4R1
Transfer function estimate |H(f)| [-]
Frequency f [Hz]
f: 7.63 Hz
f: 2.00 Hz
f: 16.38 Hz
0
1
2
3
4
5
0
10
20
30
40

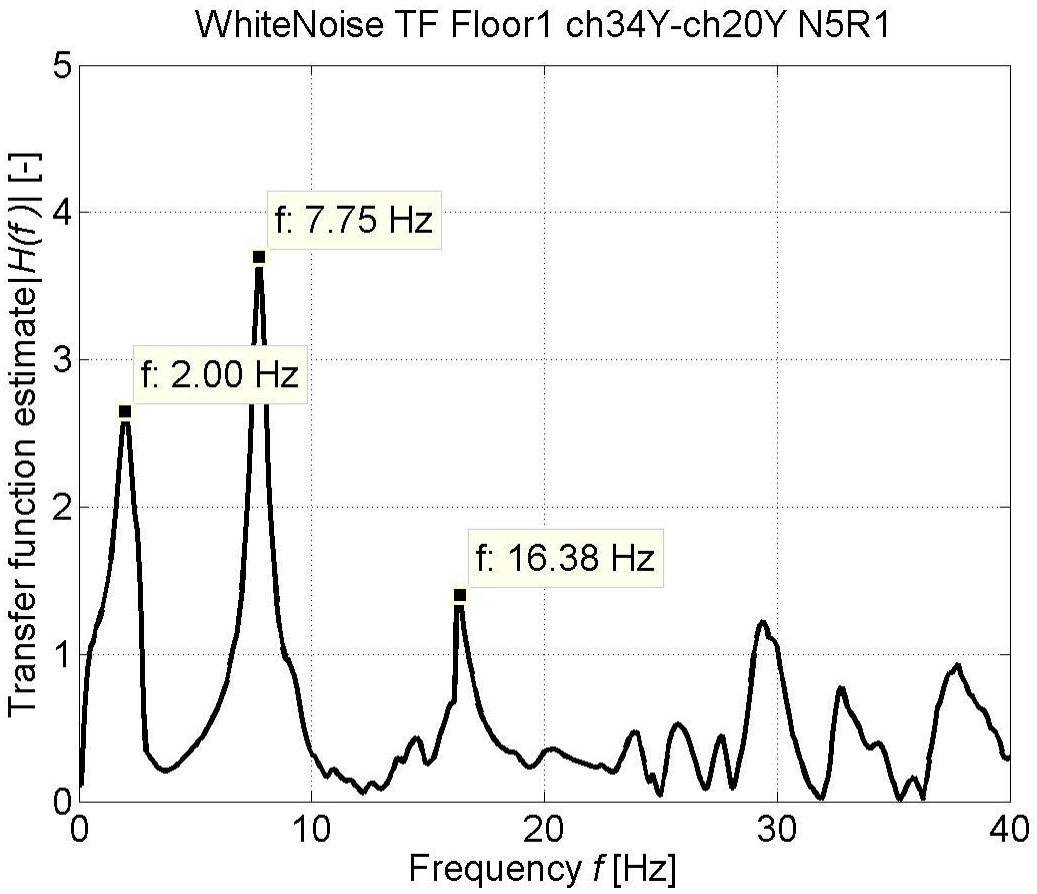
WhiteNoise TF Floor1 ch34Y-ch20Y N5R1
f: 7.75 Hz
f: 2.00 Hz
f: 16.38 Hz
Transfer function estimate |H(f)| [-]
Frequency f [Hz]
0
1
2
3
4
5
0
10
20
30
40

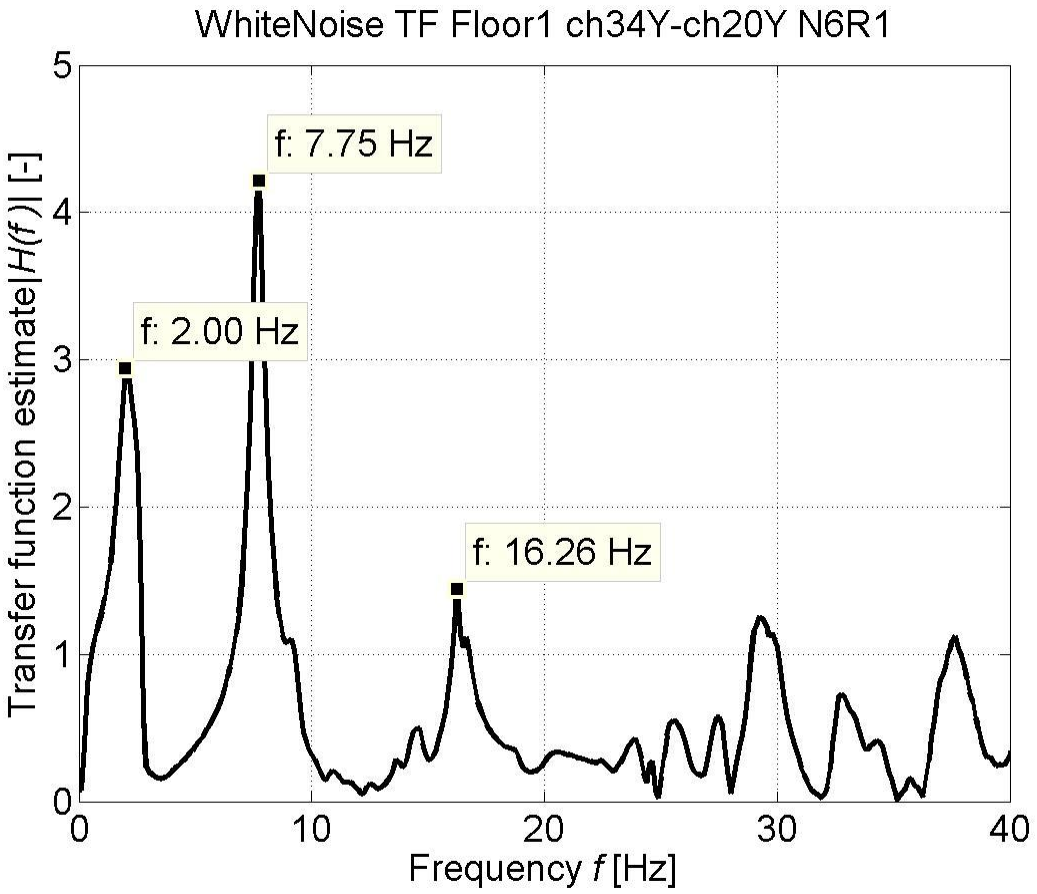
WhiteNoise TF Floor1 ch34Y-ch20Y N6R1
f: 7.75 Hz
f: 2.00 Hz
f: 16.26 Hz
Transfer function estimate |H(f)| [-]
Frequency f [Hz]
0
1
2
3
4
5
0
10
20
30
40

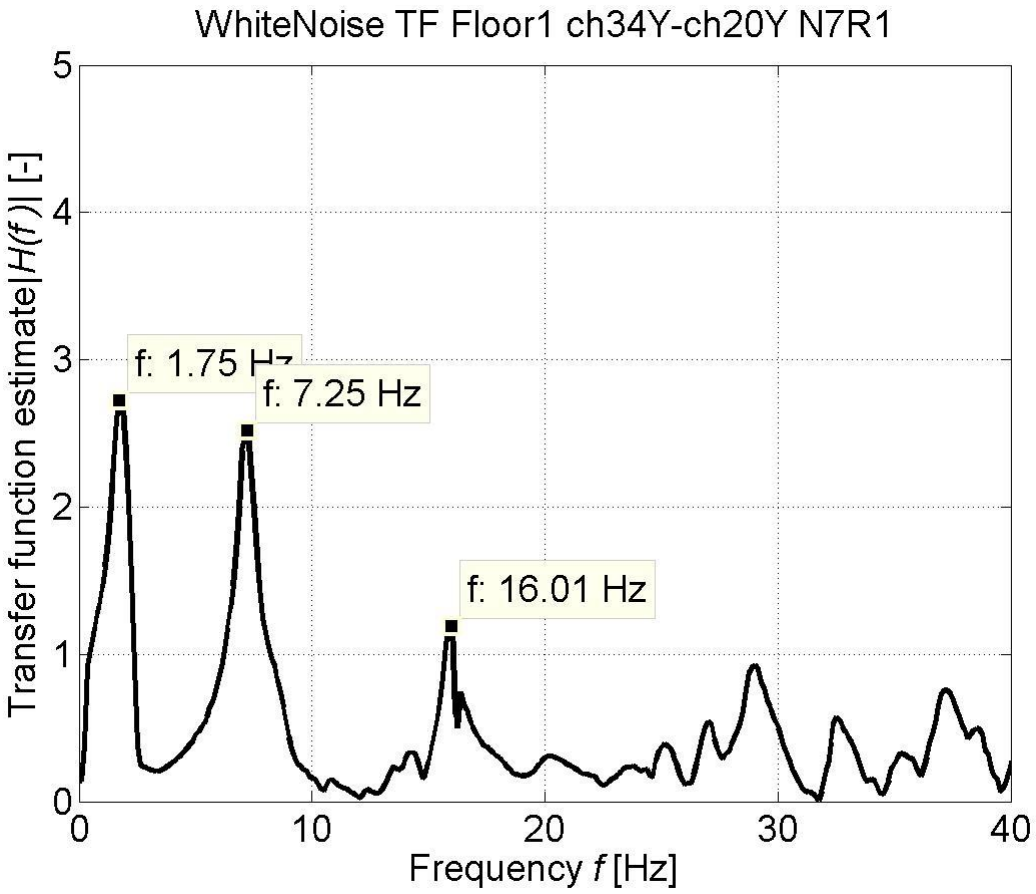

F L O O R 2

Channels 35-38

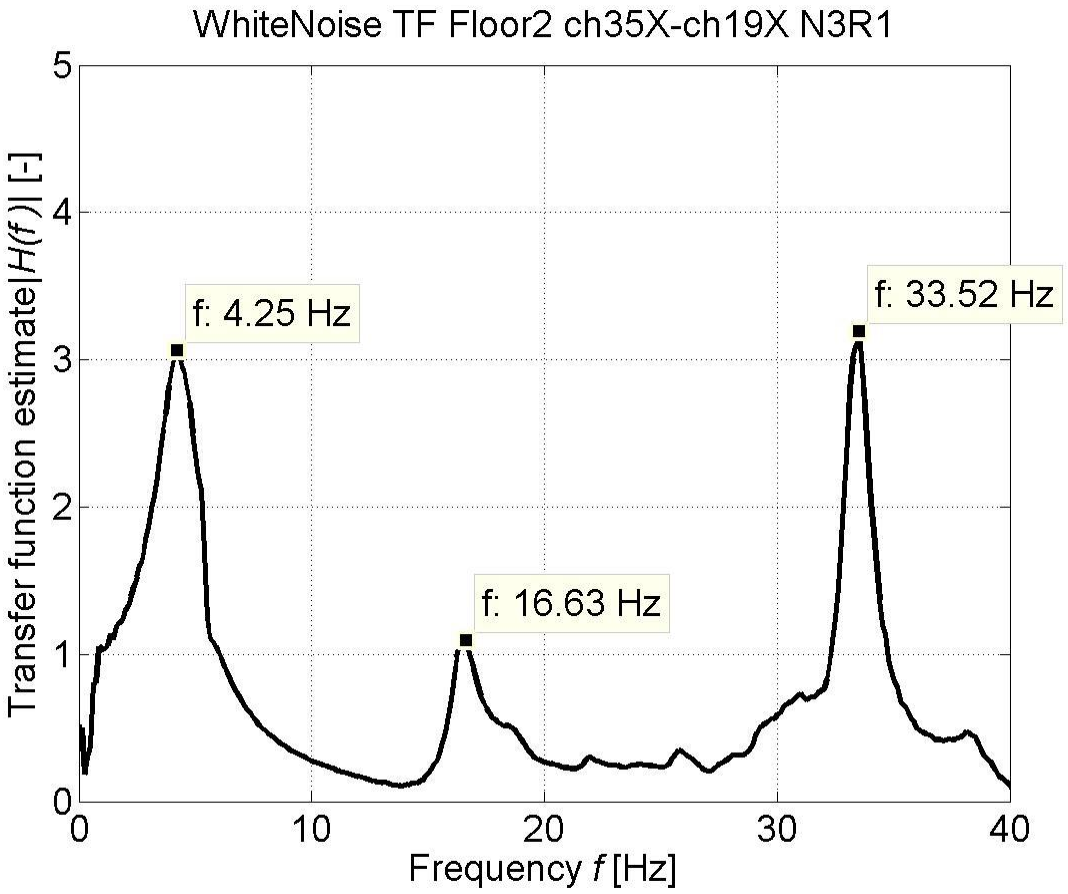
WhiteNoise TF Floor2 ch35X-ch19X N3R1
Transfer function estimate |H(f)| [-]
Frequency f [Hz]
f: 4.25 Hz
f: 16.63 Hz
f: 33.52 Hz
0
1
2
3
4
5
0
10
20
30
40

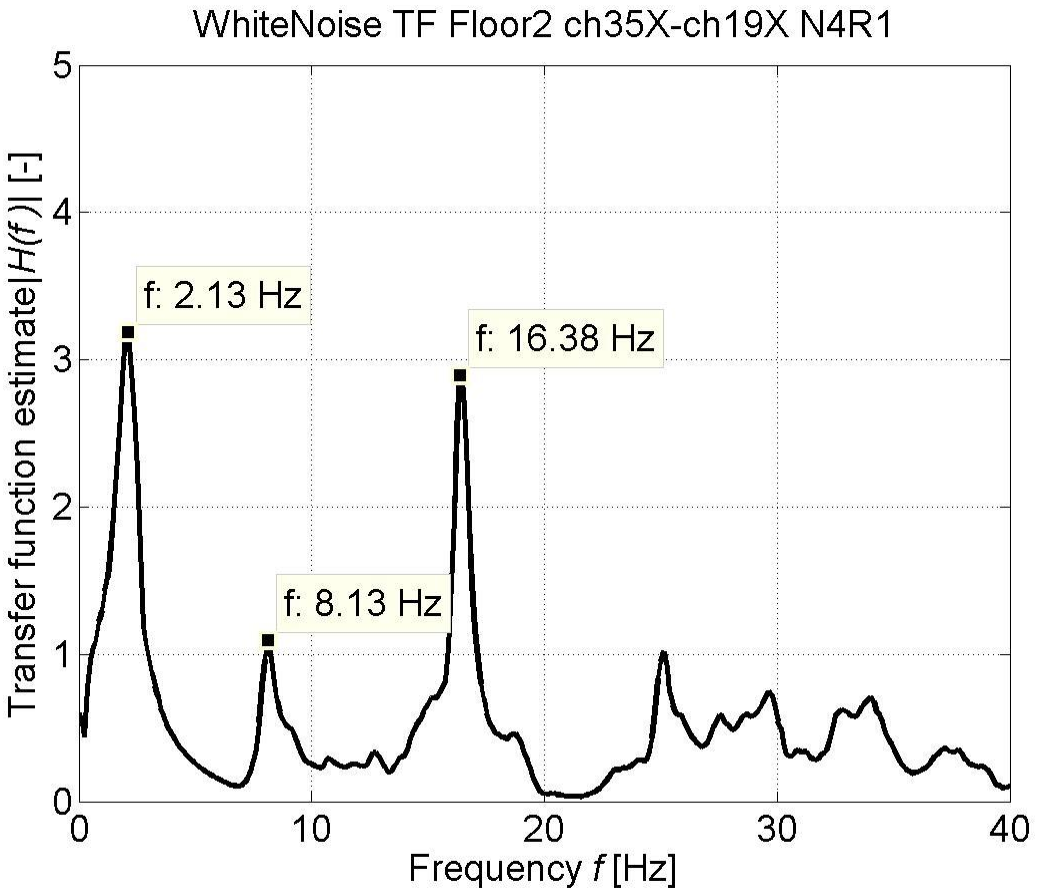
WhiteNoise TF Floor2 ch35X-ch19X N4R1
Transfer function estimate |H(f)| [-]
Frequency f [Hz]
f: 2.13 Hz
f: 8.13 Hz
f: 16.38 Hz
0
1
2
3
4
5
0
10
20
30
40

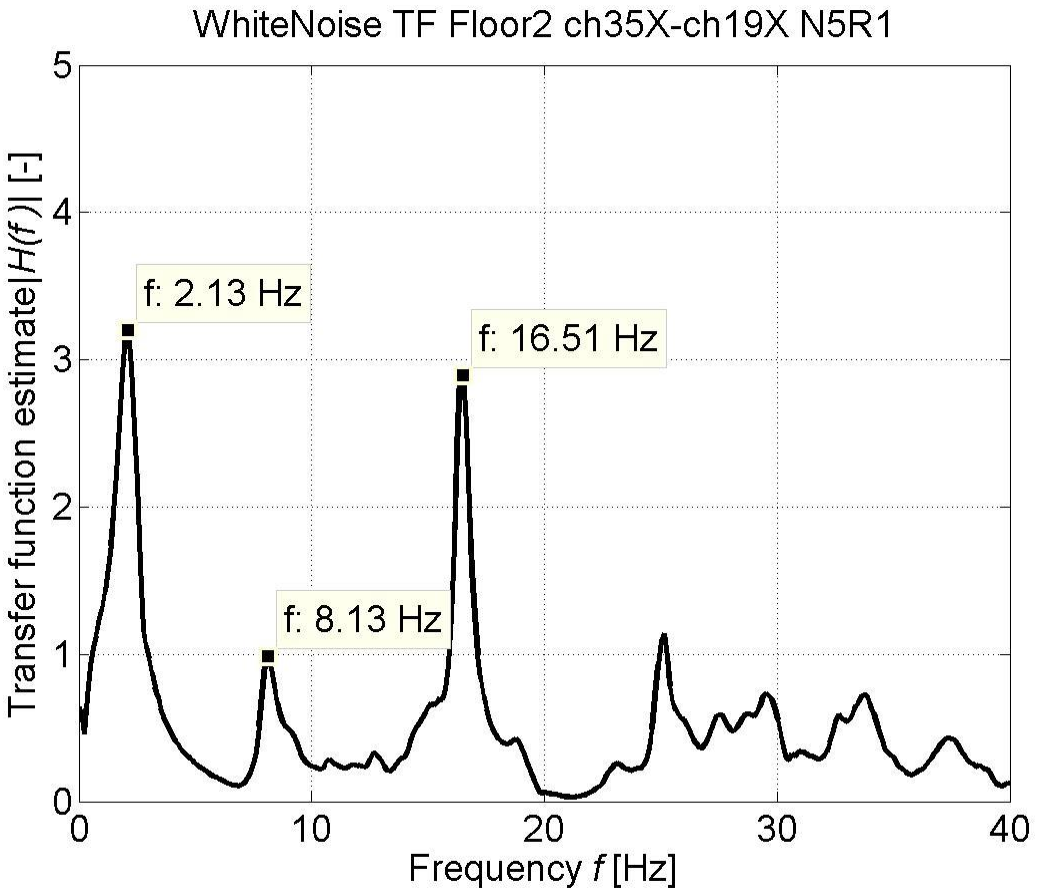
WhiteNoise TF Floor2 ch35X-ch19X N5R1
Transfer function estimate |H(f)| [-]
Frequency f [Hz]
f: 2.13 Hz
f: 8.13 Hz
f: 16.51 Hz
0
1
2
3
4
5
0
10
20
30
40

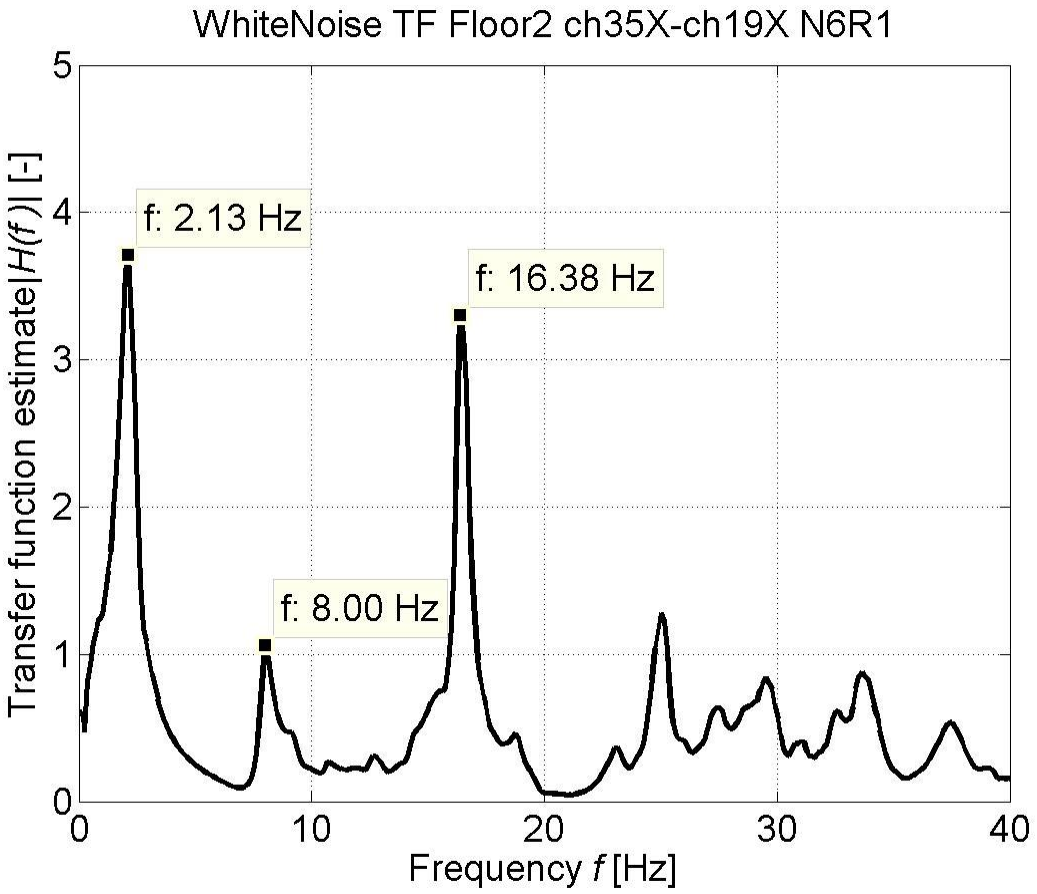
WhiteNoise TF Floor2 ch35X-ch19X N6R1
f: 2.13 Hz
f: 16.38 Hz
f: 8.00 Hz
Transfer function estimate |H(f)| [-]
Frequency f [Hz]
0
1
2
3
4
5
0
10
20
30
40

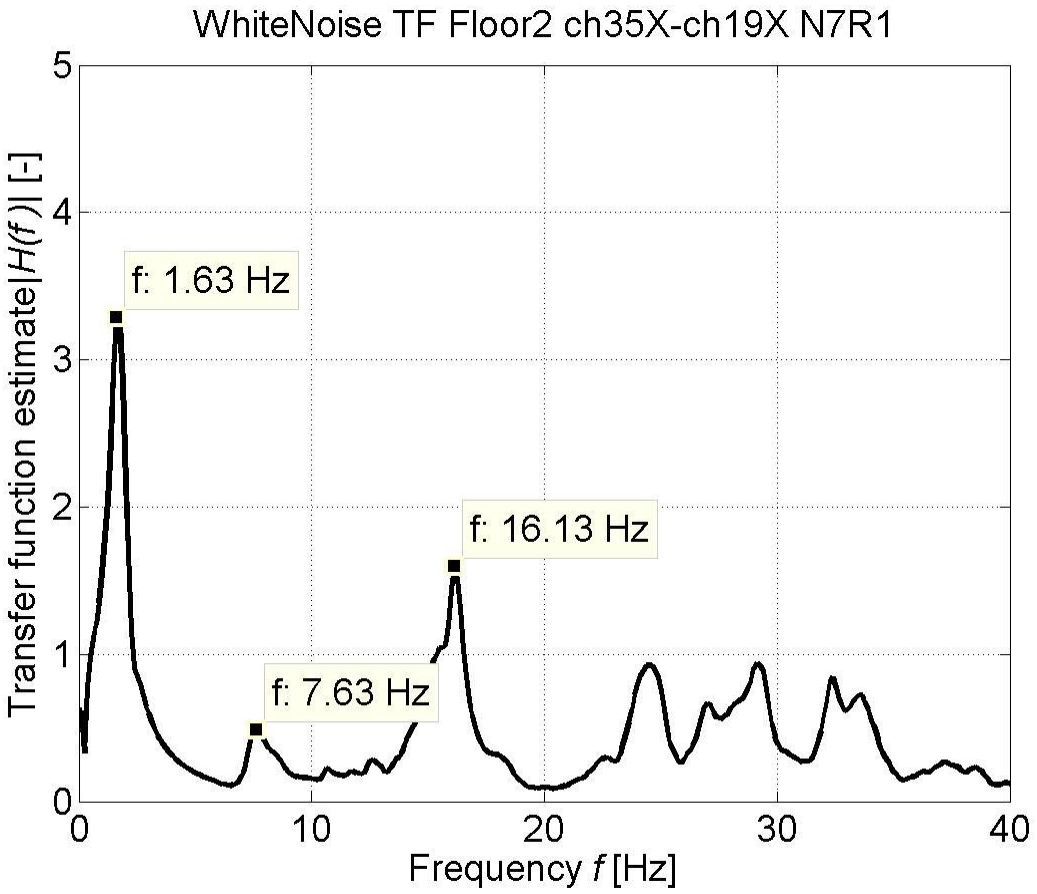
WhiteNoise TF Floor2 ch35X-ch19X N7R1
Transfer function estimate |H(f)| [-]
Frequency f [Hz]
f: 1.63 Hz
f: 7.63 Hz
f: 16.13 Hz
0
1
2
3
4
5
0
10
20
30
40

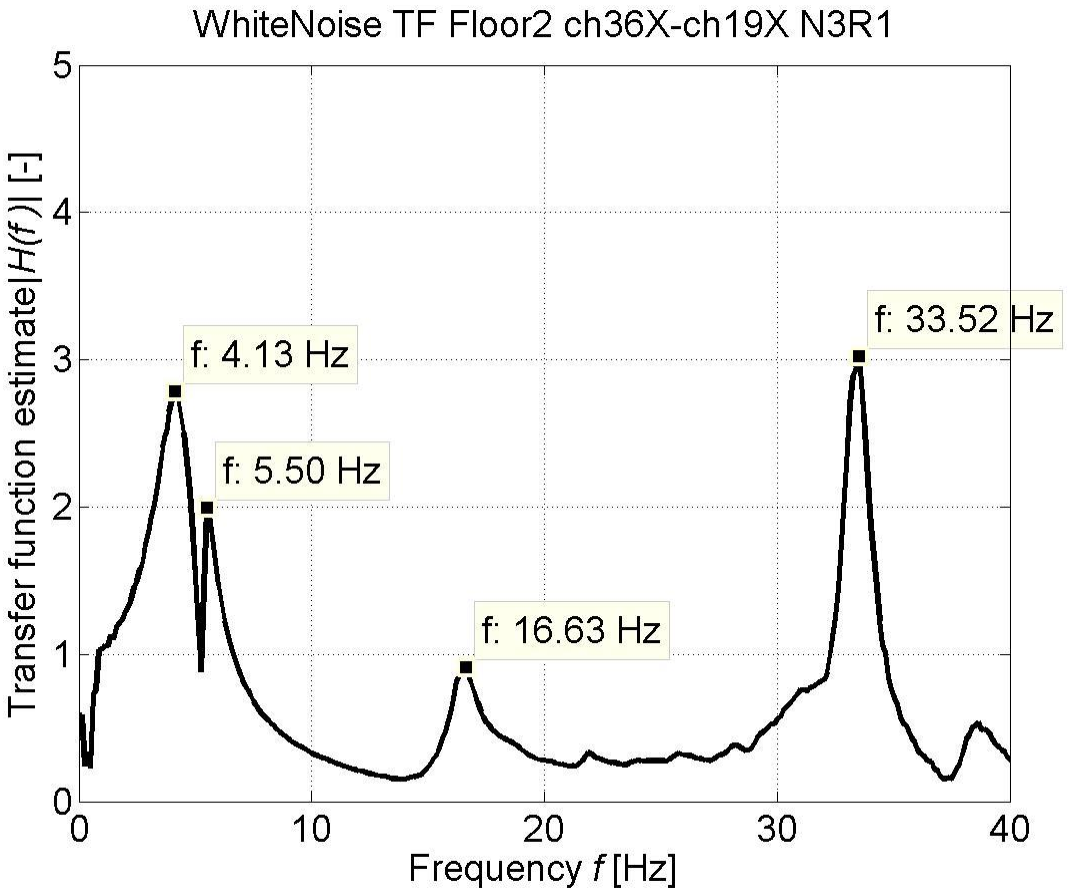
WhiteNoise TF Floor2 ch36X-ch19X N3R1
Transfer function estimate |H(f)| [-]
Frequency f [Hz]
f: 4.13 Hz
f: 5.50 Hz
f: 16.63 Hz
f: 33.52 Hz
0
1
2
3
4
5
0
10
20
30
40

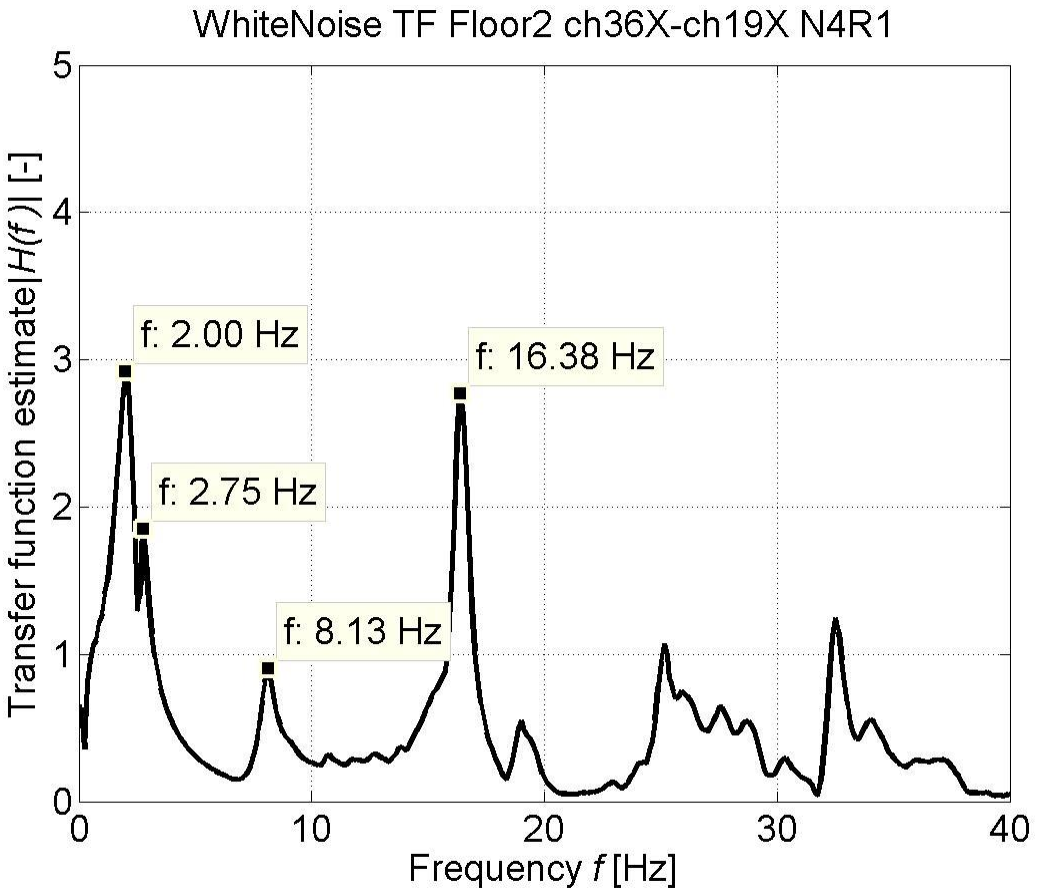
WhiteNoise TF Floor2 ch36X-ch19X N4R1
Transfer function estimate |H(f)| [-]
Frequency f [Hz]
f: 2.00 Hz
f: 2.75 Hz
f: 8.13 Hz
f: 16.38 Hz
0
1
2
3
4
5
0
10
20
30
40

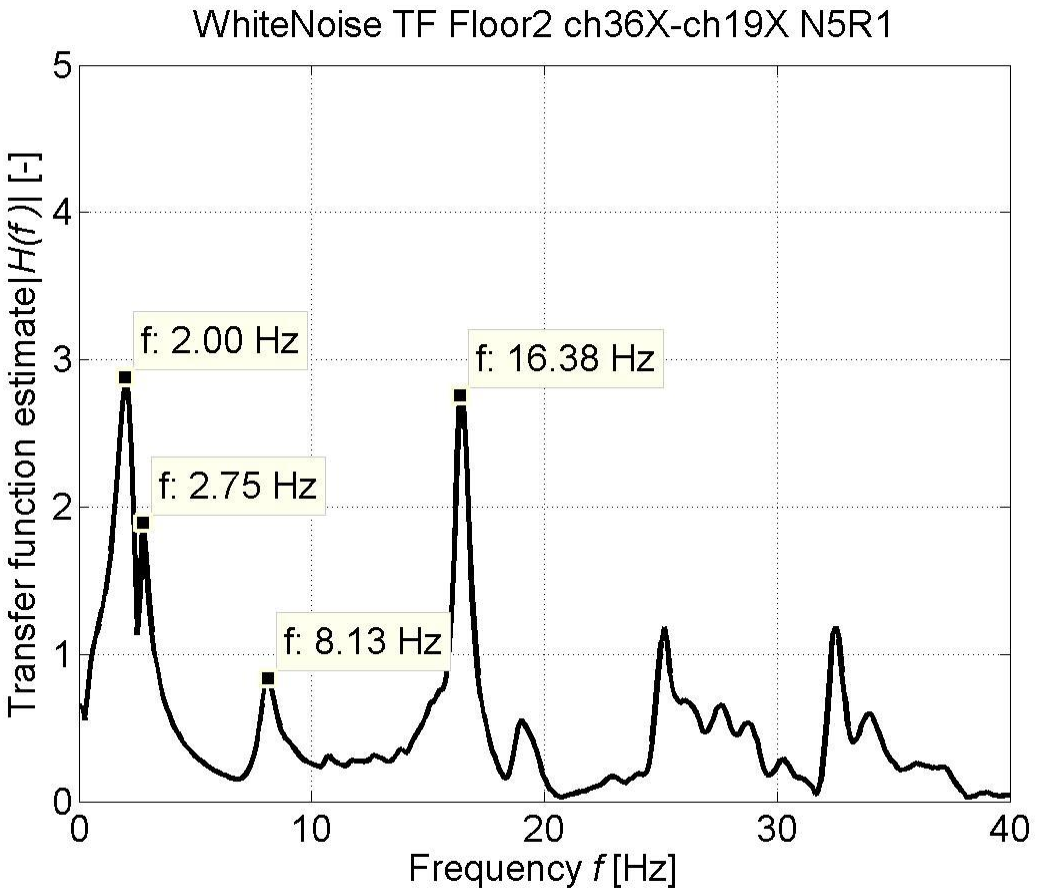
WhiteNoise TF Floor2 ch36X-ch19X N5R1
Transfer function estimate |H(f)| [-]
Frequency f [Hz]
f: 2.00 Hz
f: 2.75 Hz
f: 8.13 Hz
f: 16.38 Hz
0
1
2
3
4
5
0
10
20
30
40

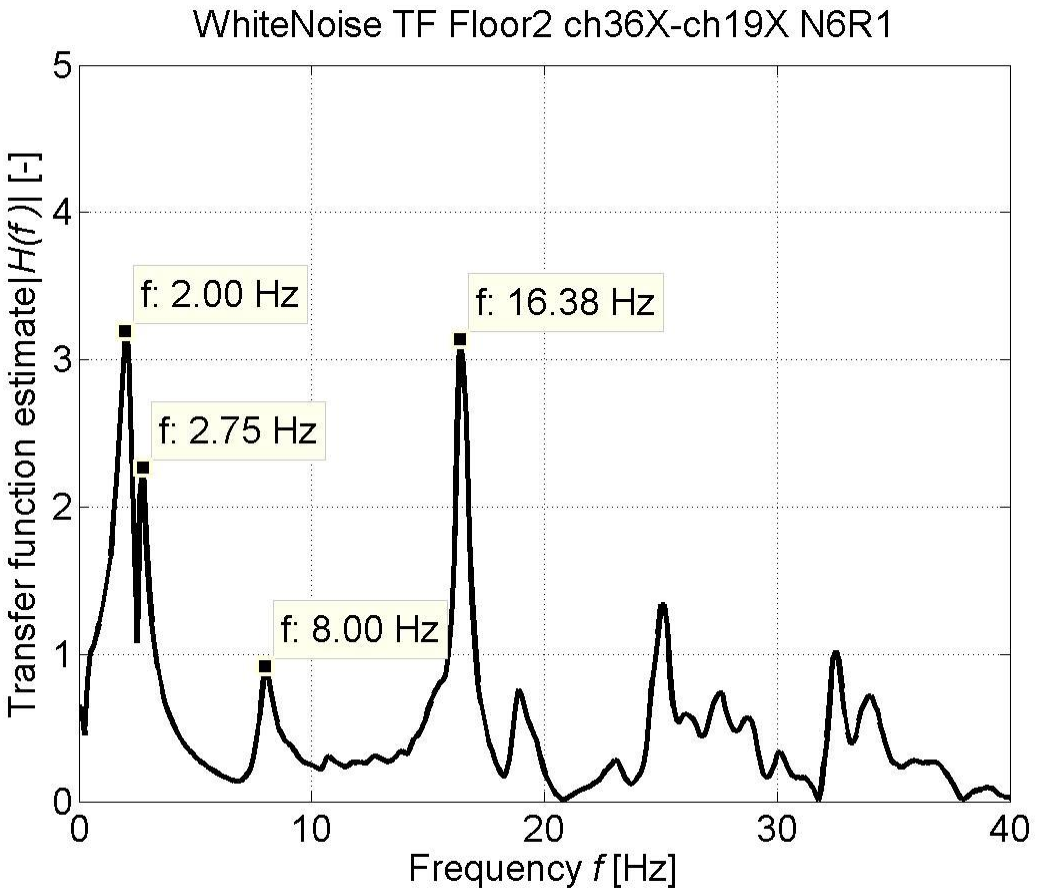
WhiteNoise TF Floor2 ch36X-ch19X N6R1
Transfer function estimate |H(f)| [-]
Frequency f [Hz]
f: 2.00 Hz
f: 2.75 Hz
f: 8.00 Hz
f: 16.38 Hz
0
1
2
3
4
5
0
10
20
30
40

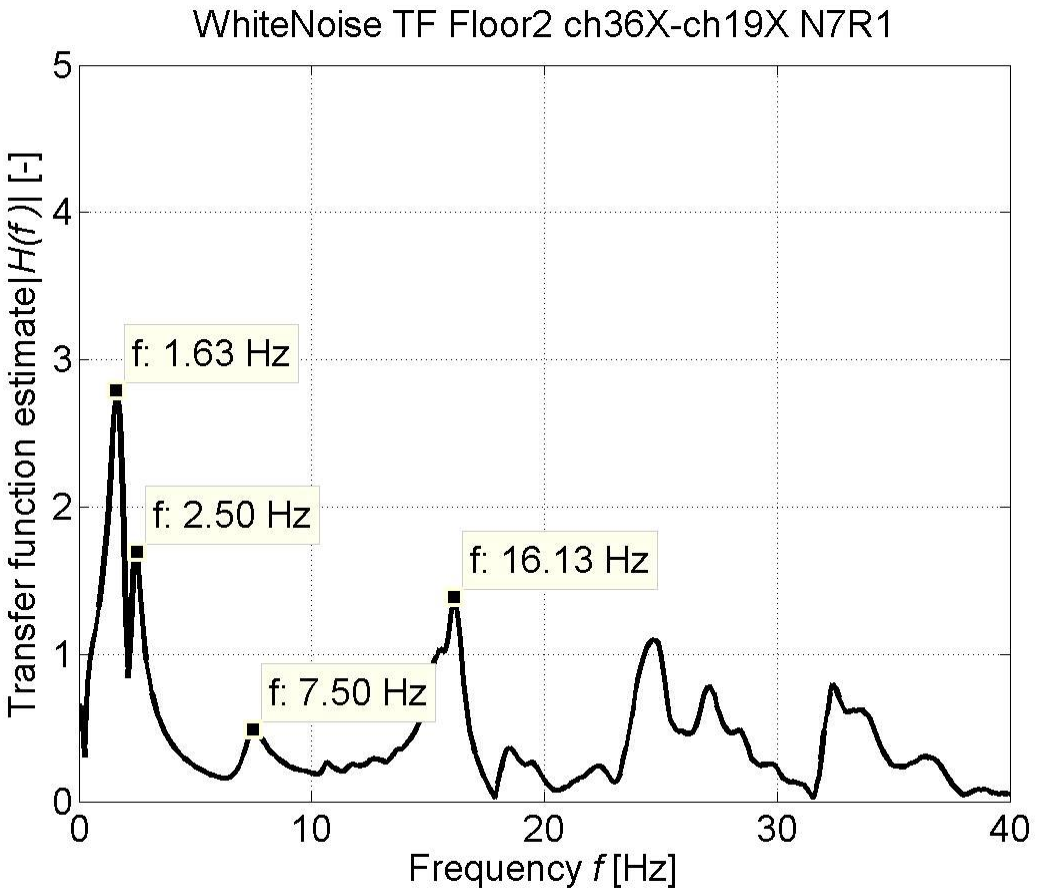
WhiteNoise TF Floor2 ch36X-ch19X N7R1
Transfer function estimate |H(f)| [-]
Frequency f [Hz]
f: 1.63 Hz
f: 2.50 Hz
f: 7.50 Hz
f: 16.13 Hz
0
1
2
3
4
5
0
10
20
30
40

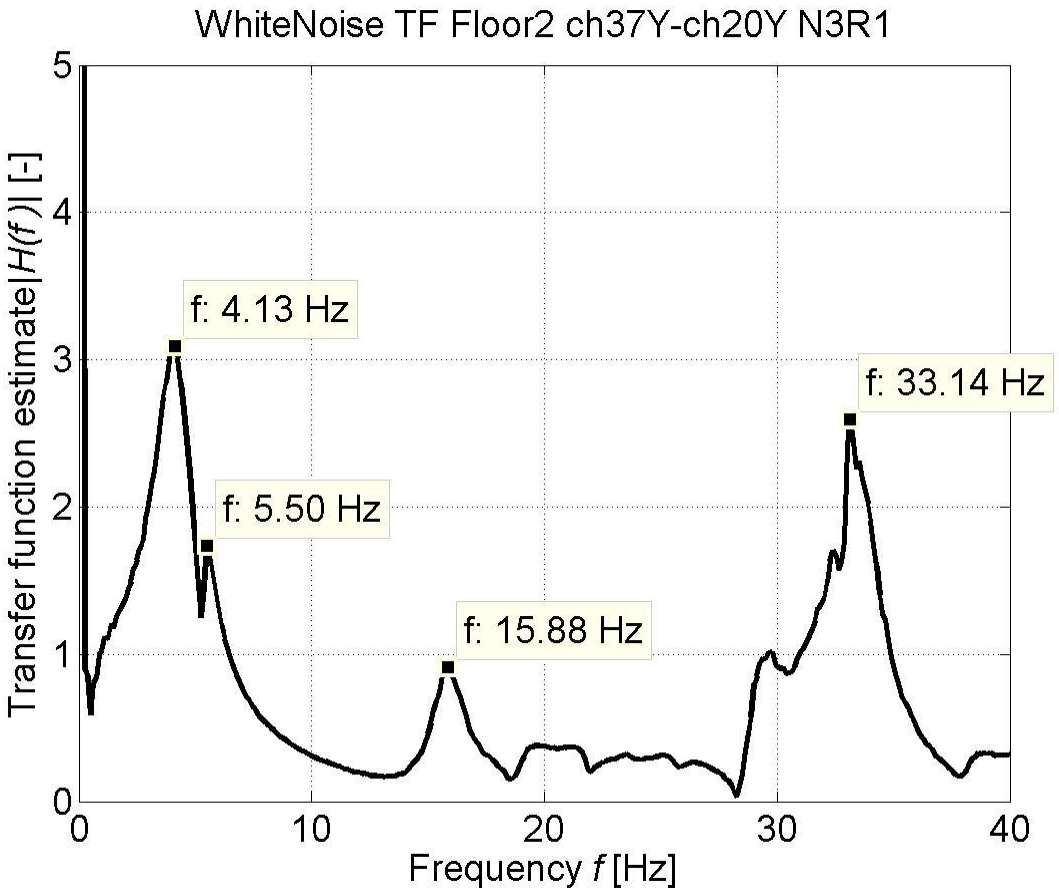
WhiteNoise TF Floor2 ch37Y-ch20Y N3R1
Transfer function estimate |H(f)| [-]
Frequency f [Hz]
f: 4.13 Hz
f: 5.50 Hz
f: 15.88 Hz
f: 33.14 Hz
0
1
2
3
4
5
0
10
20
30
40

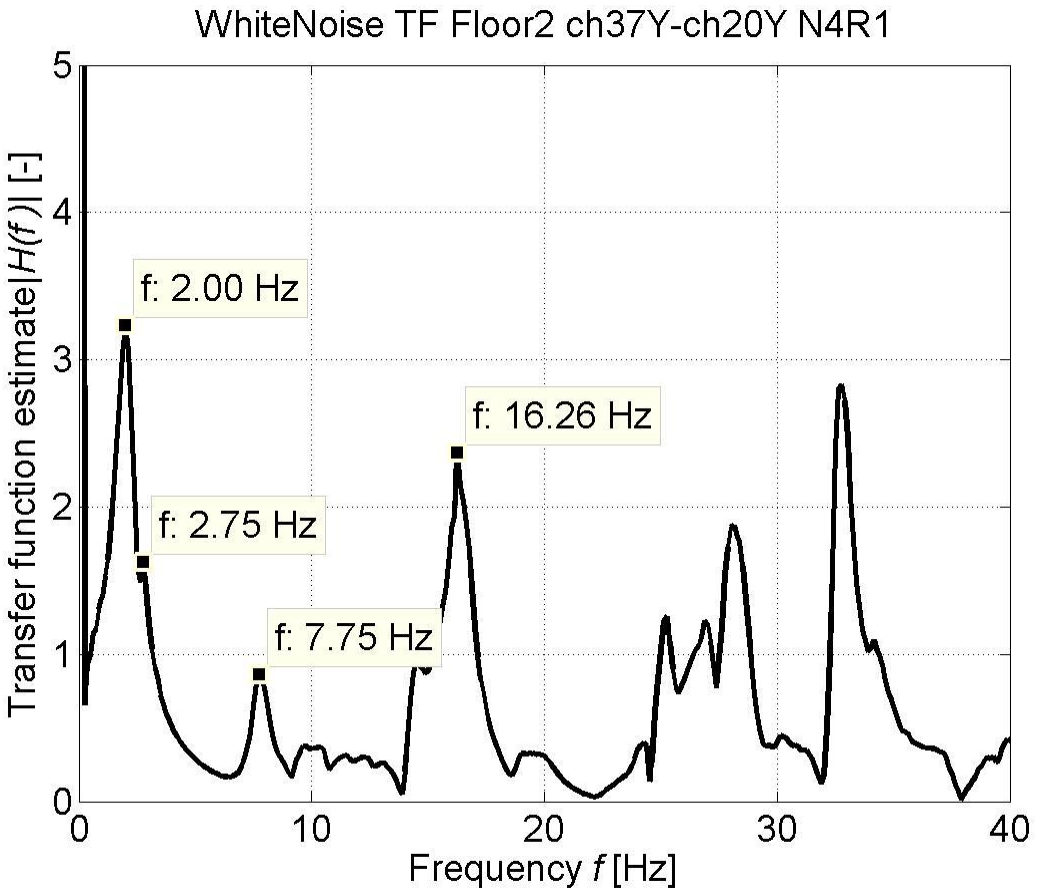
WhiteNoise TF Floor2 ch37Y-ch20Y N4R1
Transfer function estimate |H(f)| [-]
Frequency f [Hz]
f: 2.00 Hz
f: 2.75 Hz
f: 7.75 Hz
f: 16.26 Hz
0
1
2
3
4
5
0
10
20
30
40

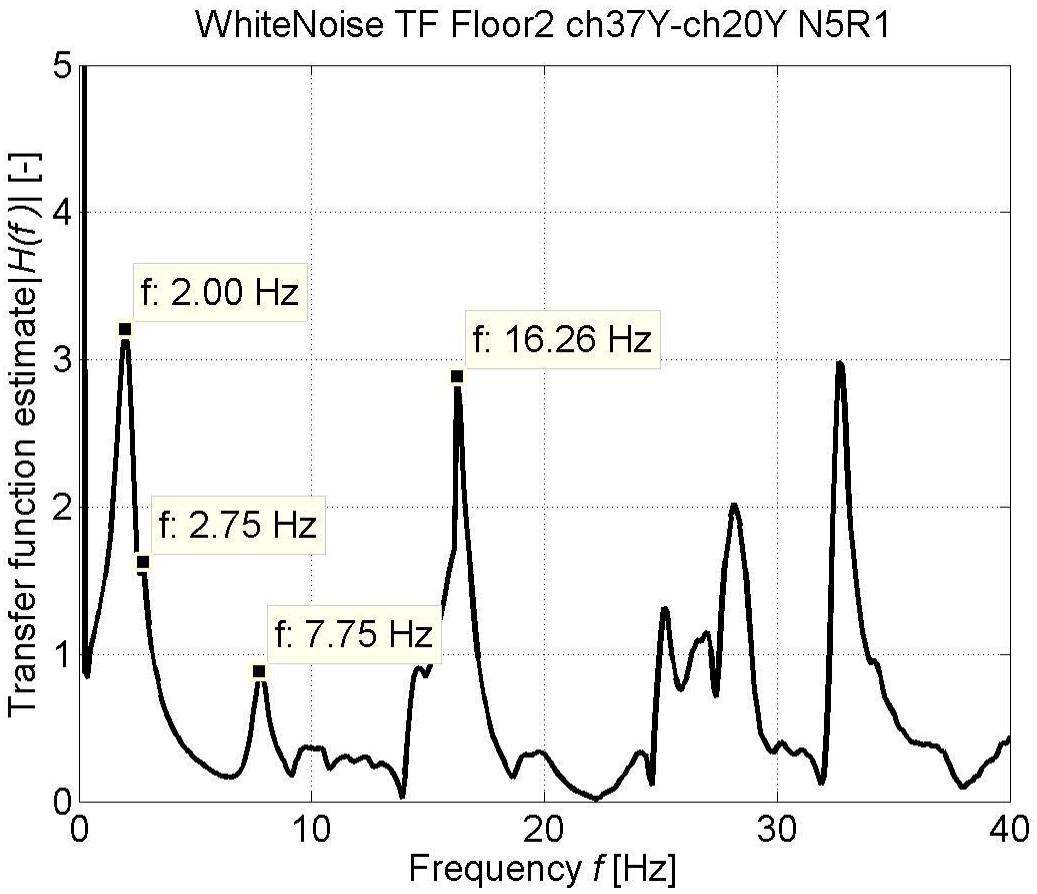
WhiteNoise TF Floor2 ch37Y-ch20Y N5R1
Transfer function estimate |H(f)| [-]
Frequency f [Hz]
f: 2.00 Hz
f: 2.75 Hz
f: 7.75 Hz
f: 16.26 Hz
0
1
2
3
4
5
0
10
20
30
40

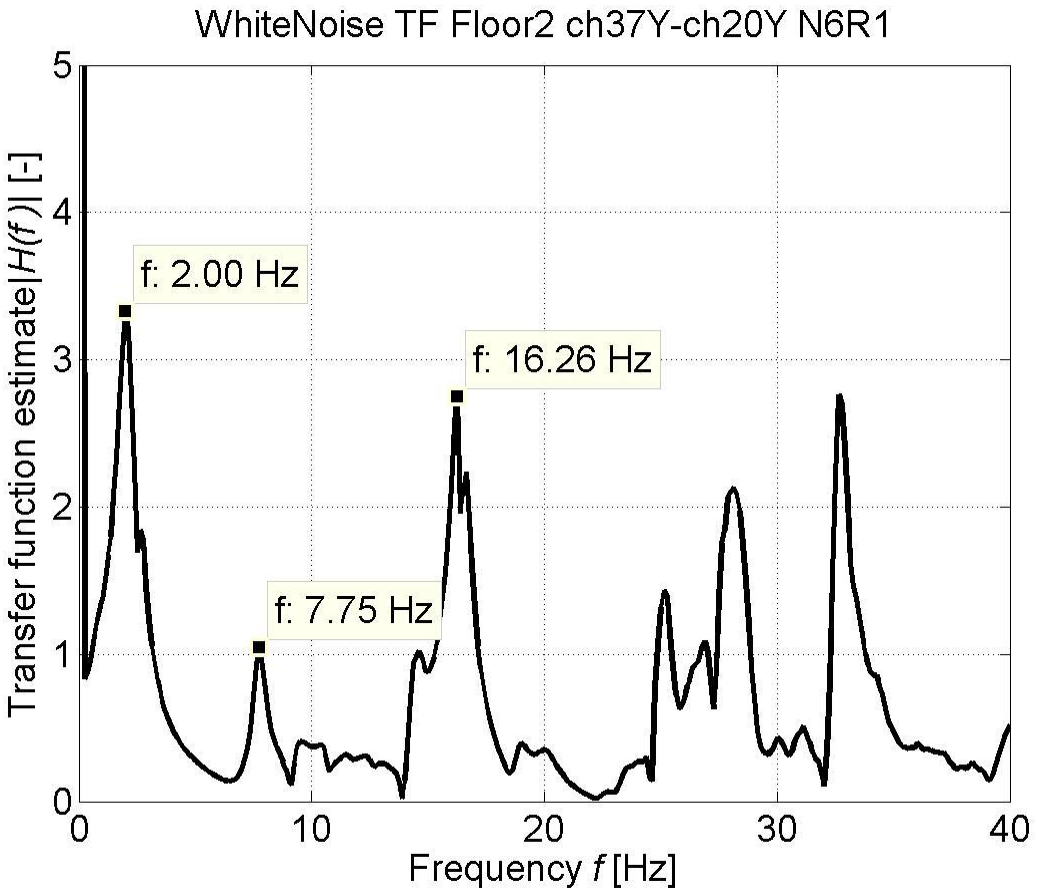
WhiteNoise TF Floor2 ch37Y-ch20Y N6R1
Transfer function estimate |H(f)| [-]
Frequency f [Hz]
f: 2.00 Hz
f: 7.75 Hz
f: 16.26 Hz
0
1
2
3
4
5
0
10
20
30
40

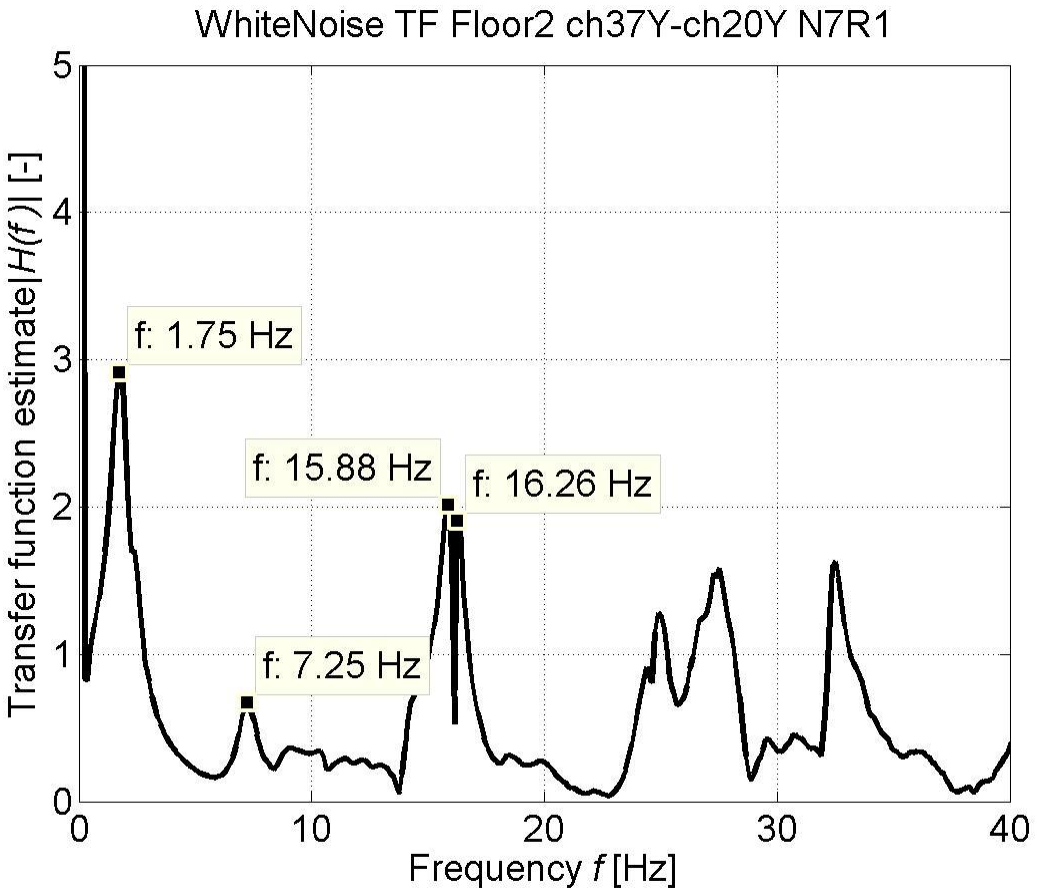
WhiteNoise TF Floor2 ch37Y-ch20Y N7R1
Transfer function estimate |H(f)| [-]
Frequency f [Hz]
f: 1.75 Hz
f: 15.88 Hz
f: 16.26 Hz
f: 7.25 Hz
0
1
2
3
4
5
0
10
20
30
40

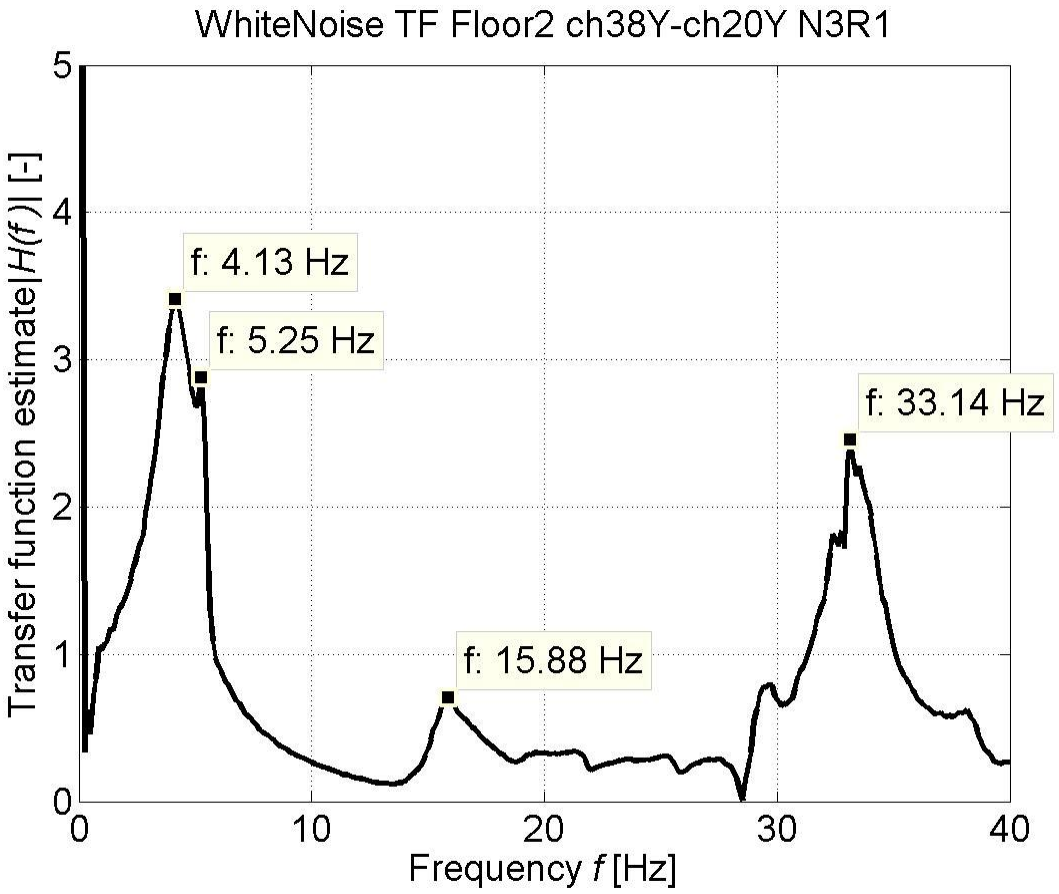
WhiteNoise TF Floor2 ch38Y-ch20Y N3R1
Transfer function estimate |H(f)| [-]
Frequency f [Hz]
f: 4.13 Hz
f: 5.25 Hz
f: 15.88 Hz
f: 33.14 Hz
0
1
2
3
4
5
0
10
20
30
40

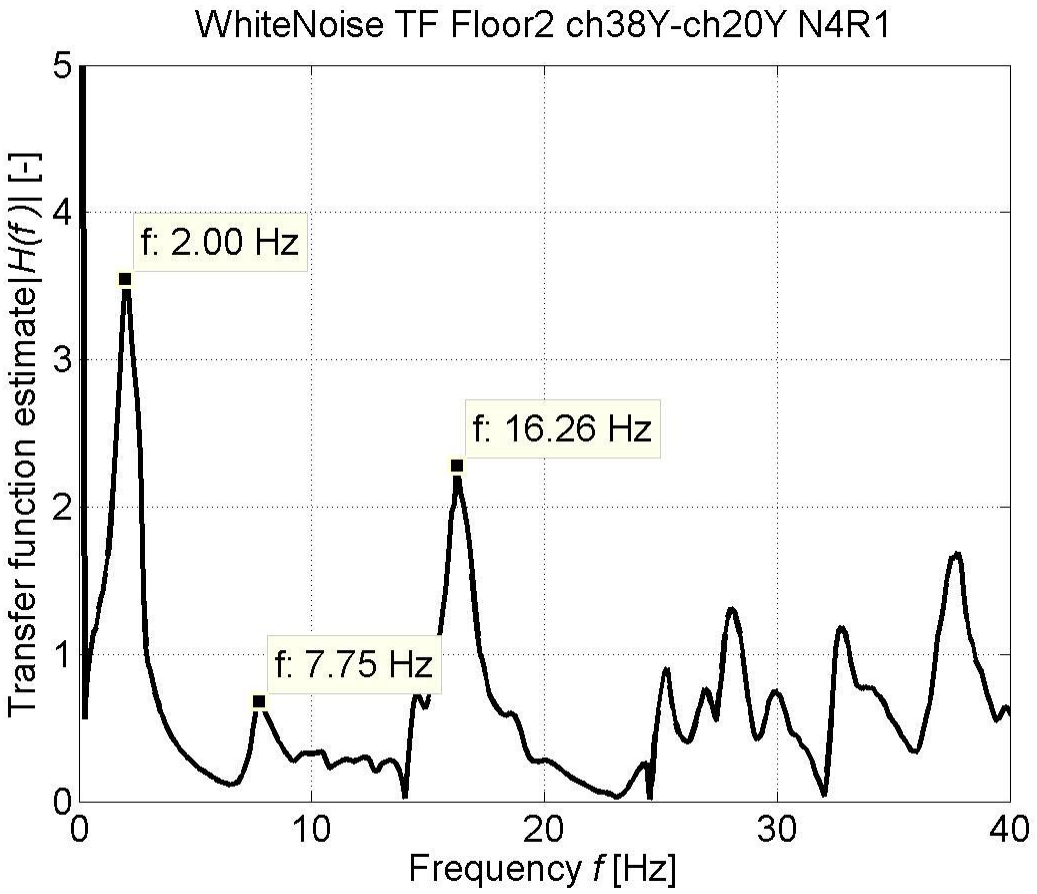
WhiteNoise TF Floor2 ch38Y-ch20Y N4R1
Transfer function estimate|H(f)| [-]
Frequency f [Hz]
f: 2.00 Hz
f: 7.75 Hz
f: 16.26 Hz
0
1
2
3
4
5
0
10
20
30
40

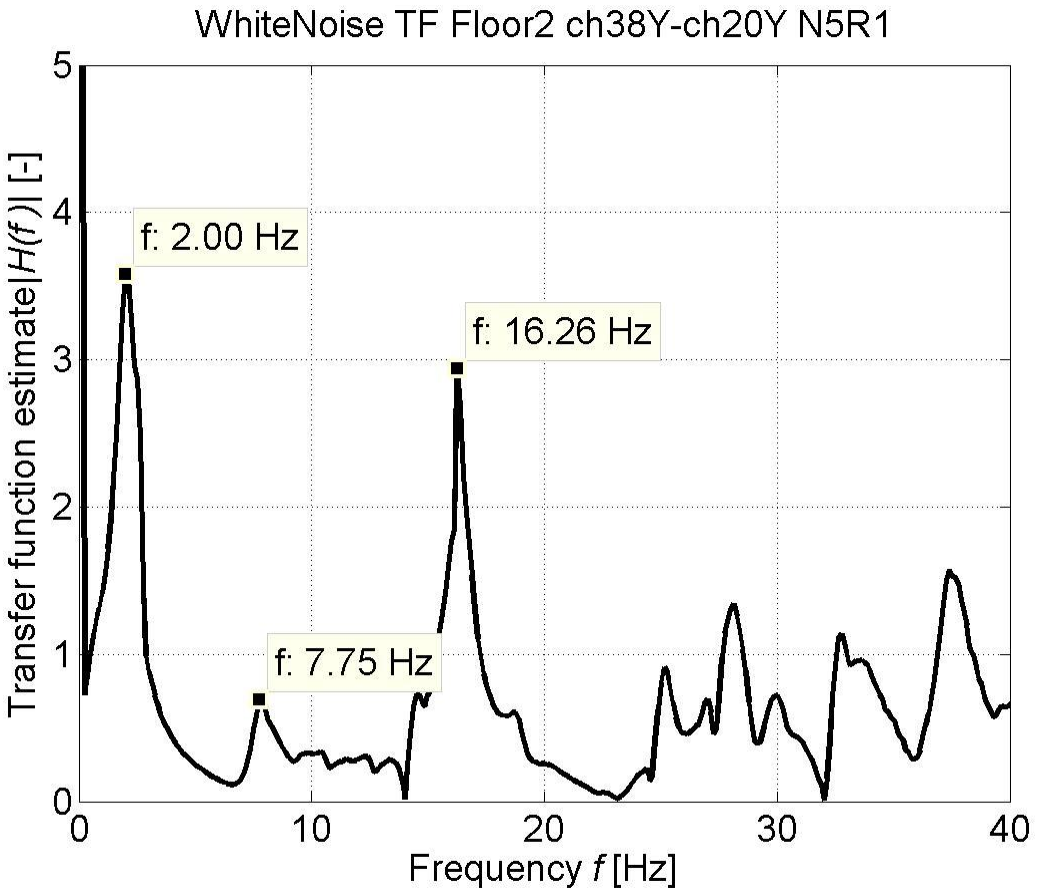
WhiteNoise TF Floor2 ch38Y-ch20Y N5R1
Transfer function estimate |H(f)| [-]
Frequency f [Hz]
f: 2.00 Hz
f: 7.75 Hz
f: 16.26 Hz
0
1
2
3
4
5
0
10
20
30
40

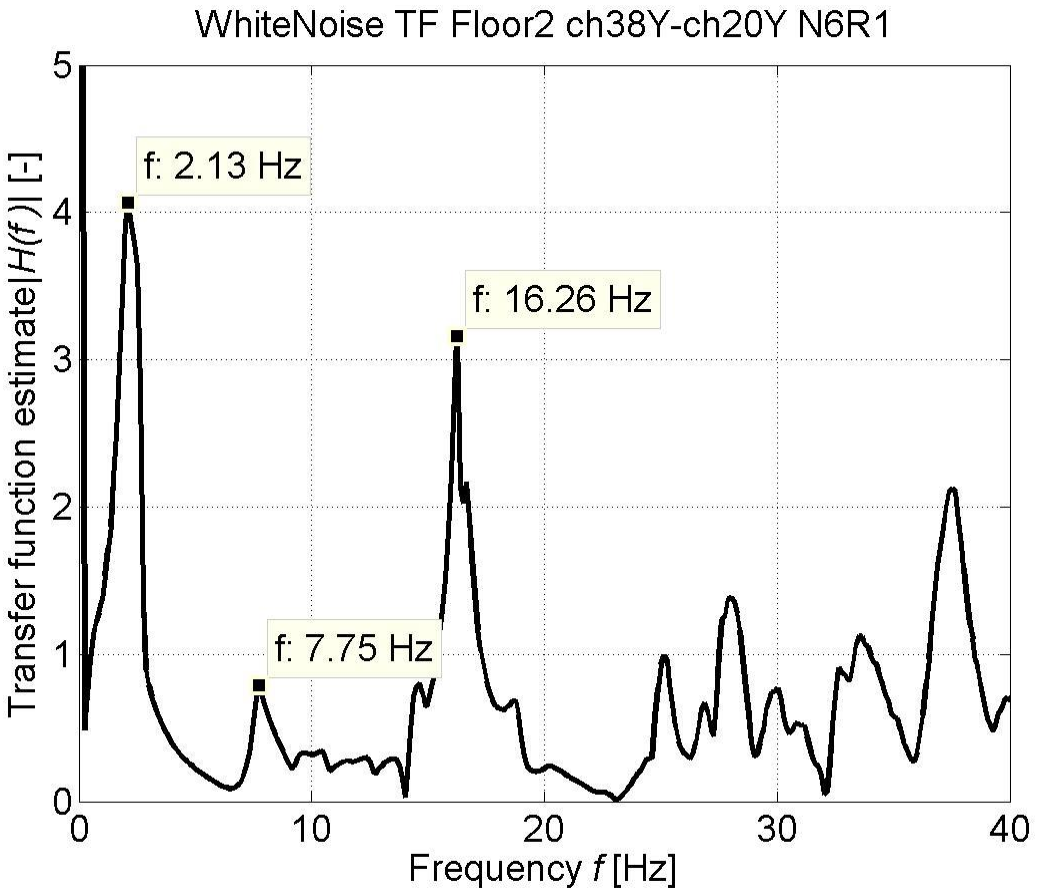
WhiteNoise TF Floor2 ch38Y-ch20Y N6R1
f: 2.13 Hz
f: 16.26 Hz
f: 7.75 Hz
Transfer function estimate |H(f)| [-]
Frequency f [Hz]
0
1
2
3
4
5
0
10
20
30
40

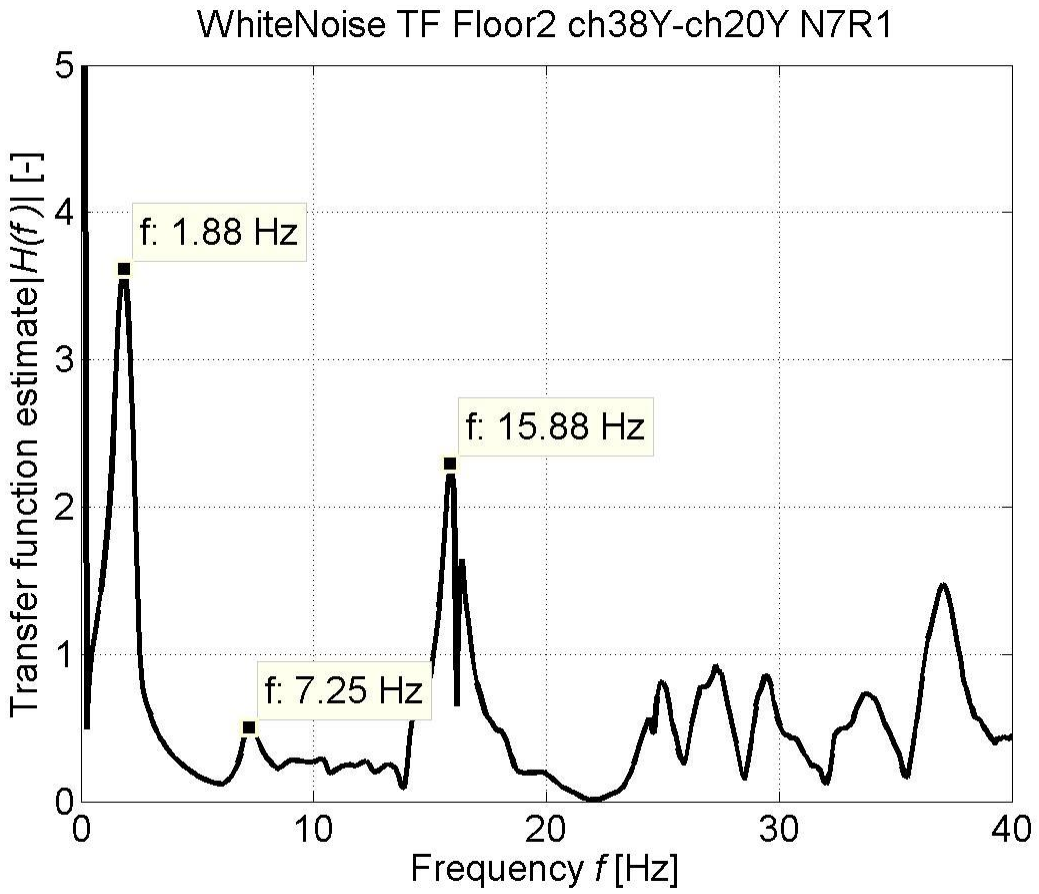

F L O O R 3

Channels 39-42

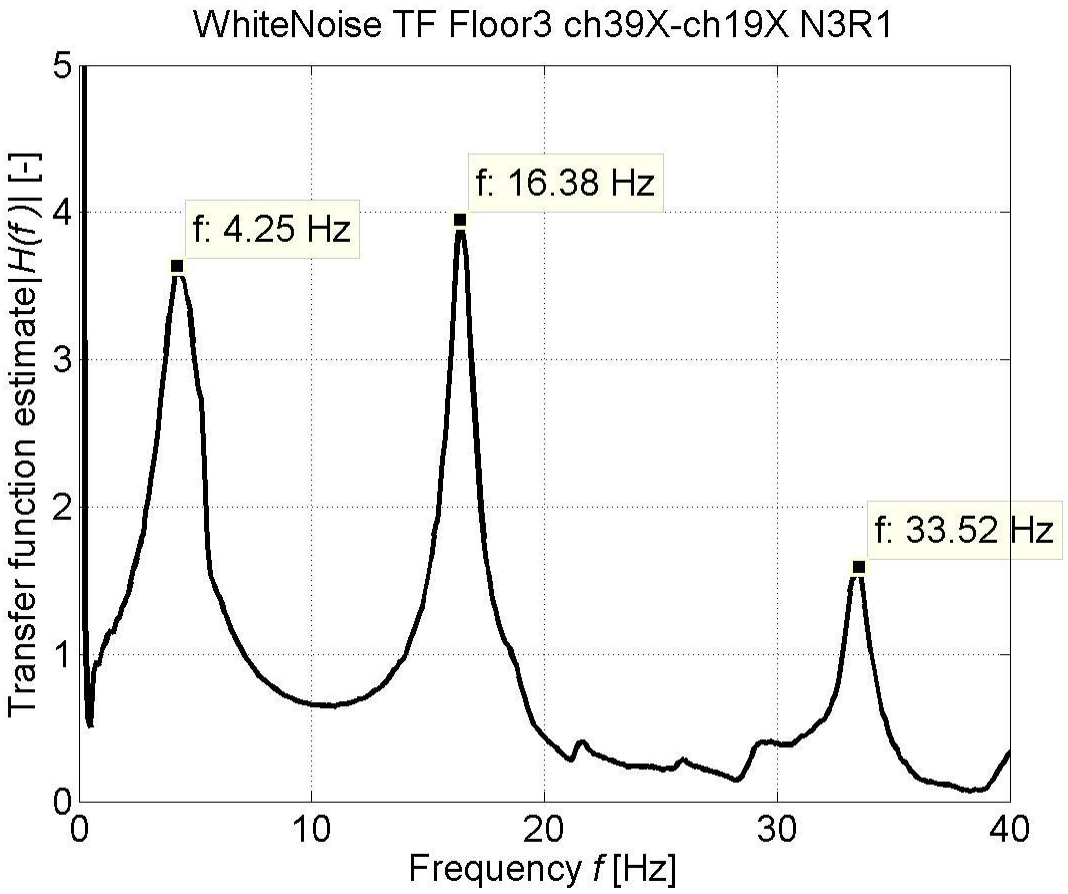
WhiteNoise TF Floor3 ch39X-ch19X N3R1
f: 4.25 Hz
f: 16.38 Hz
f: 33.52 Hz
Transfer function estimate|H(f)| [-]
Frequency f [Hz]
0
1
2
3
4
5
0
10
20
30
40

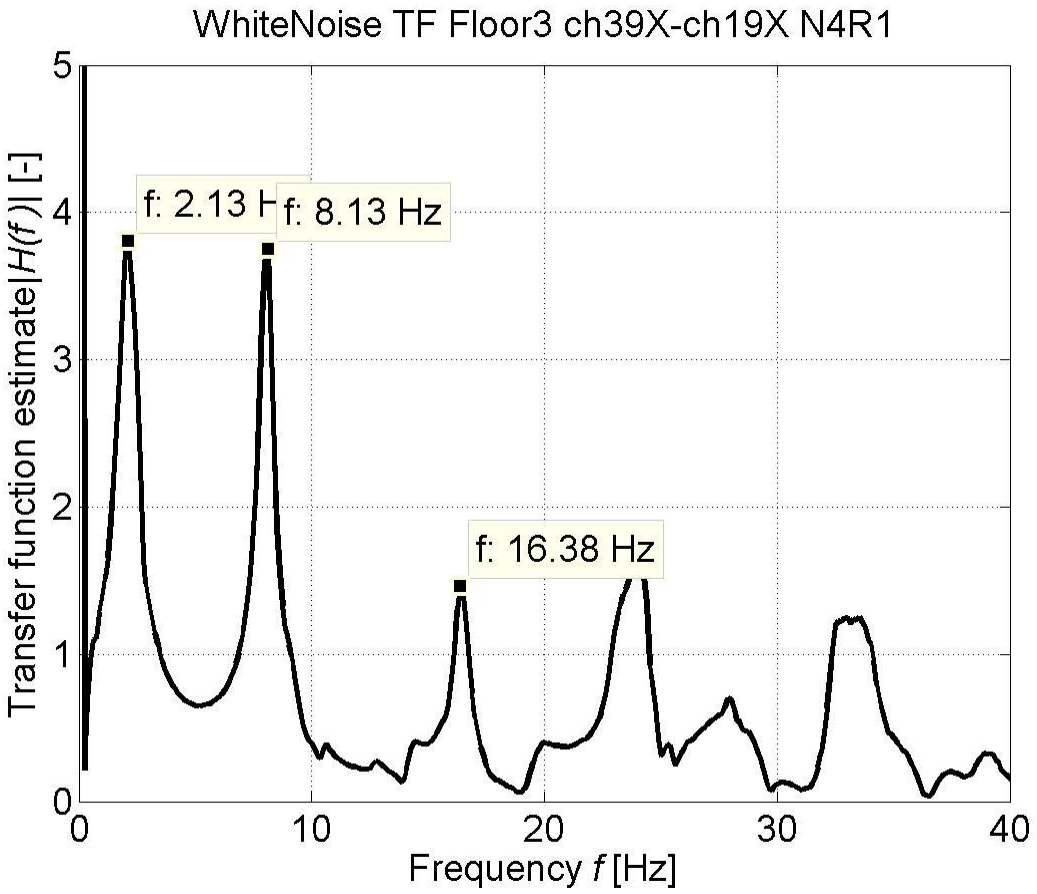
WhiteNoise TF Floor3 ch39X-ch19X N4R1
f: 2.13 H
f: 8.13 Hz
f: 16.38 Hz
Transfer function estimate |H(f)| [-]
Frequency f [Hz]
0
1
2
3
4
5
0
10
20
30
40

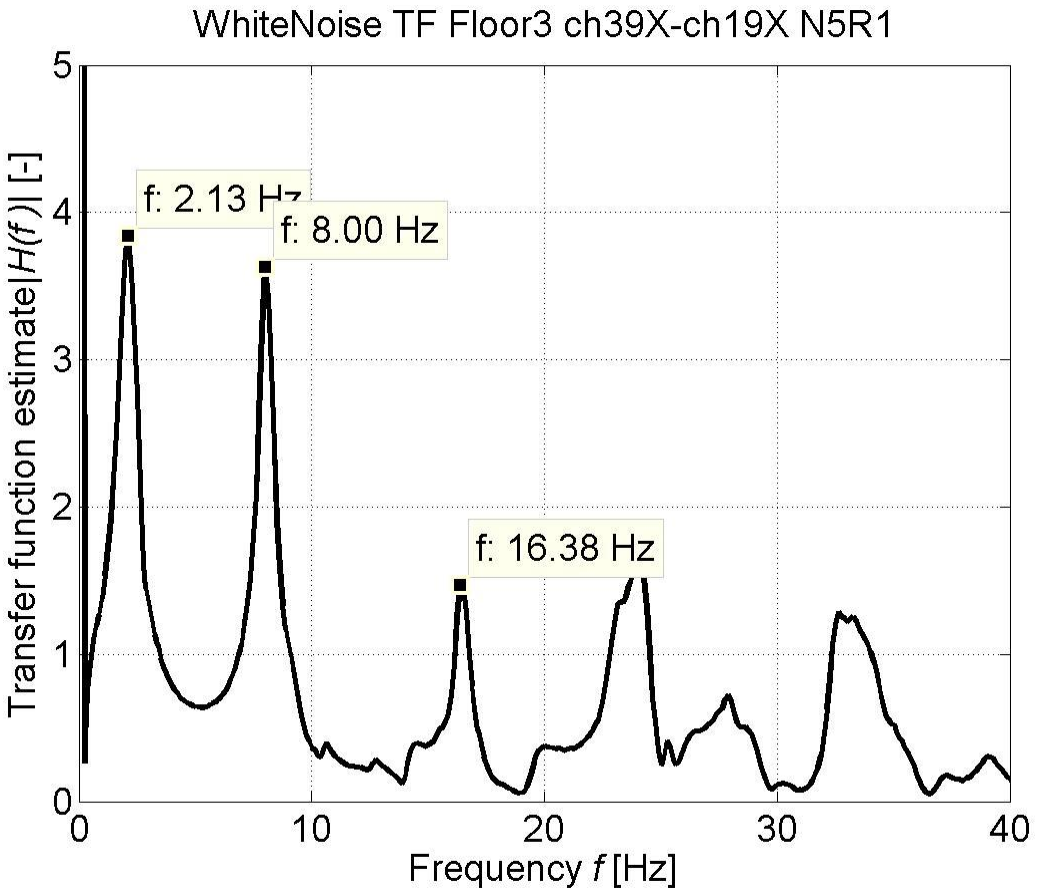
WhiteNoise TF Floor3 ch39X-ch19X N5R1
f: 2.13 Hz
f: 8.00 Hz
f: 16.38 Hz
Transfer function estimate |H(f)| [-]
Frequency f [Hz]
0
1
2
3
4
5
0
10
20
30
40

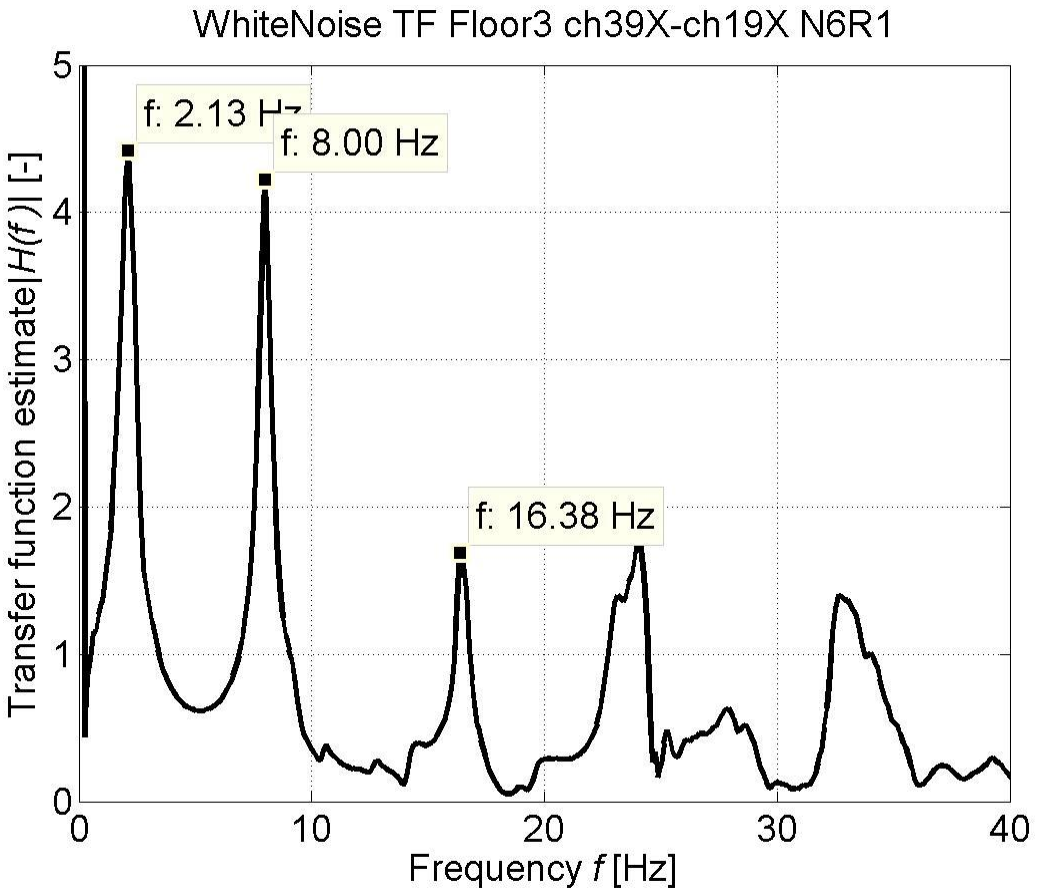
WhiteNoise TF Floor3 ch39X-ch19X N6R1
f: 2.13 Hz
f: 8.00 Hz
f: 16.38 Hz
Transfer function estimate |H(f)| [-]
Frequency f [Hz]
0
1
2
3
4
5
0
10
20
30
40

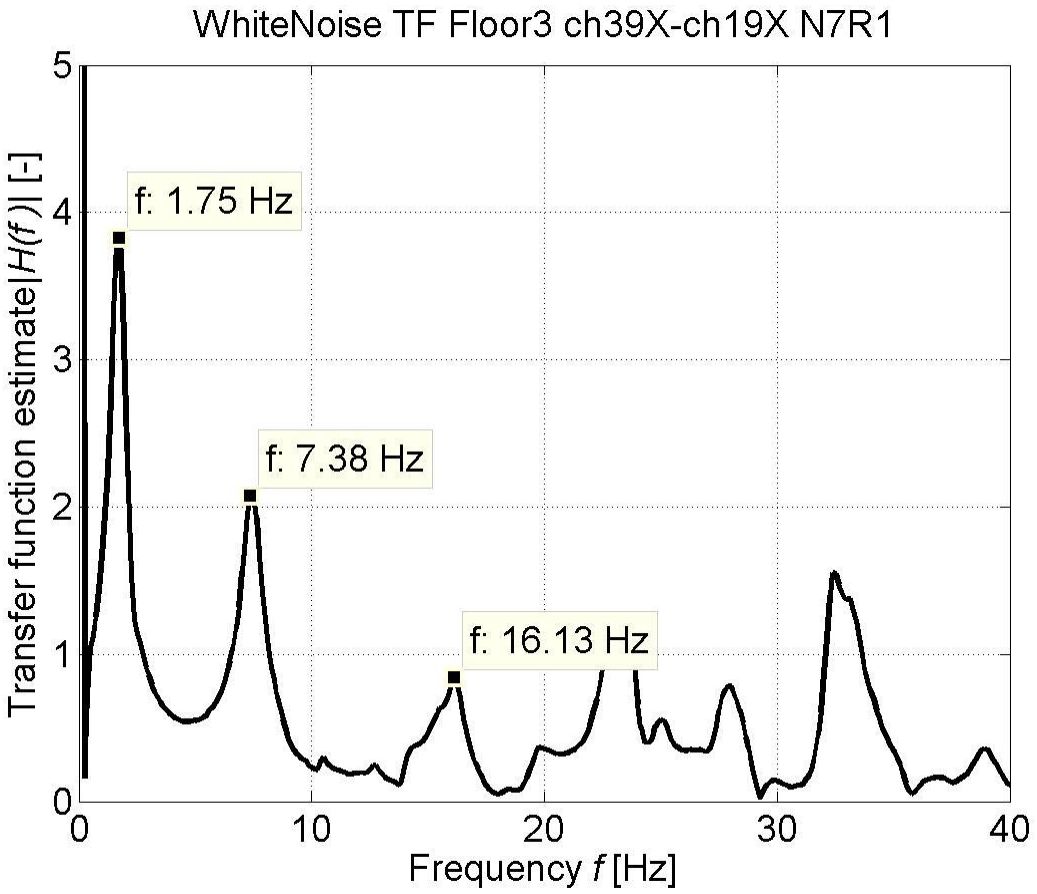
WhiteNoise TF Floor3 ch39X-ch19X N7R1
f: 1.75 Hz
f: 7.38 Hz
f: 16.13 Hz
Transfer function estimate |H(f)| [-]
Frequency f [Hz]
0
1
2
3
4
5
0
10
20
30
40

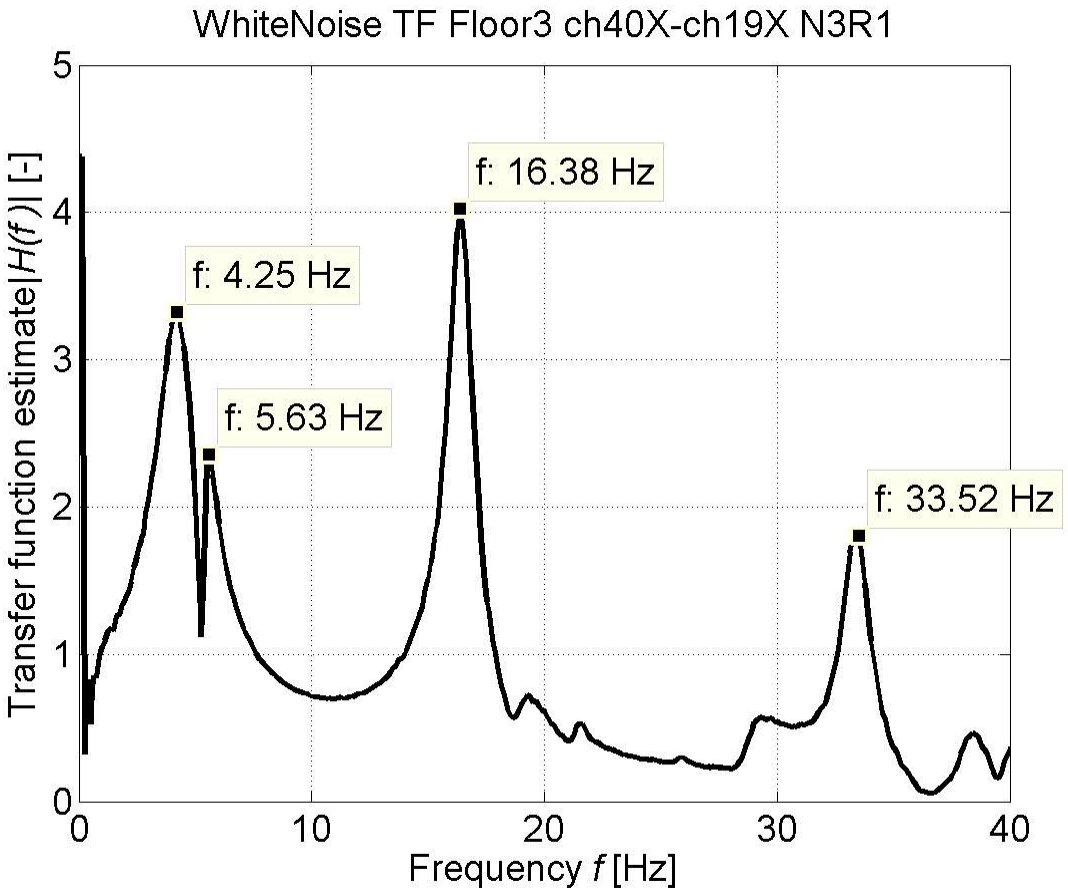
WhiteNoise TF Floor3 ch40X-ch19X N3R1
f: 16.38 Hz
f: 4.25 Hz
f: 5.63 Hz
f: 33.52 Hz
Transfer function estimate |H(f)| [-]
Frequency f [Hz]
0
1
2
3
4
5
0
10
20
30
40

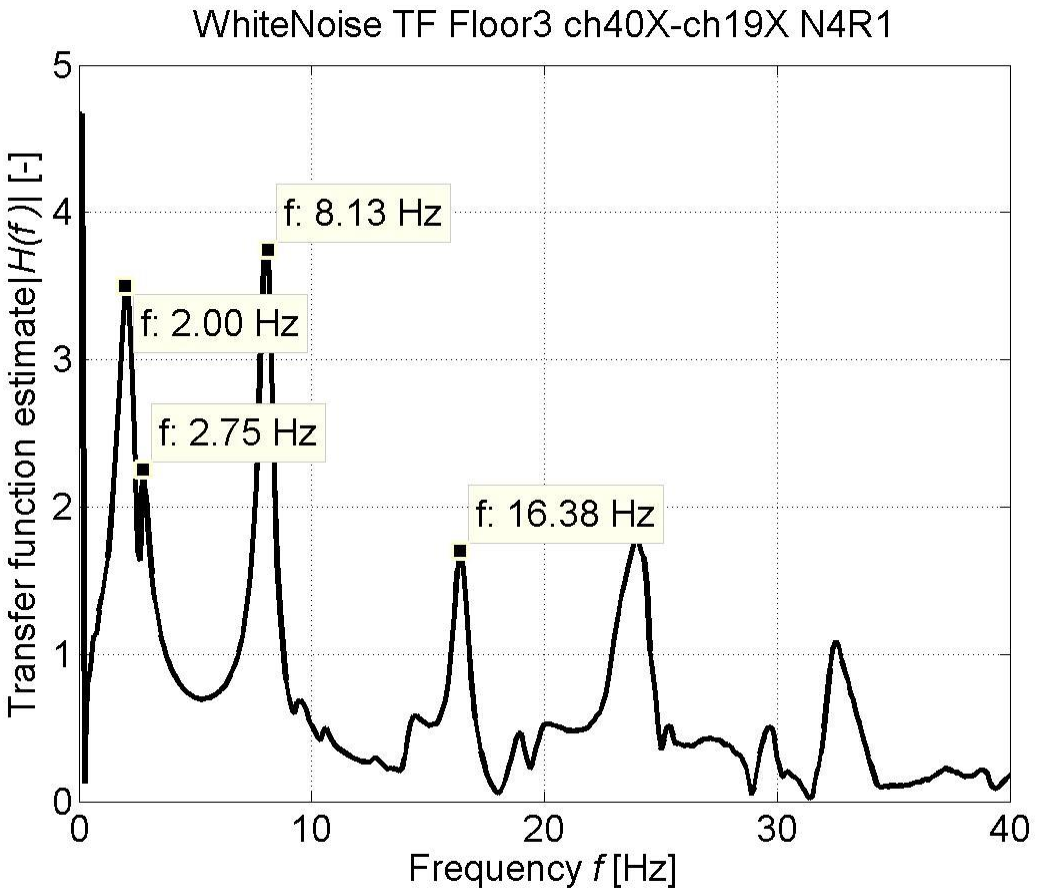
WhiteNoise TF Floor3 ch40X-ch19X N4R1
Transfer function estimate |H(f)| [-]
Frequency f [Hz]
f: 8.13 Hz
f: 2.00 Hz
f: 2.75 Hz
f: 16.38 Hz
0
1
2
3
4
5
0
10
20
30
40

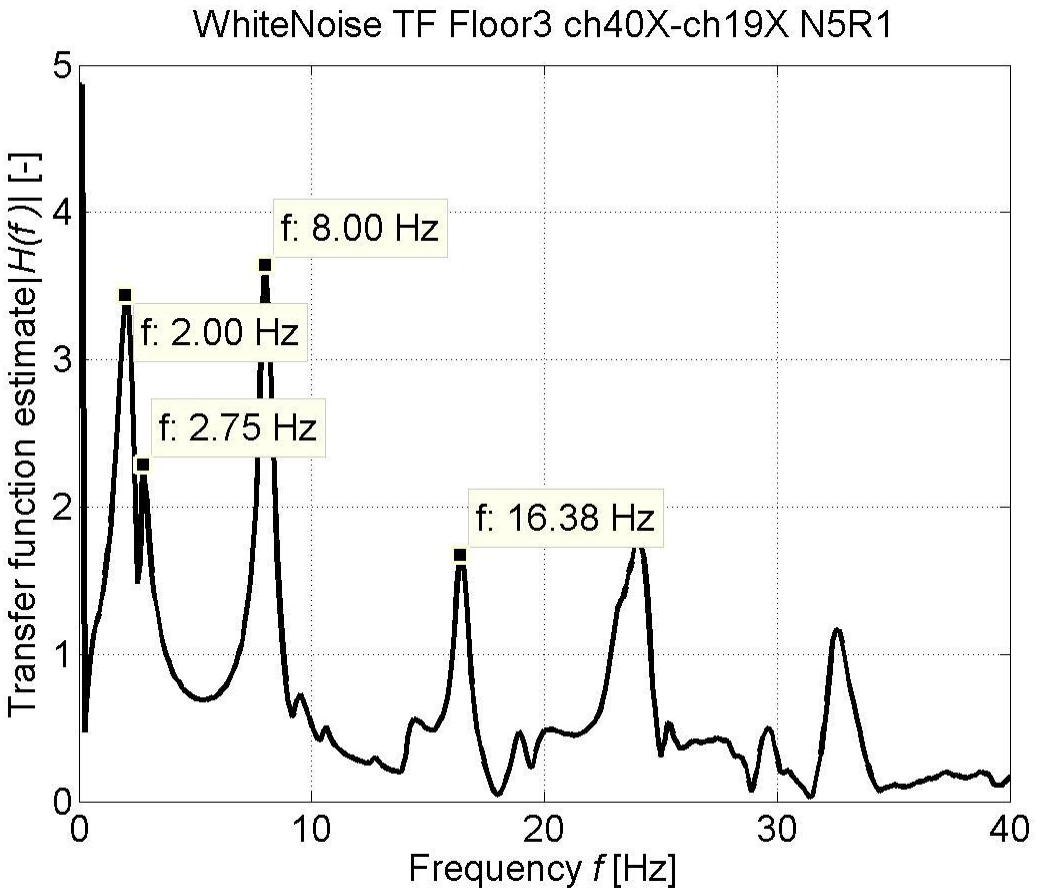
WhiteNoise TF Floor3 ch40X-ch19X N5R1
Transfer function estimate |H(f)| [-]
Frequency f [Hz]
f: 8.00 Hz
f: 2.00 Hz
f: 2.75 Hz
f: 16.38 Hz
0
1
2
3
4
5
0
10
20
30
40

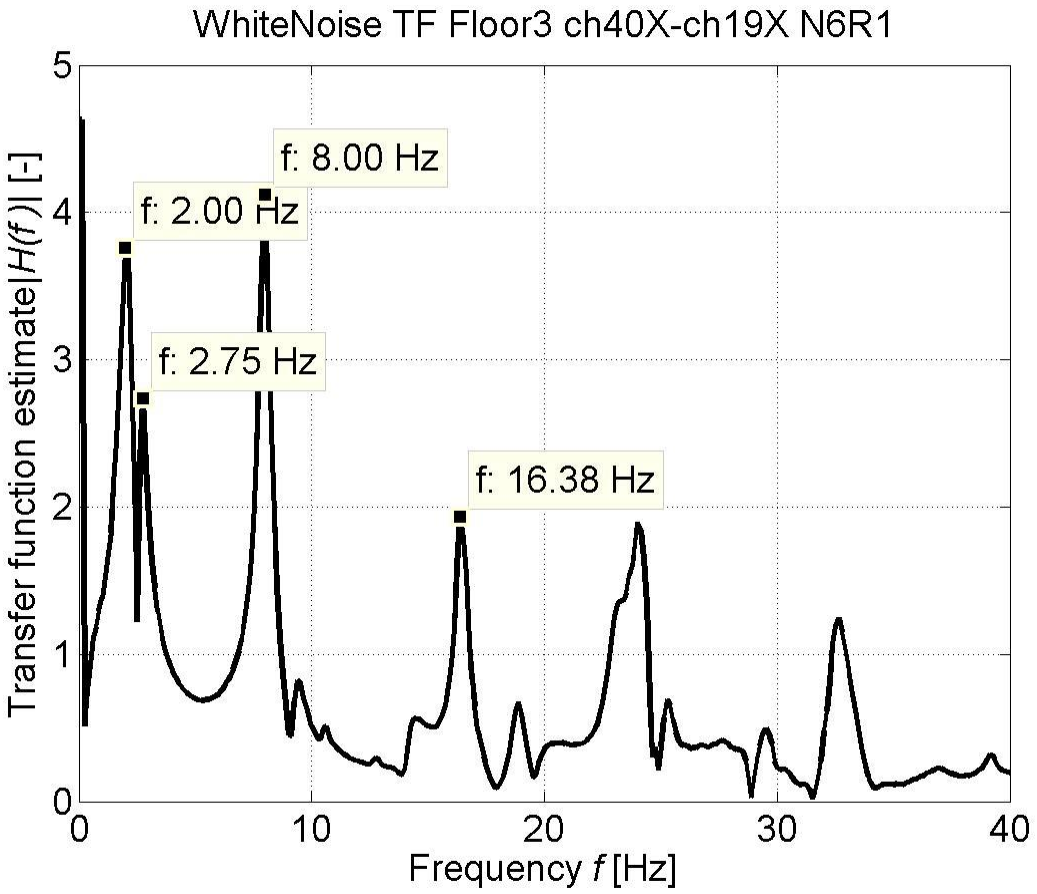
WhiteNoise TF Floor3 ch40X-ch19X N6R1
f: 8.00 Hz
f: 2.00 Hz
f: 2.75 Hz
f: 16.38 Hz
Transfer function estimate |H(f)| [-]
Frequency f [Hz]
0
1
2
3
4
5
0
10
20
30
40

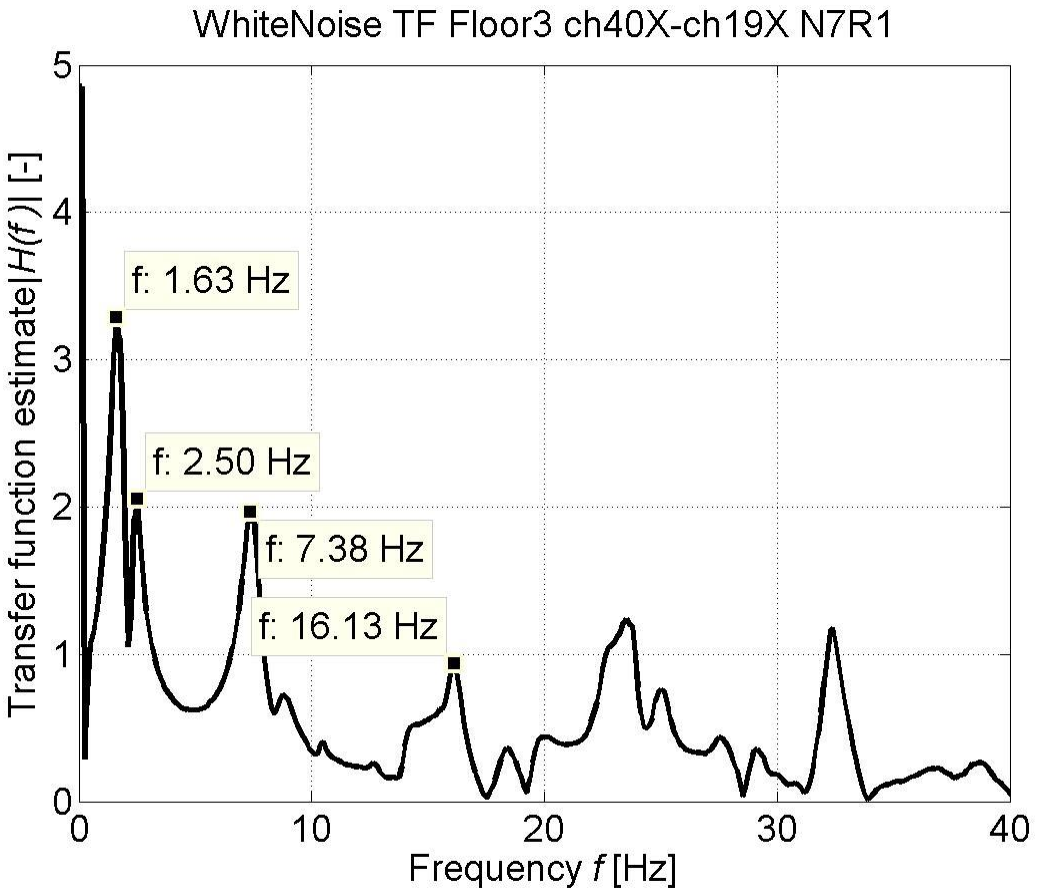
WhiteNoise TF Floor3 ch40X-ch19X N7R1
Transfer function estimate |H(f)| [-]
Frequency f [Hz]
f: 1.63 Hz
f: 2.50 Hz
f: 7.38 Hz
f: 16.13 Hz
0
1
2
3
4
5
0
10
20
30
40

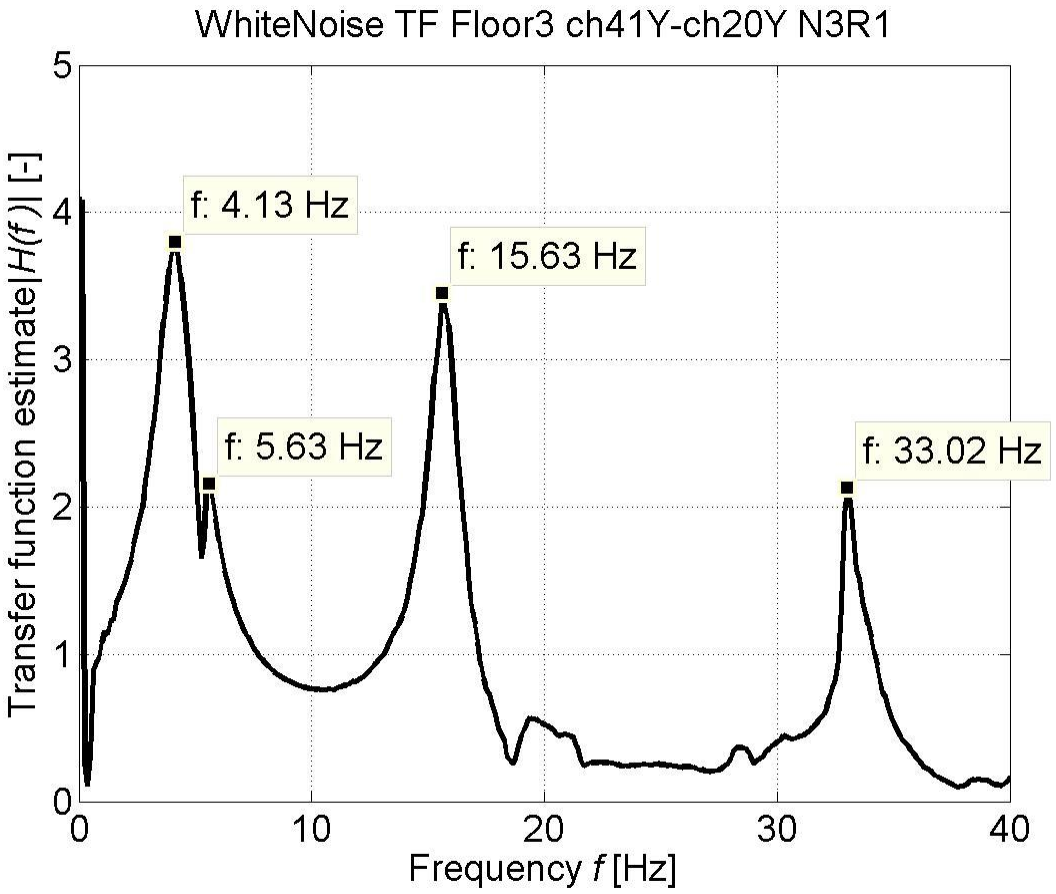
WhiteNoise TF Floor3 ch41Y-ch20Y N3R1
Transfer function estimate|H(f)| [-]
Frequency f [Hz]
f: 4.13 Hz
f: 5.63 Hz
f: 15.63 Hz
f: 33.02 Hz
0
1
2
3
4
5
0
10
20
30
40

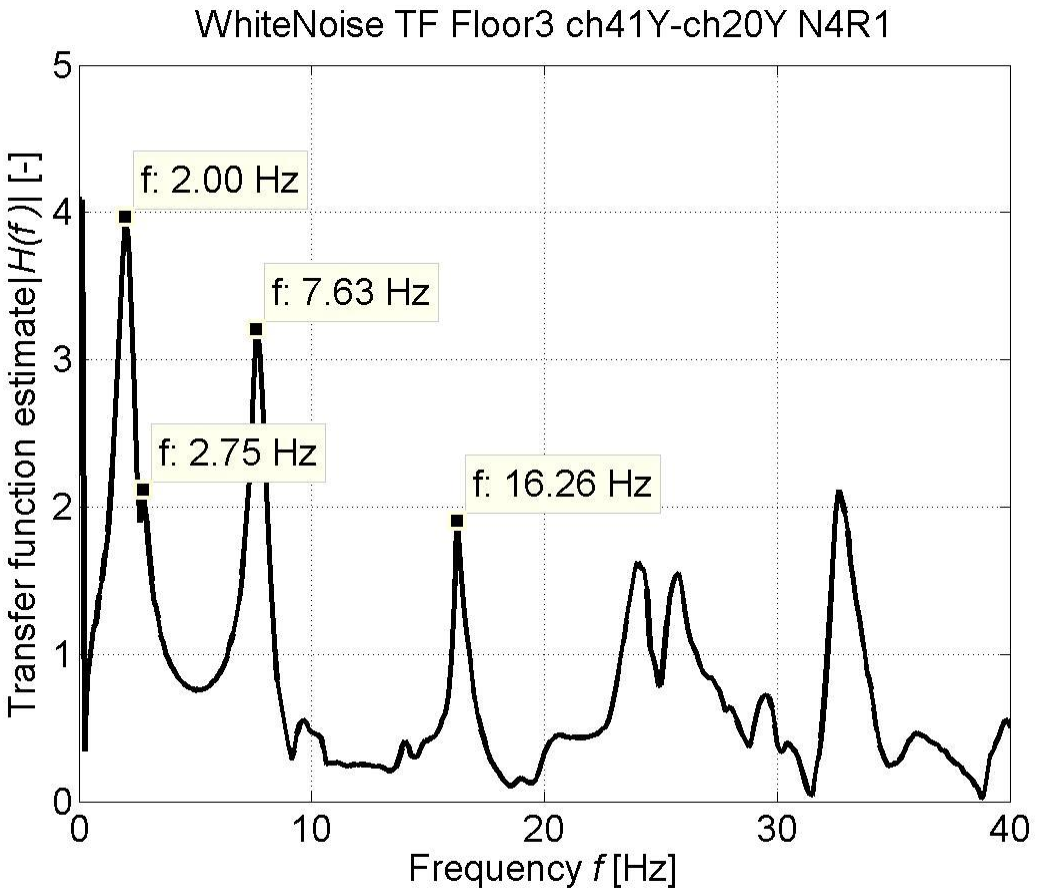
WhiteNoise TF Floor3 ch41Y-ch20Y N4R1
f: 2.00 Hz
f: 7.63 Hz
f: 2.75 Hz
f: 16.26 Hz
Transfer function estimate|H(f)| [-]
Frequency f [Hz]
0
1
2
3
4
5
0
10
20
30
40

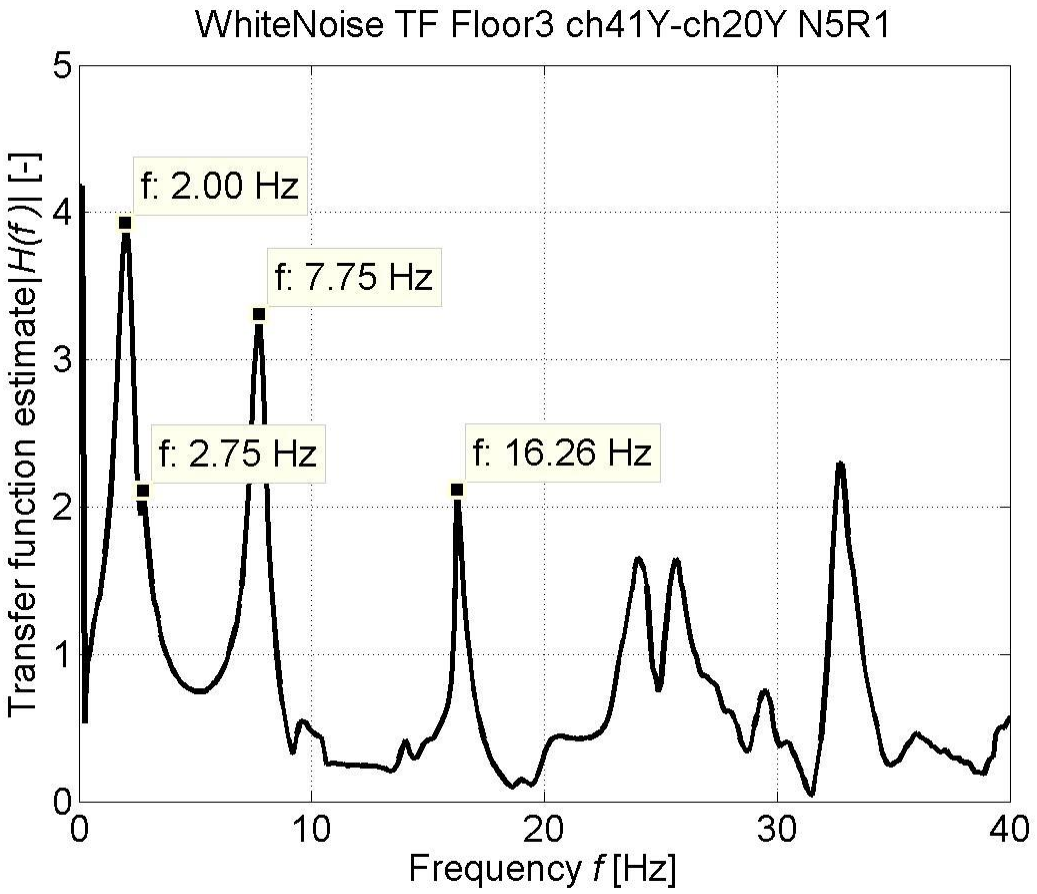
WhiteNoise TF Floor3 ch41Y-ch20Y N5R1
f: 2.00 Hz
f: 7.75 Hz
f: 2.75 Hz
f: 16.26 Hz
Transfer function estimate |H(f)| [-]
Frequency f [Hz]
0
1
2
3
4
5
0
10
20
30
40

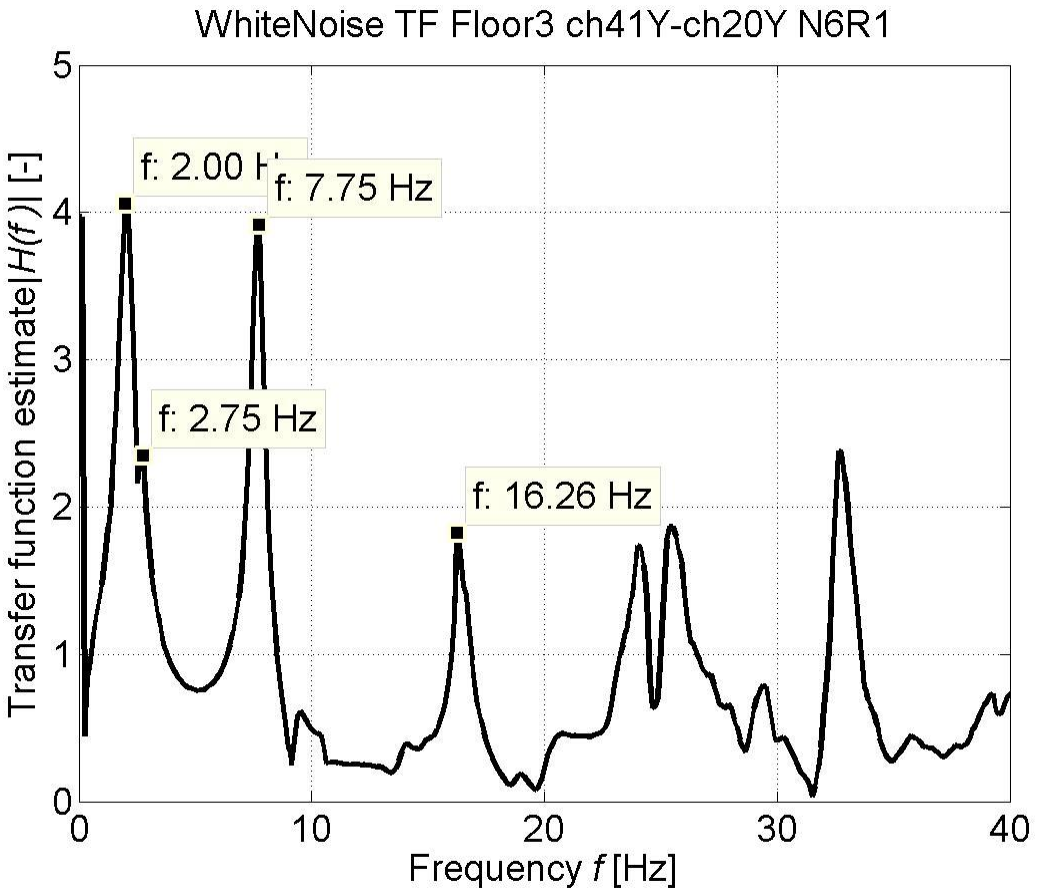
WhiteNoise TF Floor3 ch41Y-ch20Y N6R1
f: 2.00 H
f: 7.75 Hz
f: 2.75 Hz
f: 16.26 Hz
Transfer function estimate |H(f)| [-]
Frequency f [Hz]
0
1
2
3
4
5
0
10
20
30
40

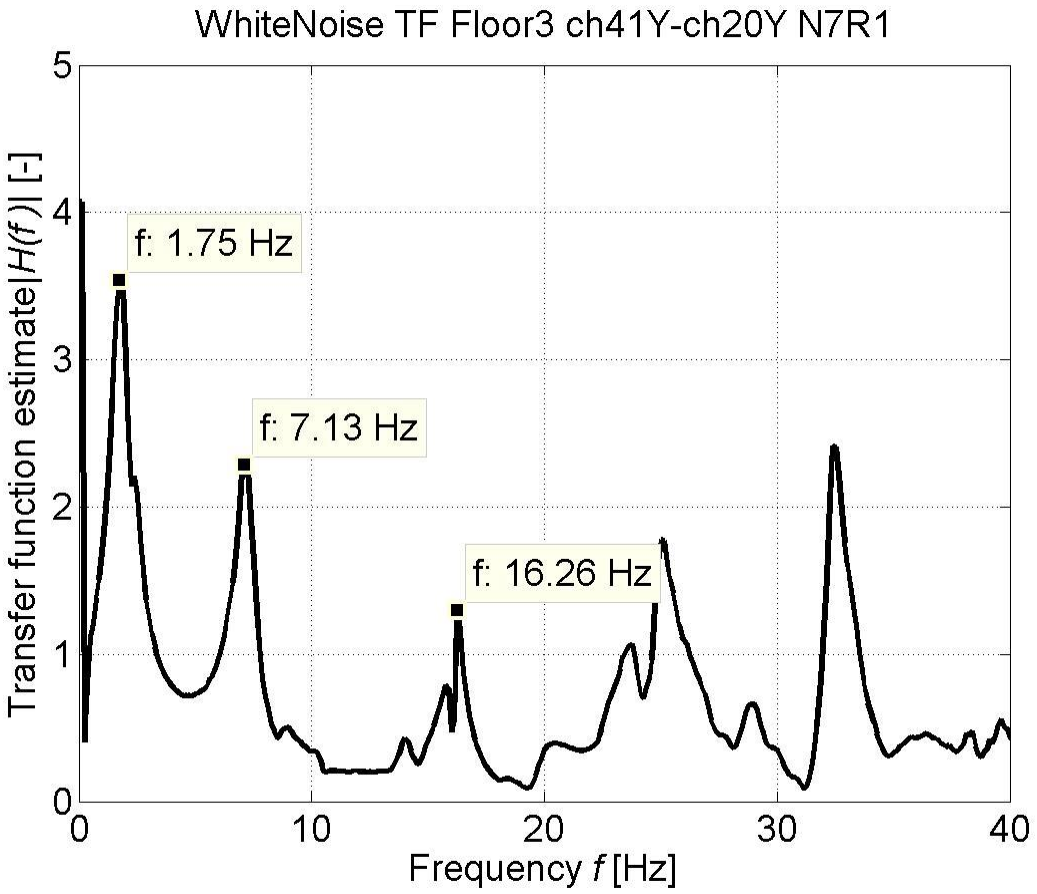
WhiteNoise TF Floor3 ch41Y-ch20Y N7R1
Transfer function estimate |H(f)| [-]
Frequency f [Hz]
f: 1.75 Hz
f: 7.13 Hz
f: 16.26 Hz
0
1
2
3
4
5
0
10
20
30
40

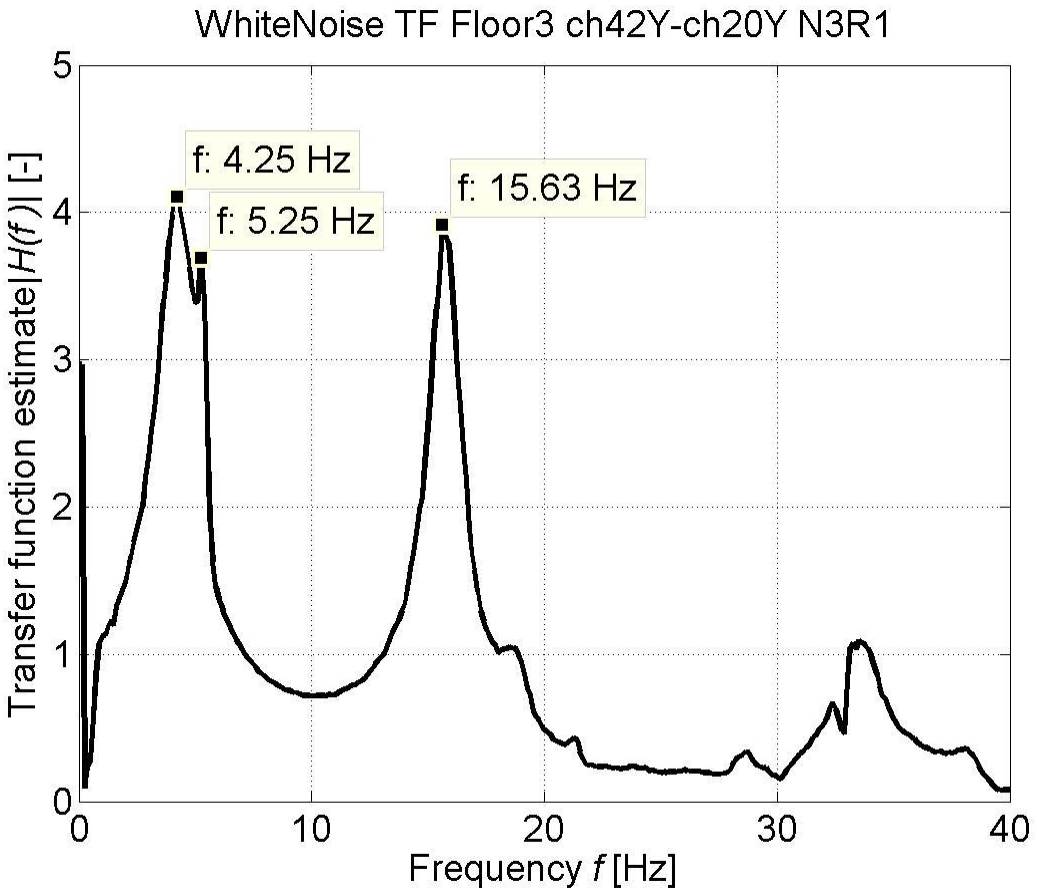
WhiteNoise TF Floor3 ch42Y-ch20Y N3R1
f: 4.25 Hz
f: 5.25 Hz
f: 15.63 Hz
Transfer function estimate |H(f)| [-]
Frequency f [Hz]
0
1
2
3
4
5
0
10
20
30
40

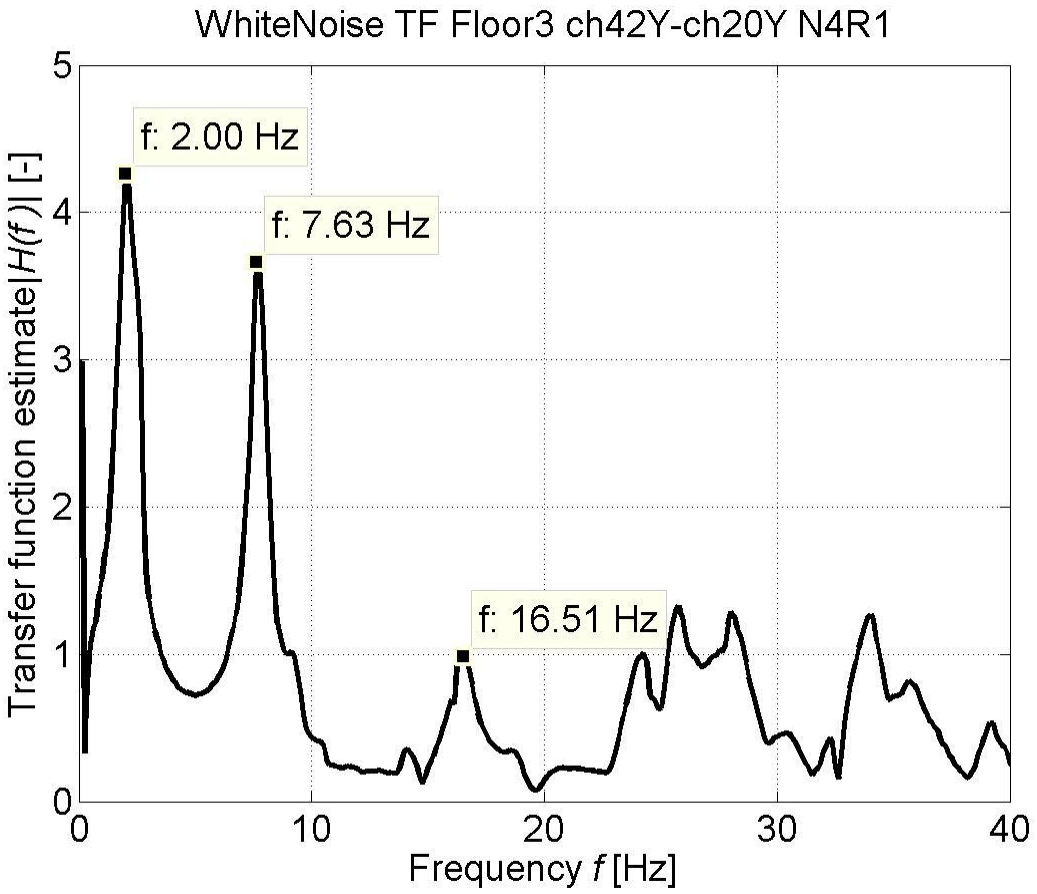
WhiteNoise TF Floor3 ch42Y-ch20Y N4R1
f: 2.00 Hz
f: 7.63 Hz
f: 16.51 Hz
Transfer function estimate |H(f)| [-]
Frequency f [Hz]
0
1
2
3
4
5
0
10
20
30
40

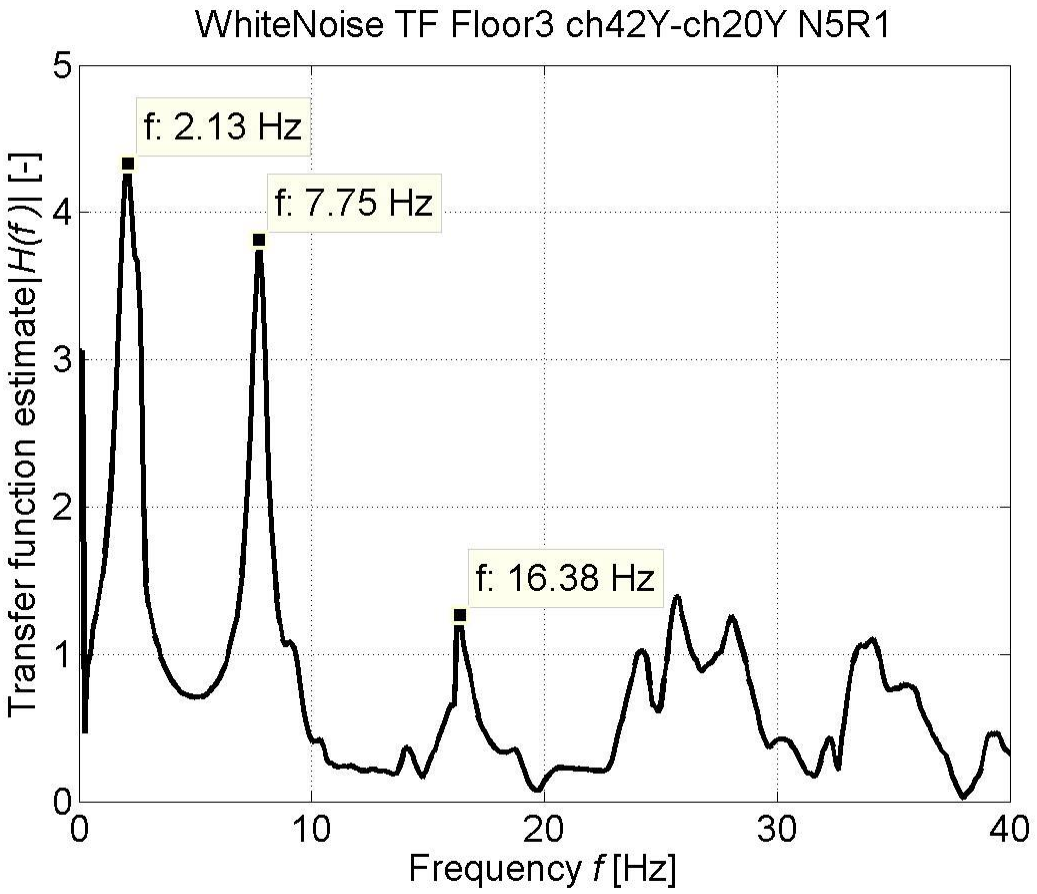
WhiteNoise TF Floor3 ch42Y-ch20Y N5R1
f: 2.13 Hz
f: 7.75 Hz
f: 16.38 Hz
Transfer function estimate |H(f)| [-]
Frequency f [Hz]
0
1
2
3
4
5
0
10
20
30
40

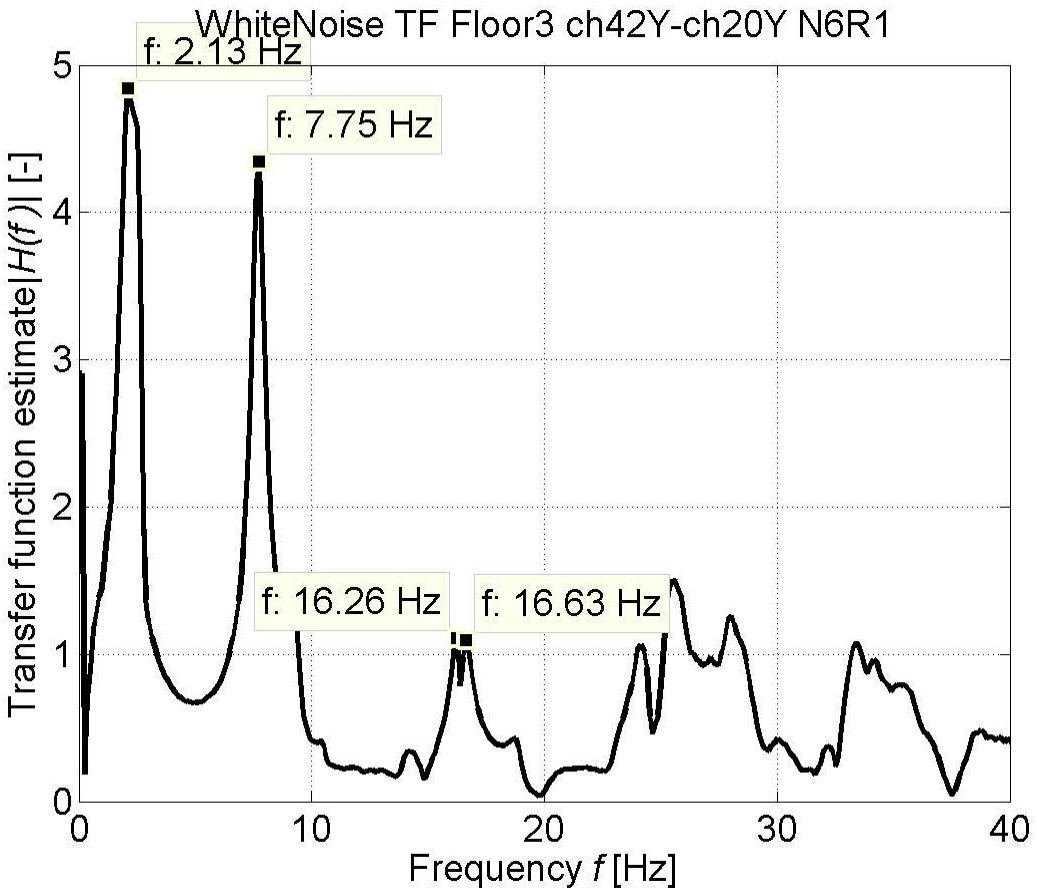
WhiteNoise TF Floor3 ch42Y-ch20Y N6R1
f: 2.13 Hz
f: 7.75 Hz
f: 16.26 Hz
f: 16.63 Hz
Transfer function estimate |H(f)| [-]
Frequency f [Hz]
0
1
2
3
4
5
0
10
20
30
40

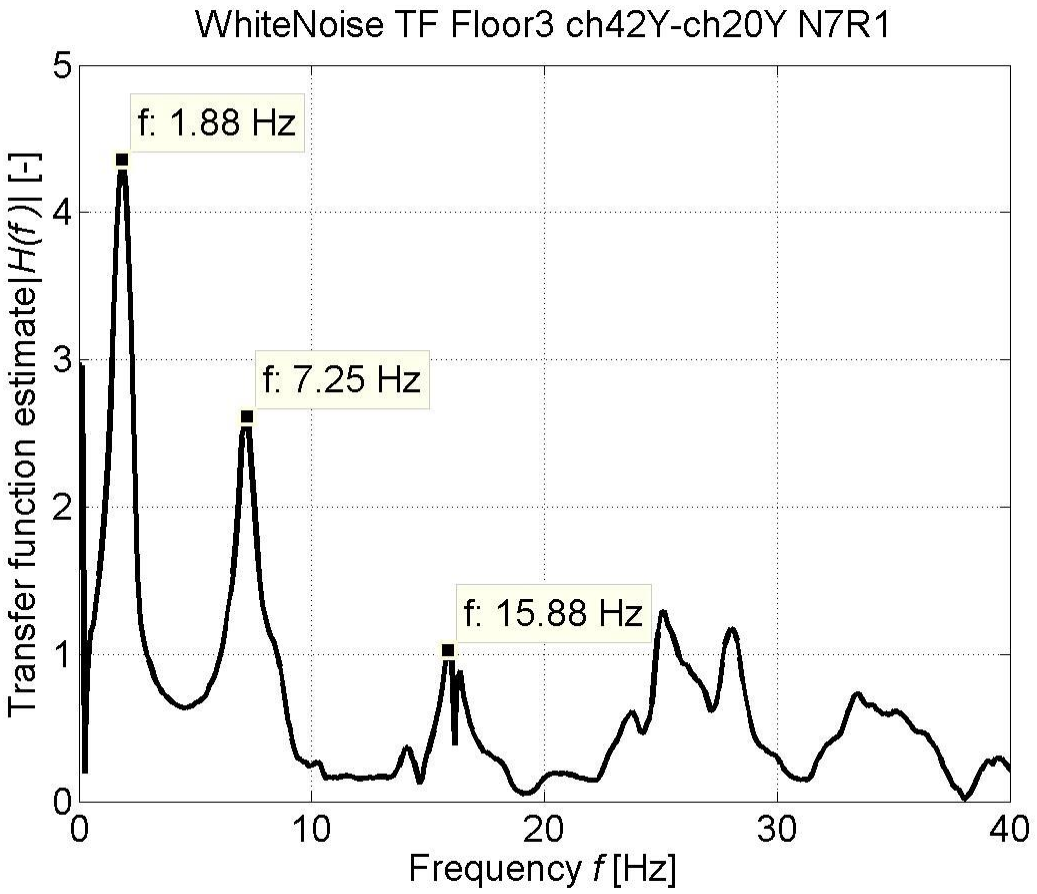
WhiteNoise TF Floor3 ch42Y-ch20Y N7R1
f: 1.88 Hz
f: 7.25 Hz
f: 15.88 Hz
Transfer function estimate|H(f)| [-]
Frequency f [Hz]
0
1
2
3
4
5
0
10
20
30
40